(2)

REPORT

Form Approved
OMB No. 0704-0188

1. AGENCY USE ONLY (Leave blank)	2. REPORT DATE	3. REPORT TYPE AND DATES COVERED
	15 Nov. 1991	Interim: 1 Oct. 90 – 30 Sept. 91

4. TITLE AND SUBTITLE

Physics and Technology of III-V Pseudomorphic Structures

5. FUNDING NUMBERS

PE61153N
R&T#414s002

6. AUTHOR(S)

C.W. Tu

7. PERFORMING ORGANIZATION NAME(S) AND ADDRESS(ES)

Department of Electrical & Computer Engineering
University of California at San Diego
La Jolla, CA 92093-0407

8. PERFORMING ORGANIZATION REPORT NUMBER

TU-ONR-90

9. SPONSORING/MONITORING AGENCY NAME(S) AND ADDRESS(ES)

Office of Naval Research
Code 1114
800 North Quincy Street
Arlington, VA 22217-5000

10. SPONSORING/MONITORING AGENCY REPORT NUMBER

11. SUPPLEMENTARY NOTES

12a. DISTRIBUTION/AVAILABILITY STATEMENT

Approved for public release; Distribution Unlimited

12b. DISTRIBUTION CODE

13. ABSTRACT (Maximum 200 words)

We have developed an *in situ* technique for determining the group-V composition in gas-source molecular beam epitaxy (GSMBE) growth of mixed group-V compounds, such as GaAsP, InAsP, and InGaAsP. The *in situ* technique consists of monitoring the intensity oscillations of group-V-induced reflection high-energy electron diffraction (RHEED). We have grown high-quality InAsP/InP strained-layer superlattices with exciton emission at 1.06, 1.3, or 1.55 μm, suitable for long-wavelength modulator applications. We have also explored the capability of GSMBE by investigating low-temperature-grown InP and *p*-type carbon doping in $In_{0.5}Ga_{0.5}As$ and $In_{0.5}Ga_{0.5}P$.

14. SUBJECT TERMS

InP, GaAsP, InAsP, InGaP, InGaAsP, MBE, GSMBE, strain, modulator, Schottky barrier, carbon, low temperature

15. NUMBER OF PAGES

16. PRICE CODE

17. SECURITY CLASSIFICATION OF REPORT	18. SECURITY CLASSIFICATION OF THIS PAGE	19. SECURITY CLASSIFICATION OF ABSTRACT	20. LIMITATION OF ABSTRACT

NSN 7540-01-280-5500

Standard Form 298 (Rev. 2-89)
Prescribed by ANSI Std. 239-18
298-102

53-85

Table of Contents

A differential reflection high energy electron diffraction measurement system

C. E. Chang, T. P. Chin, and C. W. Tu
Department of Electrical and Computer Engineering, University of California at San Diego, La Jolla, California 92093-0407

(Received 10 September 1990; accepted for publication 19 November 1990)

An economical, real-time differential reflection high energy electron diffraction (RHEED) measurement system which is effective in a high-noise environment is described. Two fiber optic cables sample the RHEED intensities from the phosphorescent screen in a molecular beam epitaxy (MBE) growth chamber. The first cable observes the RHEED oscillations with the inherent background noise while the second cable monitors the background noise. The differential RHEED unit subtracts the RHEED signal combined with the background noise from the background noise, leaving only the RHEED signal. The resultant "clean" RHEED oscillation is displayed on an IBM compatible computer.

I. INTRODUCTION

Reflection high energy electron diffraction (RHEED) has evolved to become the primary method used to observe the epitaxial growth of crystals in molecular beam epitaxy (MBE) machines. Monitoring the intensity of the RHEED oscillations allows optimization of the epitaxial growth conditions for binary and ternary compound semiconductors in the MBE growth chamber.[1] The growth rate of a single monolayer can be determined from the period of the RHEED oscillation.

Conventional low-c RHEED techniques utilize a photodiode or a photomultiplier tube to monitor the RHEED pattern intensity on the phosphorescent screen. The signal from the diode is amplified to drive an X–Y recorder. Due to the low intensity of the diffracted spot on the phosphorescent screen, background noise can approach and even exceed the RHEED signal.

The differential RHEED technique attempts to alleviate the inconveniences associated with conventional photodiode or photomultiplier RHEED techniques. This can be realized by sampling the RHEED pattern at two different points. The first point observes the RHEED pattern along with the background noise. The second point samples the background noise near the first point. The background noise may consist of surrounding lighting, MBE equipment vibrations, and diffuse background scattered electrons. Although in principle the diffuse scattering intensity also oscillates with time, its signal level is low (near the noise level); thus, the homogeneity of the background noise can be assumed. The subtraction of the RHEED information (measured RHEED intensity along with the associated background noise) from the background noise will yield the intrinsic RHEED intensity. This process should effectively remove the background noise in real time (without the inconvenient lag time between data acquisition and signal processing to display the RHEED oscillations). Figure 1 illustrates the basic setup of the differential RHEED system. A fiber optic cable sends the RHEED pattern and noise from the phosphorescent screen to a phototransistor in the phototransistor box. A second ancillary fiber optic cable conveys the noise to another matching phototransistor. Operational amplifiers inside the differential RHEED unit subtract the first signal from the second, leaving only the intrinsic RHEED intensity. An IBM compatible computer outfitted with an analog-to-digital (A/D) converter and an oscilloscope/fast Fourier transform (FFT) package will display, process, analyze, and store the RHEED oscillation. The period of oscillations (time to grow one monolayer) can be obtained with a FFT.

II. DIFFERENTIAL RHEED APPARATUS

The differential RHEED system can be subdivided into two sections. The first section deals with the differential RHEED unit while the second section deals primarily with the low-cost computer data acquisition/analysis system.

A. Differential RHEED unit

Simple mechanical arms position the fiber optic cables to the points of interest on the phosphorescent viewport of the MBE machine. The small diameter of the fiber cable allows accurate positioning of the fiber optic cable over the intensity maxima or minima of the RHEED spots. Two feet of shielded plastic fiber optic cable about 1 mm in diameter transports the low intensity RHEED information and noise to the phototransistor box. The end of the fiber optic cables are "polished" with a flame to yield a more optically transparent end.[2] The short run of fiber optic cables minimizes signal loss without sacrificing the ease of placement advantages of the fiber optic cable.

Two VarTec VT1113 phototransistors in a TO-18 package, converts the optical RHEED information or noise into an electrical signal in the phototransistor box. The common emitter configuration of the phototransistor provides enough voltage and current to drive the signal through the long length of shielded cable to the RHEED amplifier. The fiber optic cable to phototransistor interface consists of a common 3/8 to 1/4 in. Swagelok pipe fitting with a rubber cork (Fig 2). A small drop of superglue attaches the phototransistor to the 3/8 in. end of the Swagelok while the silicone sealant dries. The inside diameter

 0034-6748/91/030655-05$02.00

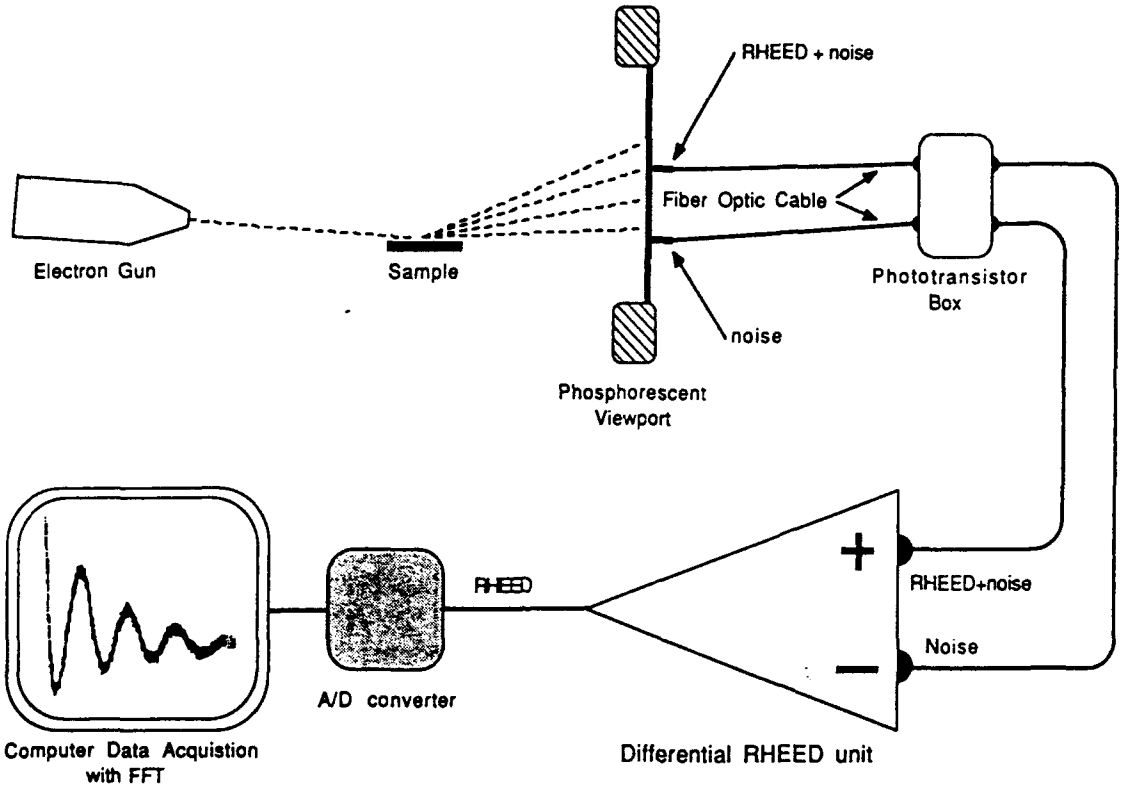

FIG. 1. Setup of the differential RHEED system. Two fiber optic cables sample the RHEED pattern from viewport. The differential amplifier subtracts the noise from the actual RHEED pattern. A computer data acquisition system displays the RHEED signal in real time.

of the Swagelok precisely fits the cylindrical TO-18 package of the phototransistor. On the other Swagelok end, a 1/4 in. diameter rubber cork with a small hole drilled in the center firmly positions the fiber optic cable over the active area in the phototransistor package. When the nut on the Swagelok is tightened, it compresses the rubber cork which, in turn, tightens its grip on the fiber optic cable. The electrical RHEED signals leave the phototransistor box via BNC connectors, and the 15 V dc required by the phototransistors enters the phototransistor box through a 1/4 in. phono plug.

The differential dc-coupled RHEED amplifier unit amplifies the signals from two phototransistors, subtracts the first signal from the second, and corrects for the dc offset. Figure 3 illustrates the schematic diagram of the RHEED amplifier unit. In the first stage, operational amplifiers (U1A and U1B) in the noninverting mode provide variable gain from 1 to 5 for the incoming signal from each of the two phototransistors. The variable gain allows matching of the noise levels of the two signals. With equal noise amplitudes in each channel a third operational amplifier (U2A) in the differential mode subtracts the first signal

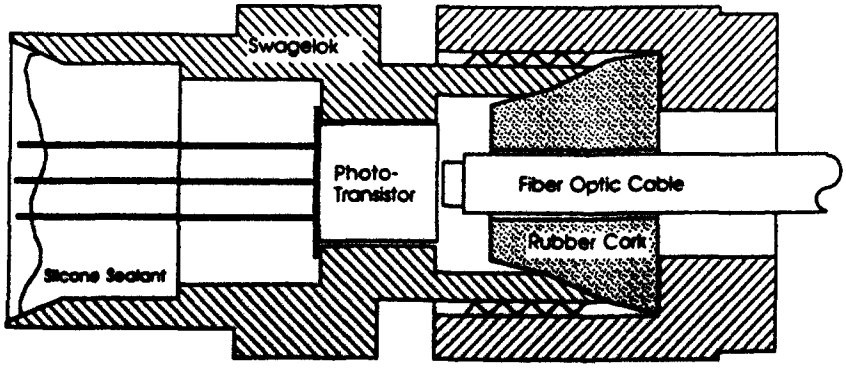

FIG. 2. A fiber optic cable to a phototransistor interface accomplished with a Swagelok pipe fitting. The rubber cork centers the cable over the active area of the phototransistor. The Swagelok nut compresses the cork to grip the fiber optic cable.

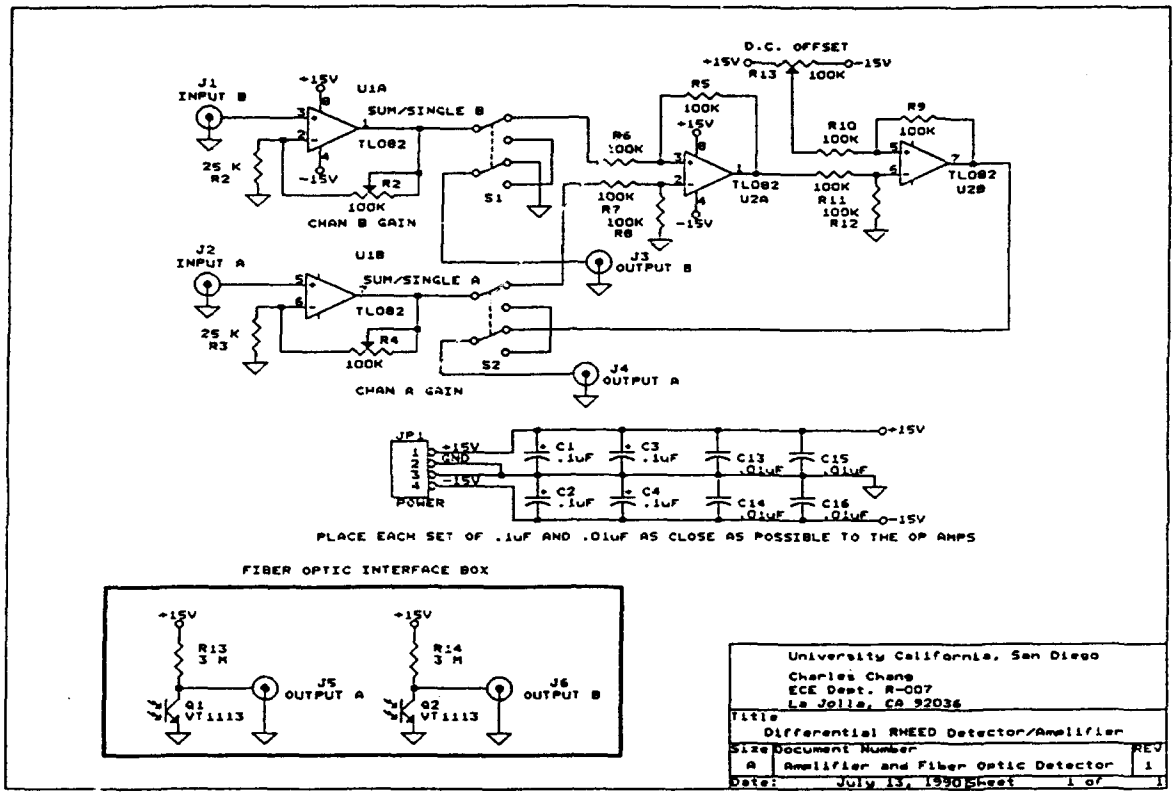

FIG. 3. Schematic diagram of the differential RHEED amplifier.

(that contains the RHEED information) from the second signal (that just contains the noise). Assuming equal phase in the noise, this will result in the actual RHEED intensity. Due to the inherent unequal dc offset in the phototransistors from the same make and batch, a fourth operational amplifier (U2B) adds or subtracts a dc constant to the RHEED oscillation signal. Capacitors could have been used to block the dc offset; however, the long period of the RHEED oscillations (about 1 s) would require large capacitor values. Furthermore, the capacitance value tolerance between two capacitors could alter the phase of the noise between channels; thus, reducing the overall effectiveness of the differential amplifier. Switches on the differential RHEED unit allow the unit to operate in the differential mode or to operate as two separate single channel amplifiers. High input resistance JFET TL082 operational amplifiers were used throughout the circuit. Capacitors (0.1 and 1 μF) bypass the line noise from the power supply to ground in order to reduce the noise, thus, they should be located as close to the operational amplifier as physically possible. To minimize the effect of line noise, a simple IC-regulated ± 15 V power supply with large computer grade electrolytic filter capacitors is used.

B. Computer data acquisition

The data acquisition computer consisted of an Intel 80286 based IBM AT compatible with a 80287 math coprocessor, VGA graphics, 1 Mb RAM, and a 40 Mb hard drive. A Metrabyte[3] DAS-8 12 bit A/D converter combined with the UnkleScope[4] software package converted the IBM AT compatible computer into a relatively low-cost computerized data acquisition system. The 12 channel A/D board provided enough resolution at a fast enough sampling rate (20 000 samples/s) to accurately digitize the RHEED intensity in real time. The Unklescope oscilloscope package effectively displays the RHEED pattern on the computer monitor. The ability to store the RHEED pattern measurement on the hard drive allows a FFT or a printer plot to be performed at a later time.

III. PERFORMANCE

The differential RHEED system is installed on a highly modified Varian Modular Gen II MBE growth chamber. Figures 4 and 5 illustrates the RHEED measurements conducted on a GaAs(100) wafer under various circumstances. Figure 4 shows the results of a single-channel RHEED measurement made with the differential RHEED system. High-frequency noise of a significant amplitude plagues the dampened sinusoidal RHEED oscillations. Conventional RHEED measurements plotted with *X–Y* plotters lack the high-frequency noise from the MBE machine since the mechanical limitations of the plotter act as a low-pass filter. The large amplitude of the background noise obscures the RHEED oscillations, thus making it difficult to determine the period of oscillations with accuracy. Although the RHEED information can be filtered in

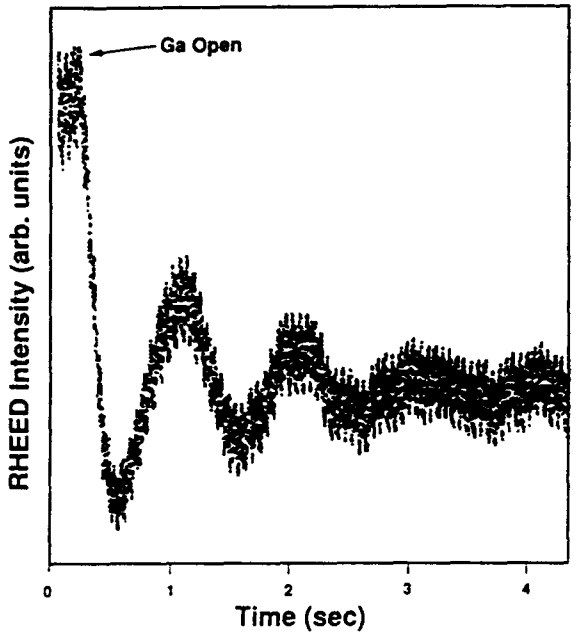

FIG. 4. RHEED oscillation of GaAs made with the differential RHEED amplifier in the single channel mode.

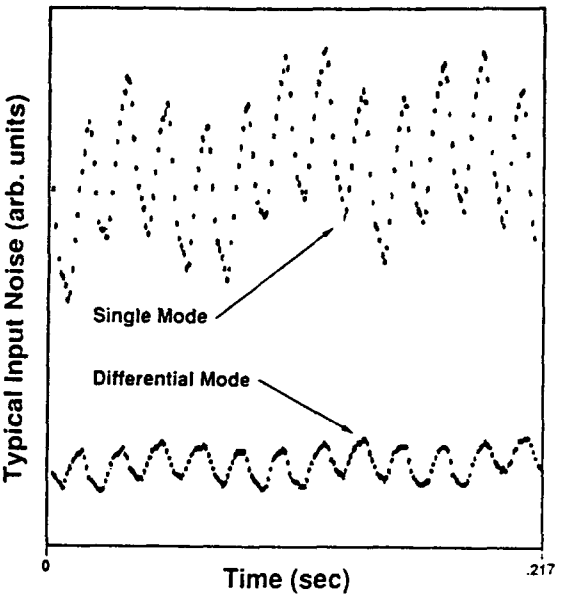

FIG. 6. Typical background MBE noise in both the single channel mode and in the differential mode.

the digital domain or converted to the frequency domain with a FFT, the IBM computer cannot process the data while acquiring data with enough resolution at the same time. Figure 5 illustrates the RHEED measurement made with the differential RHEED amplifier in the differential mode. The ancillary fiber optic cable was placed on a low intensity spot about 2 in away from the primary fiber optic cable. This clearly shows that the differential RHEED amplifier in the differential mode can effectively remove a significant quantity of the background noise, resulting in a clearly defined RHEED oscillation.

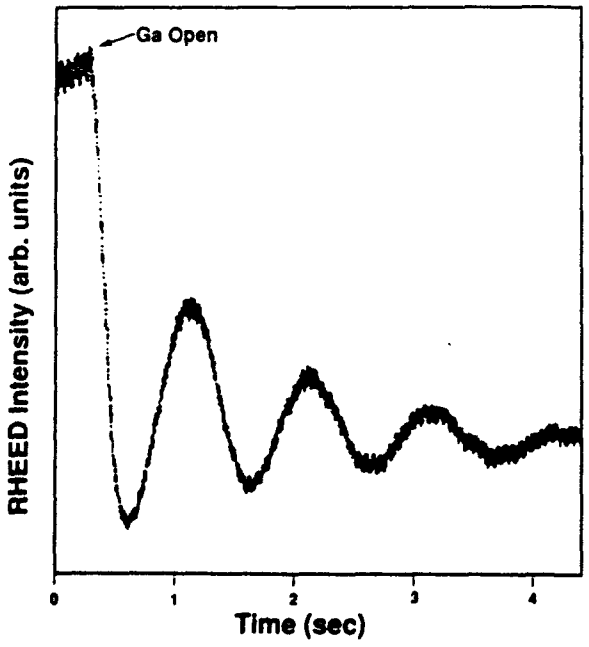

FIG. 5. RHEED oscillation of GaAs made with the differential RHEED amplifier in the differential mode.

The noise typically encountered in the RHEED information with and without the differential mode is shown in Fig. 6. In the single mode, a 60 Hz ac line-frequency signal primary from the electron gun filament dominates the background noise. Mechanical vibrations from the compressor of the Varian UHV8 cryopump caused the large 15 Hz, and those from the expander of the cryopump caused the 4 Hz (apparent in the figure as a rise in the overall noise with time) background noise. In the differential mode, the lower frequency single-source noise (4 Hz and 15 Hz) is almost completely canceled by the differential amplifier. Although the 60 Hz noise remains, it is greatly reduced in amplitude so it does not make a significant contribution to the RHEED oscillation. The residual 6 Hz noise may be caused by the noise phase difference from both the electron gun and the surrounding fluorescent lights.

IV. SUMMARY

A simple, relatively low-cost differential RHEED measurement system that effectively removes the background noise from the RHEED intensity oscillations in real time has been described. The differential option effectively removes the high-frequency noise from within the MBE machine.

ACKNOWLEDGMENTS

This work is partially supported by the Charles Lee Powell Foundation, the Air Force Wright Research and Development Center under Contract No. F33615-88-C-1862 and the Office of Naval Research under Grant No. N00014-89-J-1147. We wish to thank B.W. Liang for his valuable discussions.

[1] M. A. Herman and H. Sitter, *Molecular Beam Epitaxy* (Springer, Berlin, 1989), pp. 19–23.
[2] C. J. Sa and H.H. Wieder, Rev. Sci. Instrum. 61, 918 (1990).
[3] MetraByte Corp., 440 Myles Standish Blvd., Taunton MA 02780.
[4] Unkel Software Inc., 62 Bridge St., Lexington MA 02780.

MATERIALS RESEARCH SOCIETY SYMPOSIUM PROCEEDINGS VOLUME 216

Long-Wavelength Semiconductor Devices, Materials, and Processes

Symposium held November 26-29, 1990, Boston, Massachusetts, U.S.A.

EDITORS:

A. Katz
AT&T Bell Laboratories, Murray Hill, New Jersey, U.S.A.

R. M. Biefeld
Sandia National Laboratories, Albuquerque, New Mexico, U.S.A.

R. L. Gunshor
Purdue University, West Lafayette, Indiana, U.S.A.

R. J. Malik
AT&T Bell Laboratories, Murray Hill, New Jersey, U.S.A.

MRS MATERIALS RESEARCH SOCIETY
Pittsburgh, Pennsylvania

REFLECTION HIGH-ENERGY-ELECTRON DIFFRACTION STUDY OF InP AND InAs (100) IN GAS-SOURCE MOLECULAR BEAM EPITAXY

T. P. Chin, B. W. Liang, H. Q. Hou, and C. W. Tu
Department of Electrical and Computer Engineering 0407, University of California at San Diego
La Jolla, California 92093-0407, U. S. A.

ABSTRACT

InP and InAs (100) were grown by gas-source molecular-beam epitaxy (GSMBE) with arsine, phosphine, and elemental indium. Reflection high-energy-electron diffraction (RHEED) was used to monitor surface reconstructions and growth rates. (2x4) to (2x1) transition was observed on InP (100) as phosphine flow rate increased. (4x2) and (2x4) patterns were observed for In-stabilized and As-stabilized InAs surfaces, respectively. Both group-V and group-III-induced RHEED oscillations were observed. The group-V surface desorption activation energy were measured to be 0.61 eV for InP and 0.19 eV for InAs. By this growth rate study, we are able to establish a precise control of V/III atomic ratios in GSMBE of InP and InAs.

INTRODUCTION

Gas-source molecular-beam epitaxy (GSMBE) is a versatile tool of growing complicate heterostructures not only for its capability of tailoring the material to monolayer preciseness but also the handling of phosphorus, which is relatively more difficult in conventional MBE. Many of the mixed-group-V compounds are of great interests in optoelectronic device applications. For example, $In_xGa_{1-x}As_yP_{1-y}$ lattice-matched to InP has been used for photonic devices operating at 1.3 μm and 1.55 μm for long-wavelength optical communication.[1] Material for even longer wavelength can be achieved by increasing the InAs molar fraction in the alloy.

Reflection high-energy-electron diffraction has been shown to be a powerful in situ diagnostic technique for growth rate and composition control in MBE GaAs and related compounds, but relatively few RHEED studies have been reported for GSMBE of phosphides. Here we report a reflection RHEED study of InP and InAs in GSMBE. Different surface reconstructions were observed under various substrate temperatures and hydride flow rates. By measuring the group-V-limited growth rates under different growth temperatures and hydride flow rates, we were able to determine the V/III atomic ratio on the substrate surface in GSMBE. This is an absolute V/III ratio measurement compare to beam-flux ratio or flow-rate ratio usually used in conventional MBE or metalorganic chemical vapor deposition (MOCVD). Beam-flux ratio or flow-rate ratio measurement is rather system-dependent and easily affected by many unpredictable factors.[2,3] Substrate temperature, which plays a dominant role in the molecule incorporation process, is not considered in the beam-flux or flow-rate measurement, either. However, the ratio of group-V-limited growth rate and group-III-limited growth rate corresponds to the V/III atomic ratio on the growing surface. With the precise control of arsine and phosphine flow rates in GSMBE, we can achieve better control of growth conditions and perform more systematic investigation on the relation between the V/III ratio and layer quality. One purpose of this study is to optimize the growth condition for InP and other III-V compounds in GSMBE. In situ group-V composition control may also be obtained for mixed group-V material, e.g., $GaAs_xP_{1-x}$ or $InAs_xP_{1-x}$.

Mat. Res. Soc. Symp. Proc. Vol. 216, ©1991 Materials Research Society

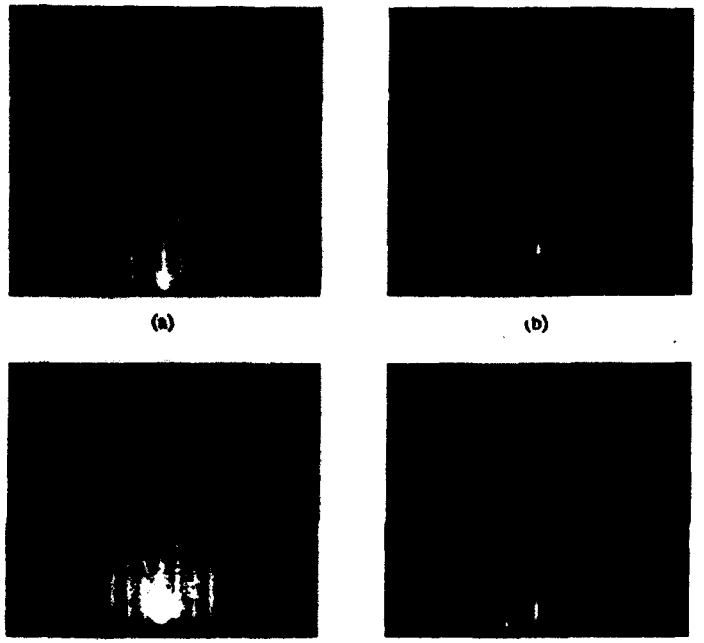

Fig. 1: RHEED patterns on InP(100) in GSMBE. (a) and (b): (2x4) is observed at In-rich surface. (c) and (d): (2x1) is observed at higher phosphine flow or lower substrate temperature.

EXPERIMENTS AND RESULTS

The GSMBE system consists of a modified Varian Modular GEN-II MBE reactor equipped with a 2200 l/s (H_2) cryopump and an ion pump (which is turned off during growth). Two separate gas cabinets house two gas-source supply systems (100% arsine and 100% phosphine) as well as scrubbers. Both gases are introduced into the growth chamber through the same Varian hydride injector. The normal cracking temperature is 1000°C. The phosphine and arsine flow rate in this study is typically 1-4 sccm. The background pressure ranges between 0.8×10^{-5} and 2×10^{-5} Torr during growth. The growth rates are monitored by the specular-beam intensity oscillation of RHEED. A dual-channel differential amplifier produces clean RHEED signals after subtracting the background noises. The oscillation is then recorded in an IBM PC AT compatible computer to measure the growth rate.[4]

InP (100) substrates were etched in a solution of H_2O_2:NH_4OH:H_2O (2:5:10), rinsed, and blown dry. Each sample was bonded onto a 3-inch Si wafer with In. The Si wafer was then mounted onto a Mo transfer ring with Ta wires. Growth temperatures were calibrated with a pyrometer and the melting point of InSb.

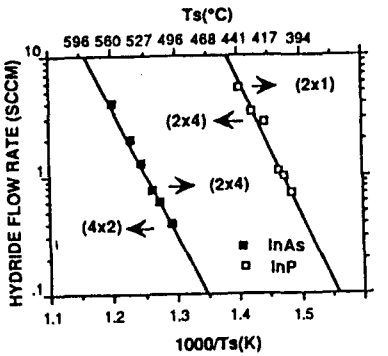

Fig. 2: Hydride flow vs. reciprocal growth temperature at which RHEED pattern occurred on InAs and InP (100).

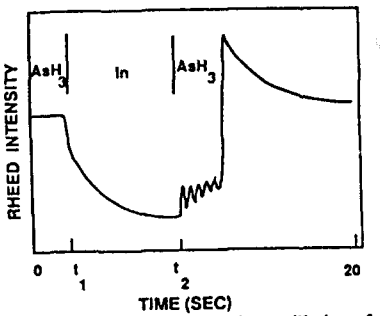

Fig. 3: As-induced RHEED oscillation of on InAs (100).

InAs was grown on InP at 460°C. InAs(100) shows (2x4) and (4x2) reconstructions for As and In stabilized surfaces, respectively. For InP(100), (2x4) was observed right after thermal cleaning. This (2x4) pattern will change to (2x1) under higher phosphine flow rate or lower substrate temperature. Fig. 1 shows RHEED patterns on InP(100). This observation is consistent with that reported by Morishita *et al.* in metalorganic MBE of InP with phosphine and trimethylindium,[5] however, is different from the conventional MBE results. (2x4) and (4x2) reconstructions were observed on InP(100) under As_4 or P_2 overpressure.[6] The corresponding pattern-transition substrate temperature and arsine flow rate are shown in Fig. 2. According to early studies in GSMBE by Panish *et al.*,[7,8] this pattern transition indicates the formation of indium droplets on the surface. Thus, one can compare the curves in Fig. 2 with the equilibrium P_2 and As_2 vapor pressure curves in a solid-liquidus system (InP+In and InAs+In) and then obtain the accommodation coefficients of P_2 and As_2 on InP and InAs, respectively. This comparison is not shown here because we need more calibration in our system to convert the hydride flow rate to molecular-beam flux.

Fig. 3 shows a typical arsenic-induced RHEED oscillation on InAs. First, the surface was As-stabilized, showing (2x4) reconstruction. Arsine was then turned off and the In shutter was opened at t_1. The RHEED pattern would switch to (4x2) and the specular-beam intensity decreased as the surface became rougher due to In accumulation. The In shutter was then closed and arsine was turned on at t_2. The RHEED oscillation resumed as the incoming arsenic molecules incorporated with the accumulated In on the surface. After the extra In was consumed, the RHEED pattern changed back to (2x4) and the specular-beam intensity increased abruptly. After this overshoot, the intensity recovered to the original level. Similar experiments were also done on InP (100). The growth rates measured here are limited by the amount of group-V flux and also dependent on substrate temperature. Fig. 4 is a plot of the group-V-limited growth rate as a function of hydride flow rate with substrate temperature as parameters. It is clear that the higher the T_s, the

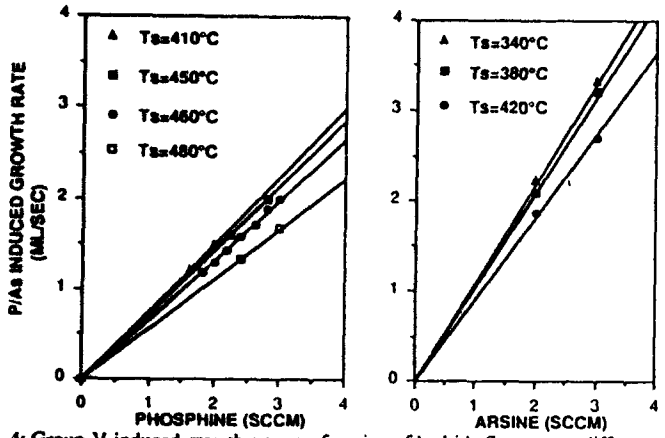

Fig. 4: Group-V-induced growth rate as a function of hydride flow rate at different growth temperature for InP (left) and InAs (right).

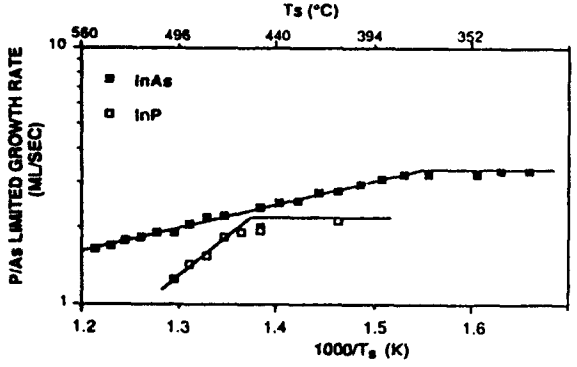

Fig. 5: Group-V-induced growth rate as a function of growth temperature. Arsine and phosphineflow rates are 3 and 2.8 sccm, respectively.

lower the growth rate due to the desorption of group-V molecules. Fig. 5 is the Arrhenius plot of the As- and P-limited growth rates of InAs and InP, respectively, as functions of substrate temperatures. RHEED oscillations were difficult to observe at higher or lower temperatures.

DISCUSSION

Fig. 4 demonstrates one of the advantages of using gas sources, namely, The arsine or phosphine flow can be controlled by a mass flow controller rapidly and accurately. Similar experiments were also performed on GaP, AlP, and GaAs.[9] One can find a curve in Fig. 4 for a corresponding T_s and then adjust the As- or P-limited growth rate by setting the mass flow controller appropriately. The ratio of As- or P-limited growth rate and In-limited growth rate represents the V/III ratio of the atoms incorporated onto the surface. This provides a precise measurement of V/III atomic ratio other than ion-gauge measurements, which is difficult to be used in GSMBE due to the high hydrogen background pressure (typically $1x10^{-5}$ Torr). Preliminary results shows that higher V/III ratio results in higher impurity concentration and lower mobility. Table 1 shows the Hall measurement results of three undoped 3-μm InP samples grown under different V/III ratios at 450°C. The carrier concentration at 77K increases and mobility decreases as the growth temperature increases. The mobility at room temperature is relatively low probably due to lattice scattering by structural defects. The best result so far is a 3-μm-thick InP layer with a 77K mobility of 62,600 cm^2/V-sec and a background carrier concentration of $5.1x10^{14}$ cm^{-3}, achieved under V/III=1 condition.

Group-V molecules will desorb from the surface as the substrate temperature increases. This results in the the group-V-limited growth rate decreasing at higher substrate temperature as shown in Fig. 5. The As-limited growth rate of InAs is constant for T_s<400°C and decreases linearly on an Arrhenius plot as T_s increases. The arsenic and phosphorus surface desorption activation energy (E_a) can be obtained from the slope of the curves. We find E_a=0.19 eV for InAs and E_a=0.61 eV for InP. Similar experiments in conventional MBE has been done by Chow and Fernandez,[10] they measured E_a to be 0.2 eV for GaAs. These thermodynamic data are currently being used in modeling the $InAs_xP_{1-x}$ growth.

		300K		77K	
sample #	V/III ratio	n	μ	n	μ
C083	1.1	2.3E15	3870	1.7E15	38500
C086	2	5.3E15	3700	3.6E15	31500
C088	3	5.6E15	3780	4.0E15	24000

Table 1: 3μm undoped InP grown under different V/III ratios. The growth temperature was 450°C.

SUMMARY

A RHEED study was performed on InP and InAs (100) grown by GSMBE. (2x4) and (2x1) patterns were observed on InP, while (4x2) and (2x4) patterns were observed on InAs for In-stabilized and for As-stabilized surfaces, respectively. By measuring both group-V and group-III limited growth rates, an accurate V/III ratio control was then established for different III-V compounds in GSMBE. The electrical property of InP was affected by the V/III ratio. As and P surface desorption activation energies on InAs/InP were also measured.

ACKNOWLEDGEMENT

This work is partially supported by the Office of Naval Research and Powell Foundation. The authors would also like to thank C. E. Chang and M. C. Ho for building the RHEED amplifier and valuable discussions.

REFERENCES

1. M.B. Panish and H. Temkin, Annu. Rev. Mater. Sci.19, 209 (1989).

2. R. Fernandez, J. Vac. Sci. Technol. B 6, 745 (1988).

3. R. Chow and R. Fernandez, Mat. Res. Soc. Symp. Proc. 145, 13 (1989).

4. C.E. Chang, T.P. Chin, and C.W. Tu, unpublished.

5. Y. Morishita, S. Maruno, M. Gotoda, Y. Nomura, and H. Ogata, Appl. Phys. Lett. 53 (1), 42, (1988).

6. E. H. C. Parker, *The Technology and Physics of Molecular Beam Epitaxy*, (Plenum, New York, 1985).

7. M.B. Panish and H. Temkin, Annu. Rev. Mater. Sci. 19, 209 (1989).

8. M.B. Panish and S. Sumski, J. Appl. Phys. 55 (3), 3571 (1984).

9. T.P. Chin, B.W. Liang, H.Q. Hou, M.C. Ho, C. E. Chang, and C.W. Tu, Appl. Phys. Lett, Jan. 21, 1991.

10. R. Chow and R. Fernandez, Mat. Res. Soc. Symp. Proc. 145, 13 (1989).

Determination of V/III ratios on phosphide surfaces during gas source molecular beam epitaxy

T. P. Chin, B. W. Liang, H. Q. Hou, M. C. Ho, C. E. Chang, and C. W. Tu
Department of Electrical and Computer Engineering 0407, University of California, San Diego, La Jolla, California 92093-0407

(Received 6 August 1990; accepted for publication 21 October 1990)

Phosphorus-controlled growth rate of homoepitaxial (100) InP, GaP, and AlP on GaP substrates by gas source molecular beam epitaxy was investigated. Elemental group-III sources and thermally cracked phosphine were used. The growth rate was monitored by the specular beam intensity oscillations of reflection high-energy electron diffraction. This technique gives exact values of V/III ratio on the surface by measuring the amount of phosphorus which is actually incorporated into the film. Here the V/III ratio is defined as P-controlled growth rate divided by group-III-controlled growth rate instead of the beam flux V/III ratio. Also the phosphorus surface desorption activation energies were measured to be 0.61 eV and in the range between 0.89 and 0.97 eV for InP and GaP, respectively.

Considerable potential exists for phosphorus-containing semiconductor materials in electronic and optoelectronic device applications. InP is a promising material for microwave sources and amplifiers operating at high power and high frequencies with lower noise. Long-wavelength (1.3 or 1.55 μm) optical-fiber communication systems also employ InP devices. GaP and AlP have been proposed for high-temperature electronic devices due to the large band gap and small lattice mismatch between each other.[1,2] Heterojunction bipolar transistors (HBTs) of GaP/$Al_xGa_{1-x}P$ working at temperatures as high as 550 °C have been reported.[3] GaP has been widely used to make yellow, red, and green light-emitting diodes.[4]

Many of the applications described above will require multilayer structure and abrupt changes in composition or doping. Gas source molecular beam epitaxy is a viable technique for growing phosphides because it may provide more precise control of phosphorus flux than conventional molecular beam epitaxy (MBE) and better layer thickness control than liquid phase epitaxy or vapor phase epitaxy.[5] Critical issues of high quality epilayer growth are the growth temperature and V/III ratio. In conventional MBE, the V/III ratio is obtained by measuring beam equivalent pressure. In gas source molecular beam epitaxy (GSMBE) the high hydrogen background pressure (typically 1×10^{-5} Torr) makes accurate V/III ratio measurement by ion gauge difficult. Another problem is that the V/III ratio at the substrate surface depends on the growth temperature, thus it will be different from the beam flux ratio. Panish and Sumski demonstrated a calculation of the group-V beam flux at the substrate surface by converting the equilibrium group-V partial pressure in a solid plus liquidus system for GaAs and InP in GSMBE.[6] Group-V-controlled growth rate measurement goes even further by measuring the amount of group V incorporated into the epilayer regardless of the chamber geometry, ionization factor of the ion gauge, and high hydrogen background pressure.[7,8] A similar experiment of arsenic-controlled growth rate measurement in conventional MBE has been used to measure the arsenic incorporation rate and sticking coefficients of both As_2 and As_4 on GaAs (100).[9] Here we report for the first time on phosphorus-controlled growth rate measurement of InP, GaP, and AlP in GSMBE.

The GSMBE system consists of a modified Varian Modular GEN-II MBE reactor equipped with a 2200 ℓ/s (H_2) cryopump and an ion pump (which is turned off during growth). Two separate gas cabinets house two gas source supply systems (100% arsine and 100% phosphine) as well as scrubbers. Both gases are introduced into the growth chamber through the same Varian hydride injector. The normal cracking temperature is 1000 °C. The phosphine flow rate in this study is typically 1–4 sccm. The background pressure ranges between 0.8×10^{-5} and 2×10^{-5} Torr during growth. The growth rates are monitored by the specular beam intensity oscillation of reflection high-energy electron diffraction (RHEED). A dual-channel differential amplifier[10] produces clean RHEED signals after subtracting the background noises. The oscillation is then recorded in an IBM PC AT compatible computer to measure the growth rate.

InP (100) substrates were degreased in a 1% Alconox solution and then rinsed with de-ionized (DI) water. They were etched afterwards in a solution of H_2O_2:NH_4OH:H_2O (2:5:10), rinsed, and blown dry. For GaP (100), there is an additional step of 50% HCl dip before the final rinse. Each sample was bonded onto a 3 in. Si wafer with In. The Si wafer was then mounted onto a Mo transfer ring with Ta wires. Growth temperatures were calibrated with a pyrometer and the melting point of InSb.

Figure 1(a) illustrates a typical RHEED oscillation and shutter operating sequence during the growth of GaP at 610 °C. It started with a phosphorus-stabilized surface. Then Ga-induced oscillation was observed after the Ga shutter was opened. The RHEED intensity decreased after the phosphine shutter was closed due to the Ga accumulation on the substrate which formed a rough surface. The final step involved closing the Ga shutter and opening the phosphine shutter again. Here the oscillation resumed with incoming phosphorus species and previous Ga accumulated on the surface. This represents phosphorus-controlled

 0003-6951/91/030254-03$02.00

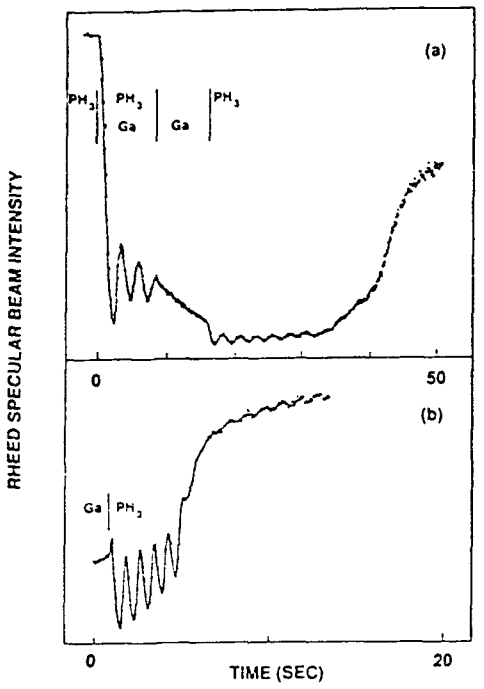

FIG. 1. (a) RHEED oscillations of Ga and phosphorus-controlled growth on GaP(100). The intensity decreases when the Ga is deposited. (b) Typical phosphorus-induced RHEED oscillation observed. The intensity recovers after Ga is consumed. The vertical scale and the sample azimuthal angle are different from those in (a) in order to observe better oscillations.

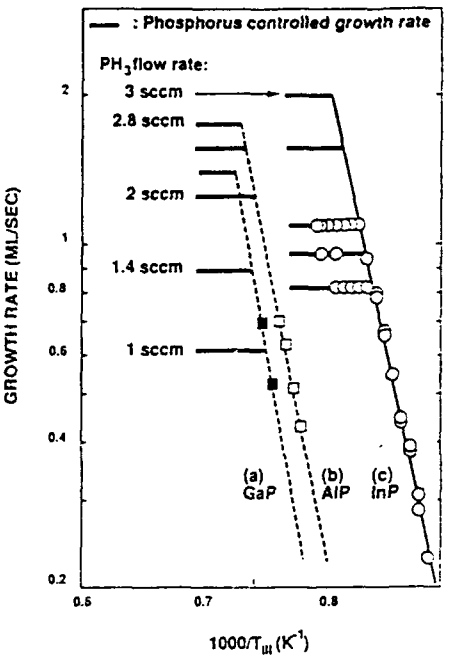

FIG. 2. Growth rate vs reciprocal group-III cell temperatures for (a) GaP, (b) AlP, and (c) InP.

growth because there was an excess amount of Ga atoms on the surface and the available amount of phosphorus limited the growth rate. While routinely taking data, we just deposited several layers of Ga on the surface without phosphine, then closed the Ga shutter and opened the phosphine shutter at the same time. The resultant oscillation is shown in Fig. 1(b). The same experiments were performed in growing InP at 470 °C and AlP at 615 °C. Figure 2 shows the growth rates of (a) GaP, (b) AlP, and (c) InP as a function of the reciprocal group-III cell temperatures. The phosphorus-controlled growth rates, as measured by the procedures just mentioned, are shown with thick lines. They are independent of group-III fluxes.

For the case of InP, a different approach was also used to obtain phosphorus-controlled growth. With the phosphine flow rate fixed, the In-controlled growth rate was measured under various In fluxes. As the open circles show in Fig. 2(c), the natural logarithm of the growth rate increases linearly with the reciprocal In cell temperature. This linear dependence stops at certain points; then the growth rate becomes constant as In flux increases more. These points at which the growth rate saturates indicates unity V/III ratios; that is, In-controlled growth rate equals P-controlled growth rate. Growth rate in the plateau region is controlled by the phosphine flow rate, independent of the In flux. Figures 3(a) and 3(b) show RHEED oscillations of InP using different In fluxes. Both oscillations were taken under indium-rich conditions. At time t_1 the In shutter was opened. Since the V/III ratio was less than unity in this region, the excess In atoms were accumulated on the surface so that the growth continued even when the In shutter was closed at t_2. The V/III ratio in Fig. 3(b) was even smaller than that in Fig. 3(a). This resulted in more oscillations after t_2 in Fig. 3(b) than that in Fig. 3(a). One important feature of these oscillations is that the growth rate between t_1 and t_2 is the same as the growth rate after t_2. This identifies phosphorus-limited growth and the

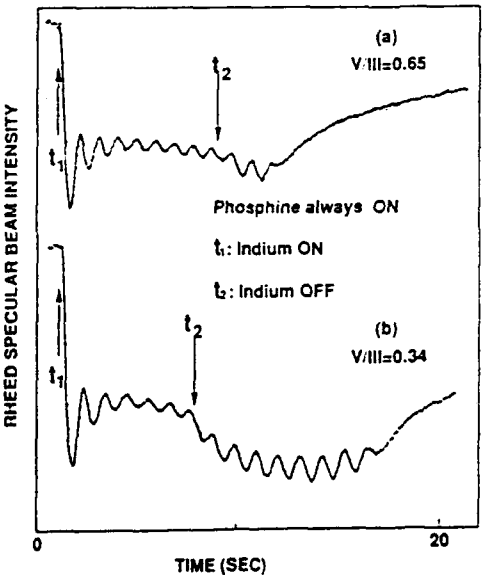

FIG. 3. RHEED oscillations on InP (100) for $V/III_b < V/III_a < 1$. Notice growth continues after the In shutter is closed at t_2 due to accumulated In on the surface.

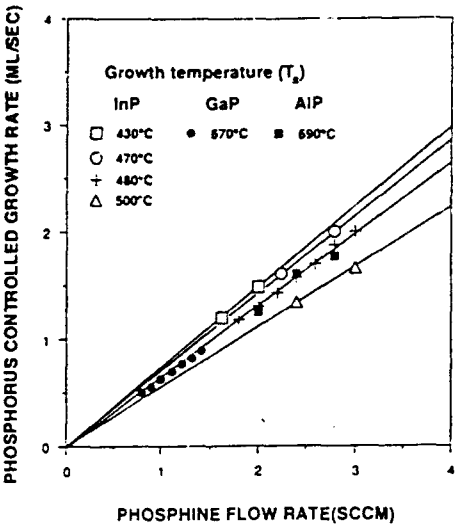

FIG. 4. Phosphorus-controlled growth rate vs phosphine flow rate.

growth rate in this region depends only on the phosphine flow rate. Figure 4 combines the data from InP, GaP, and AlP. It shows linear behavior of phosphorus-limited growth rate versus phosphine flow rate in GSMBE. This demonstrates the precise flux control capability of GSMBE. The slope strongly depends on growth temperature.

From the results in Figs. 2 and 4, we can obtain an accurate measure of the V/III ratio while growing all phosphides. For a given group-III flux and V/III ratio, we can set the corresponding phosphine flow rate accurately. An InP layer with 77 K mobility 62 600 cm^2/V s and background carrier concentration N_d-N_a of 5.1×10^{14} cm^{-3} was achieved under V/III$\simeq$1 condition. Electrical and optical properties of epilayers grown under different V/III ratios are currently under investigation. Preliminary study of growth of arsenides by arsine in GSMBE yields similar results. Accurate V/III ratio control is very important for composition control in growing compounds containing mixed group-V elements, e.g., $GaAs_xP_{1-x}$ and $In_yGa_{1-y}As_xP_{1-x}$. The value of x in these compounds is not easily determined by the flow rate or the beam flux measured by an ion gauge. Combining the results of both phosphine and arsine will provide a convenient and precise way to control the x value in mixed group-V compounds.[11]

The substrate temperature (T_s) dependence of phosphorus-controlled growth was also investigated on GaP and InP. The results are shown in Fig. 5. On InP, the growth rate starts to decrease for T_s>440 °C. The P_2 surface desorption activation energy is estimated to be 0.61

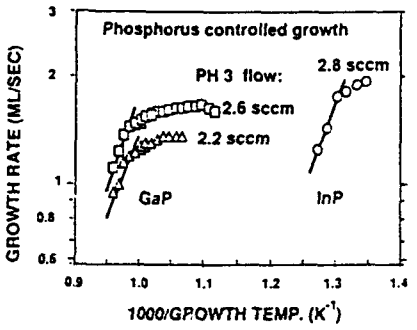

FIG. 5. Arrhenius plot of phosphorus-controlled growth rate vs substrate temperature.

eV. For GaP the phosphorus-controlled growth rate is fairly constant at substrate temperatures from 550 to 650 °C and then decreases for T_s> 650 °C due to phosphorus desorption. The activation energy is measured to be in the range of 0.89–0.97 eV on the Arrhenius plot. These values are much larger compard to the As_2 incorporation activation energy obtained by Chow and Fernandez,[9] which were measured to be 0.2 eV on GaAs with similar experiments in conventional MBE.

In conclusion, the phosphorus-controlled growth of InP, GaP, and AlP by GSMBE was determined experimentally. Growth rates were measured under different group-III fluxes, phosphine flow rates, and substrate temperatures. This technique, which measures the amount of phosphorus actually being incorporated in the epilayer growth, can achieve precise control of the V/III ratio. Phosphorus surface desorption activation energies are also measured for GaP and InP.

This work is partially supported by the Air Force Wright Research and Development Center, the Office of Naval Research and the Powell Foundation. We wish to thank Professor H. H. Wieder for critical reading of the manuscript.

[1] T. E. Zipperian and L. R. Dawson, Appl. Phys. Lett. 39, 895 (1981).
[2] D. L. Keune, M. G. Crawford, A. H. Herzog, and B. J. Fitzpatrick, J. Appl. Phys. 43, 3417 (1972).
[3] T. E. Zipperian and L. R. Dawson, J. Appl. Phys. 54, 6019 (1983).
[4] E. W. Williams and R. Hall, *Luminescence and the Light Emitting Diode* (Pergamon, Oxford, 1978).
[5] M. B. Panish and H. Temkin, Annu. Rev. Mater. Sci. 19, 209 (1989).
[6] M. B. Panish and S. Sumski, J. Appl. Phys. 55, 3571 (1984).
[7] B. F. Lewis and R. Fernandez, J. Vac. Sci. Technol. B 4, 560 (1986).
[8] R. Fernandez, J. Vac. Sci. Technol. B 6, 745 (1988).
[9] R. Chow and R. Fernandez, Mater. Res. Soc. Symp. Proc. 145, 13 (1989).
[10] C. E. Chang, T. P. Chin, and C. W. Tu, Rev. Sci. Instrum. (to be published).
[11] H. Q. Hou, B. W. Liang, T. P. Chin, and C. W. Tu (unpublished).

High-resolution x-ray diffraction of InAlAs/InP superlattices grown by gas source molecular beam epitaxy

J. C. P. Chang, T. P. Chin, K. L. Kavanagh, and C. W. Tu
Department of Electrical and Computer Engineering, 0407, University of California, San Diego, La Jolla, California 92093-0407

(Received 8 October 1990; accepted for publication 14 January 1991)

Structural properties of InAlAs/InP superlattices grown by gas source molecular beam epitaxy on (001)InP were investigated extensively with high-resolution x-ray diffraction. Very high quality material was obtained as indicated by narrow peak widths, numerous satellite peaks, and distinct Pendellosung fringes. Intermixing of group-V elements at each interface was quantified by dynamical simulations of (004), (002), and (115) reflections. The accuracy of the fits to both peak positions and peak intensities for all three reflections provides strong evidence for the proposed four-layer periodic structure.

In this letter we present high-resolution x-ray diffraction (HRXRD) data from InAlAs/InP superlattices grown by gas source molecular beam epitaxy (GSMBE) on (001)InP. Narrow peak widths and clear Pendellosung oscillations are observed, indicative of very high quality material both in lateral uniformity and periodicity. We also quantify from theoretical simulations of the data based on dynamical x-ray diffraction theory the intermixing which occurs at each interface. Such intermixing is to be expected from this system since the growth requires that the group-V elements, As and P, be switched at each heterointerface. Evidence for compositional intermixing and localized strain have been detected by HRXRD and other techniques at similar heterointerfaces including InGaAs/InP[1,2] superlattices, InGaP/GaAs[3] multiple quantum wells, and AlInP/GaAs[4] single quantum wells. In this work we quantify the composition and thickness of the interfacial layers occurring at InAlAs/InP superlattices. Simulations of (004), (002), and (115) x-ray rocking curves with excellent fits to the data are obtained if one-monolayer-thick strained intermixed layers are included in the superlattice structure.

The InAlAs/InP superlattice samples were grown by GSMBE using elemental group-III effusion cells and thermally cracked arsine and phosphine.[5] The shutter/valve sequence for growing superlattices and the nominal structure are shown in Fig. 1(a). The growth temperature of the structure was 520 °C. The 4 s hydride (arsine or phosphine) flow before growing each new layer was implemented to stabilize the gas flow while switching the hydrides.

X-ray rocking curves were recorded using a diffractometer with a four-reflection monochromator consisting of two channel-cut germanium crystals (220 reflections), as first proposed by DuMond[6] and later described by Bartels.[7] This arrangement provides a very clean, symmetric beam profile with a full width at the half maximum (FWHM) of 12 arcsec. Cu $K\alpha_1$ radiation ($\lambda = 1.54056$ Å) was used for all reflections.

Simulations were performed with a PC386 computer using dynamical diffraction theory based on the solution of the Takagi-Taupin equations.[8] In the simulation, we consider each sample to be subdivided into layers of constant lattice parameter (i.e., constant strain) and structure factor. The effect of the four-reflection monochromator in a $(+,-,-,+)$ orientation was included in the calculation following the procedures described by Tanner[9] and Slusky and Macrander.[10] The effects of vertical divergence of the beam were ignored. Only the reflecting power from the σ polarization was simulated since the monochromator effectively blocks the π-polarized radiation.[10] The FWHM of our simulated rocking curve of the four-reflection monochromator was 12 arcsec, exactly the same as calculated by Bartels.[7] This curve was then correlated with the reflectivity curve of the sample crystal to give the final rocking curve. Peak broadening due to sample curvature was simulated by convolving a rectangle of width 10 arcsec with the intensities derived from a flat sample.

Figure 2(a) shows the (004) scan of a 20-period 80 Å $In_xAl_{1-x}As$/80 Å InP superlattice with a nominal composition $x = 0.52$ grown on (001)InP. Sharp and well defined satellite peaks could be detected up to order $n = -5$. The FWHM's of the experimental and simulated (without curvature) zeroth-order satellite peak are 50 and 48 arcsec,

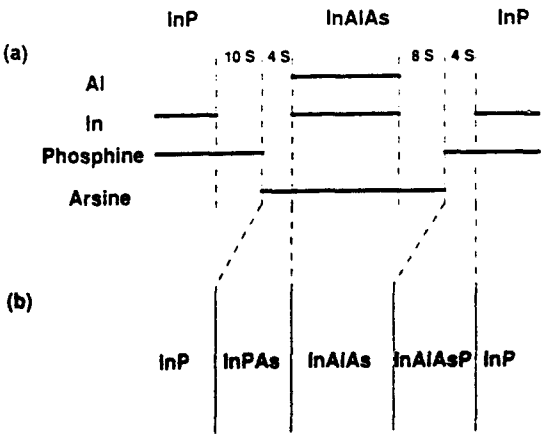

FIG. 1. (a) Shutter and valve sequences for the growth of InAlAs/InP superlattices. The solid lines indicate when beams are on. There is a 4 s interruption while arsine and phosphine flow are switched. (b) The four-layer model including strained interfacial layers formed by As-P exchange.

 0003-6951/91/141530-03$02.00

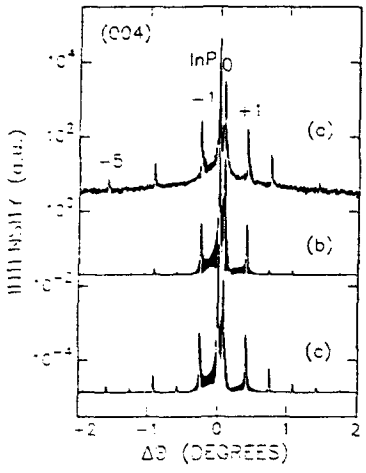

FIG. 2. (a) Experimental and simulated (004) x-ray rocking curves of a 20-period superlattice consisting of (b) 78 Å $In_{0.49}Al_{0.52}As$/78 Å InP (abrupt interface) or (c) 76 Å $In_{0.477}Al_{0.523}As$/3 Å $In_{0.477}Al_{0.523}As_{0.95}P_{0.05}$/73 Å InP/3 Å $InP_{0.40}As_{0.60}$ (four-layer model).

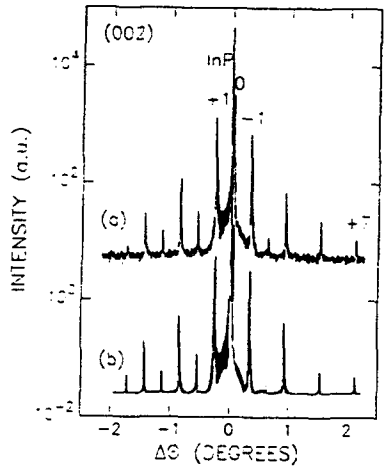

FIG. 3. (a) Experimental and (b) calculated rocking curves for the (002) reflection from a 20-period superlattice assuming a four-layer model as in Fig. 2(c).

respectively. Such comparable FWHMs indicate that the superlattice crystal quality is nearly perfect. Pendellosung oscillations, clearly seen in the wings of the substrate peak, zeroth-order peak, + 1 and − 1 peaks suggest high crystal quality and perfection in the epilayer surface and interface. The fact that the highest intensity peak within the envelope of superlattice reflections appears at a larger Bragg angle than the substrate implies the material is negatively strained, instead of perfectly lattice matched. The simulated rocking curve shown in Fig. 2(b) was obtained if we assume a perfect 20 period structure with abrupt interfaces, i.e., a bilayer model with layer thicknesses 78 Å for InP and $In_xAl_{1-x}As$ layers and $x = 0.49$. This model resulted in a poor fit to the relative peak intensities of the superlattice peaks to the substrate peak, although it fit the peak positions very well. Since no physically viable combination of layer thicknesses and In compositions could make the $|n| > 1$ satellite peaks increase in intensity by one order of magnitude, we therefore decided that the bilayer model must be modified by the addition of a strained layer at each interface. This four-layer model, shown in Fig. 1(b), considered the top several monolayers of each InP layer to have some mixture of As and formed $InP_{1-x}As_x$ at the InAlAs-on-InP interface, while the top several monolayers of $In_xAl_{1-x}As$ were replaced by a quaternary compound $In_xAl_{1-x}As_{1-y}P_y$ at the InP-on-InAlAs interface. Figure 2(c) shows a simulation with the best fit obtained with a four-layer model consisting of 73 Å of InP, 3 Å of $InP_{0.40}As_{0.60}$, 76 Å of $In_{0.477}Al_{0.523}As$, and 3 Å of $In_{0.477}Al_{0.523}As_{0.95}P_{0.05}$. This fit is excellent both in the shape of the superlattice envelope function and the intensities of the superlattice reflection relative to the substrate peak. Better fits to the experimental rocking curves could not be obtained either by choosing different lattice-parameter thickness profiles or by using 2 or 3 monolayers of interdiffused material. A three-layer model with only one intermixed layer at either the InAlAs-on-InP or InP-on-InAlAs interface also was not useful. Over 500 simulations of systematically chosen layer structures revealed that the intensity of the satellite peaks was very sensitive to the composition of the interfacial region and layer thickness. We found that the InPAs layer with positive strain affected the intensity of the $n < 0$ satellite peaks, while the InAlAsP layer with negative strain was crucial for the intensities of the $n > 0$ satellite peaks.

A uniqueness theorem for the fit to a rocking curve has not been mathematically proven.[11,12] It is possible that a quite different structure could also fit our data rather well. However, since a sufficient number of parameters (substrate materials, elements in the epilayers, numbers of layers, reflection plane, and wavelength) are known from growth procedures and the rocking curve is remarkably sensitive to structural variations, it is unlikely that an ambiguity would remain in the major features of the structure.[1,11,12] To support the validity of this four-layer model,[2,13] (002) rocking curves were also recorded and calculated using the best fit structure obtained from the (004) simulation. Although the (002) reflection is less suitable for calculation of strain, the satellite peaks are much stronger compared to those of the (004) reflections. Hence, the (002) reflection is more sensitive to superlattice properties. As shown in Fig. 3(a), sharp and well defined satellite peaks could be seen up to $n = +7$ in the (002) experimental data. Excellent agreement between the simulated curve, shown in Fig. 3(b), and the experimental (002) curve clearly shows the self-consistency of this model.

Symmetric reflections are sensitive to perpendicular strain only, while asymmetric reflections measure both perpendicular and parallel strains.[14] To investigate the coherency of the strained layers, the (115) reflection was measured and the result is shown in Fig. 4(a). Figure 4(b) was calculated using the best fit parameters from the (004) simulation with a parallel x-ray strain[15] (with respect to the substrate lattice constant) $\epsilon_{\parallel}$ equal to zero. The excel-

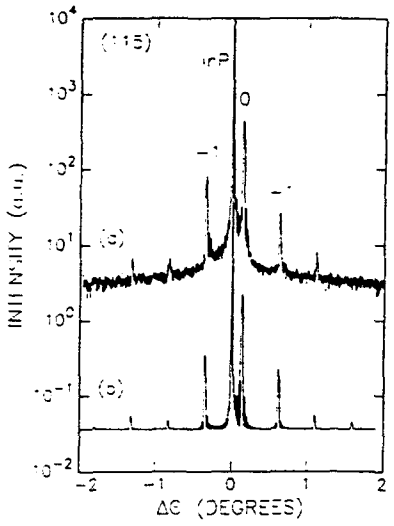

FIG. 4. (a) Experimental and (b) calculated rocking curves for the (115) reflection from a 20-period superlattice assuming a four-layer model as in Fig. 2(c).

lent fit again adds further support to the self-consistency of the four-layer model and confirms that plastic relaxation had not occurred.

The best structure determined by x-ray rocking curve simulations indicates that one monolayer of $InP_{0.4}As_{0.6}$ formed before InAlAs is grown and one monolayer of $InAlAs_{0.95}P_{0.05}$ formed on top of the InAlAs layer. We conclude that during growth 60% of the phosphorus on the top monolayer of InP was replaced by arsenic during the 4 s surface passivation by arsine. However, only 5% of arsenic in the top monolayer of InAlAs was exchanged by phosphorus within the same period of time. This is a reasonable result due to the low congruent evaporation temperature of InP(365 °C). At the growth temperature of 520 °C, the evaporation of phosphorus from InP and substitution of phosphorus vacancies by arsenic under arsenic overpressure is expected. Furthermore, due to the higher melting temperature of AlAs (2013 K), InAlAs is expected to be stable at the growth temperature.

We have also considered the possibility of exchange or interdiffusion between In and Al occurring in addition to intermixing of As and P. This could form an unstrained InAlAsP (instead of InPAs) interfacial layer which would have the advantage of being thermodynamically stable. However, this model was ruled out by further simulations. Extra stain or large variations in structure factors from the interfacial region is necessary to produce the observed modulation in the satellite peak intensities. If the interface layers are unstrained the structure factor difference becomes the only factor. However, the magnitude of the structure factors of any of these layers is dominated by the In component, and hence they vary very little. Furthermore, simulations have shown that interfacial layers with strains of opposite sign at the two interfaces are necessary to make the intensities of odd satellites stronger than those of even ones,[16] as is observed in our experimental curves. Thus, highly strained interfacial layers of opposite sign (in our case, InPAs layer with strain 3.7% and InAlAsP layer with strain −0.75%) must be formed to have the observed marked effect on the modulation of satellite peak intensities.

In summary, we have used HRXRD to characterize the interface intermixing of As and P in InAlAs/InP superlattices. Excellent fits to (004), (002), and (115) rocking curves were obtained by simulations based on dynamical theory with the inclusion at each interface of a one-monolayer-thick strained intermixed layer. These simulations indicate that only As-P exchange occurs, and the composition of the interfacial layers are $InP_{0.40}As_{0.60}$ and $In_{0.477}Al_{0.523}As_{0.95}P_{0.05}$ at the InP and InAlAs surfaces, respectively.

We gratefully acknowledge partial support from IBM, Northern Telecom, the Powell Foundation, and the Office of Naval Research. We wish to thank I. Bassignana, B. K. Bowen, S. N. G. Chu, H. Q. Hou, and B. W. Liang for many useful discussions.

[1] J. M. Vandenberg, M. B. Panish, R. A. Hamm, and H. Temkin, Appl. Phys. Lett. 56, 910 (1990).
[2] M. A. G. Halliwell and M. H. Lyons, paper presented at the Electrochemical Society Meeting, Montreal, Quebec, May 1990.
[3] H. Y. Lee, M. J. Hafich, and G. Y. Robinson, J. Cryst. Growth 105, 244 (1990).
[4] S. Nagao, M. Takashima, Y. Inoue, M. Katoh, and H. Gotoh, Paper presented at Sixth International Conference on Molecular Beam Epitaxy, La Jolla, California, August 27–31, 1990.
[5] T. P. Chin, B. W. Liang, H. Q. Hou, M. C. Ho, C. E. Chang, and C. W. Tu, Appl. Phys. Lett. 58, 254 (1990).
[6] J. W. M. DuMond, Phys. Rev. 52, 872 (1937).
[7] W. J. Bartels, J. Vac. Sci. Technol. B 1, 338 (1983).
[8] S. Bensoussan, C. Malgrange, and M. Sauvage-Simkin, J. Appl. Cryst. 20, 222 (1987).
[9] B. K. Tanner, Adv. X-ray Anal. 33, 1 (1990).
[10] S. E. G. Slusky and A. T. Macrander, J. Appl. Cryst. 20, 552 (1987).
[11] S. Cockerton, S. J. Miles, G. S. Green, and B. K. Tanner, J. Cryst. Growth 99, 1324 (1990).
[12] D. K. Bowen, S. T. Davies, and S. Swaminathan, Adv. X-ray Anal. 29, 345 (1986).
[13] M. H. Lyons and M. A. Halliwell, Inst. Pys. Conf. Ser. No. 76, 445 (1985).
[14] V. S. Speriosu, M.-A. Nicolet, S. T. Picraux, and R. M. Biefield, Appl. Phys. Lett. 45, 223 (1984).
[15] C. R. Wie, H. M. Kim, and K. M. Lau, SPIE 887, 41 (1988).
[16] E. G. Scott, M. H. Lyons, M. A. Z. Rejman-Greene, and G. J. Davies, J. Cryst. Growth 105, 249 (1990).

Submitted to J. Electrochem. Soc.
8/91

Selective Chemical Etching of InP Over InAlAs

Yan He, B. W. Liang, N. C. Tien, and C. W. Tu

University of California, San Diego
Department of Electrical and Computer Engineering
La Jolla, CA 92093-0407

ABSTRACT

We report the selective chemical etching of InP/InAlAs heterostructures. The selectivity of InP over InAlAs by 1:1:2 of $HCl:H_3PO_4:CH_3COOH$ is above 85. Better-defined mesa etching patterns, however, are obtained by a solution with lower CH_3COOH content such as 1:1:1 with a selectivity of 34. The etching recipe reported here is promising for *InP*-based heterostructure device applications.

Introduction

Selective etching is a key process for heterostructure device fabrication. There have been a number of selective etching recipes for GaAs/AlGaAs and other material systems. The selective etching of InAlAs (or InGaAs) over InP by 1:1:38 of H_2O_2:H_3PO_4:H_2O has been widely used. It shows an etch rate of ~1000Å/min for InAlAs (or InGaAs) but does not attack InP (1). Despite the successful selective etching of InAlAs over InP, no data have been reported on InP over InAlAs. Recently, there has been an increasing demand on selective etching of InP over InAlAs, especially in InP-channel FETs with an InAlAs buffer such as InAlAs/InP/InAlAs modulation-doped FETs (MODFETs) or doped-channel FETs (2,3). On the other hand, it is worthwhile to note that much work has been reported on InP over InGaAsP (4-6). HCl:H_3PO_4 (1:1), HCl:H_2O_2 (1:1), and HCl:CH_3COOH (1:1) have been proven to be the successful selective etchants for this material system.

In this paper, the etching behaviors of HCl:H_3PO_4:CH_3COOH on InP/InAlAs are investigated. With the emphases on selectivity, mesa etching profiles are also presented.

Experimental Procedures

The InP/InAlAs wafers were grown on (100) InP substrate by gas-source molecular beam epitaxy. An $In_{0.52}Al_{0.48}As$ layer was first grown, followed by an InP layer. Both InP and InAlAs layers are 0.5 μm thick and all undoped. The growth temperature was 480 °C.

The wafer was then covered with BPR100 positive photoresist as an etching mask. The rectangular mesa patterns were defined by lithography with one side along the [110] direction and the other side along the $[1\bar{1}0]$ direction. These directions are easily determined by the oval defect orientation, which is along $[1\bar{1}0]$ on a (100) wafer. The samples were kept in stagnant etching solutions during the etching process.

The photoresist was then removed off the etched wafers. The mesa depth was measured by a Sloan Dektak surface profile measuring system. The minimum detectable step in the system is less than 25Å. The selectivity was obtained by the etching rate ratio of InP over InAlAs. The mesa profiles were observed by scanning electron microscope (SEM).

Results

For heterostructure device applications, the appropriate etchant should exhibit high selectivity, well-defined mesa, and smooth surface on etched wafers. HCl:H_3PO_4:CH_3COOH solutions were found to possess these features on InP/InAlAs heterostructures. The volume ratio of this etchant is designated as 1:1:χ, and the CH_3COOH content χ was varied from 0 to 5. The etching rate to both InP and InAlAs and the selectivity were found to be a strong function of CH_3COOH volume content χ. The highest selectivity of 85 is obtained at χ=2.0

with an etching rate of 3860Å/min for InP and 45Å/min for InAlAs. The results are shown in Fig. 1.

Notice that the selectivity of GaAs over AlGaAs by chemical etching is in the range of ~30 (7), which is successful for removing the GaAs cap layer in AlGaAs/GaAs MODFETs. Our selectivity result of InP over InAlAs is higher, and it should satisfy the device processing requirements for InP-based devices.

The mesa etching profiles were observed by SEM in both [110] and [1$\bar{1}$0] directions. In general, the mesa edges along [1$\bar{1}$0] and [110] directions are all outward-sloped with an angle of approximately 12° and 22°, respectively. The solution without CH_3COOH (χ=0) showed the most well-defined mesa etching patterns with sharp, clean and straight edge. As CH_3COOH content χ increases, mesa edge becomes less sharp and has some burrs on the edge along the [110] direction. Although a lower CH_3COOH content χ produces a better mesa etching pattern, the undercut to InP and the etching to InAlAs are greater than those in higher χ solution. If one consider both the selectivity and mesa etching profile data, the solution with χ=1.0 is preferable for selectively removing InP from InAlAs in device fabrication.

Fig. 2 shows the mesa etching pattern of InP stopped on the InAlAs layer. The smooth InAlAs surface indicates the successful selective etching of InP by the 1:1:1 $HCl:H_3PO_4:CH_3COOH$ solution. The solution with this volume ratio shows a selectivity of 34 with etch rate of 10530Å/min for InP and 310Å/min for InAlAs.

Conclusions

In summary, the selective chemical etching of InP over InAlAs has been investigated. The highest selectivity of 85 was obtained with 1:1:2 of $HCl:H_3PO_4:CH_3COOH$ solution. Better-defined mesa etching patterns, however, were obtained with a solution of lower CH_3COOH content. For device mesa etching application, a 1:1:1 solution with a selectivity of 34 is preferable in order to realize both selectivity and better-defined mesa profile requirements. This recipe is expected to have its applications in InP-based heterostructure devices.

Acknowledgement

We wish to thank partial support from TRW under the California MICRO program and the Office of Naval Research.

REFERENCES

1. H. Ohno and J. Barnard, in "GaInAsP Alloy Semiconductors," T. P. Pearsall, Editor, p.447, John Willey and Sons, Chichester(1982).

2. O. Aina, M. Serio, M. Mattingly, E. Hempfling, Electronics Letters, **26**, 651(1990).

3. M. A. Fathimulla, T. Loughran, L.Stecker, E. Hempfling, M. Mattingly, and O. Aina, IEEE Electron Device Lett., **EDL-9**, 223(1988).

4. F. Fiedler, A. Schlachetzki, G. Klein, J. Mater. Sci., **17**, 2911(1982).

5. S. B. Phatak and G. Kelner, This Journal, **126**, 287(1979).

6. S. Adachi, Y. Noguchi, and H. Kawaguchi, This Journal, **129**, 1053(1982).

7. J. J. Lepore, J. Appl. Phys., **51**, 6441(1980).

FIGURE CAPTIONS

Figure 1. Etch rate to both InP and InAlAs as well as selectivity of InP over InAlAs by 1:1:χ of $HCl:H_3PO_4:CH_3COOH$ solution. The best selectivity of >85 is obtained at volume ratio of 1:1:2. The lines were drawn to guide the eyes.

Figure 2. SEM of InP selective mesa etch stopped on InAlAs by 1:1:1 of $HCl:H_3PO_4:CH_3COOH$. Selectivity is 34 with etch rate of 10530Å/min for InP and 310Å/min for InAlAs. The smooth InAlAs surface indicates the successful selective etching by this solution.

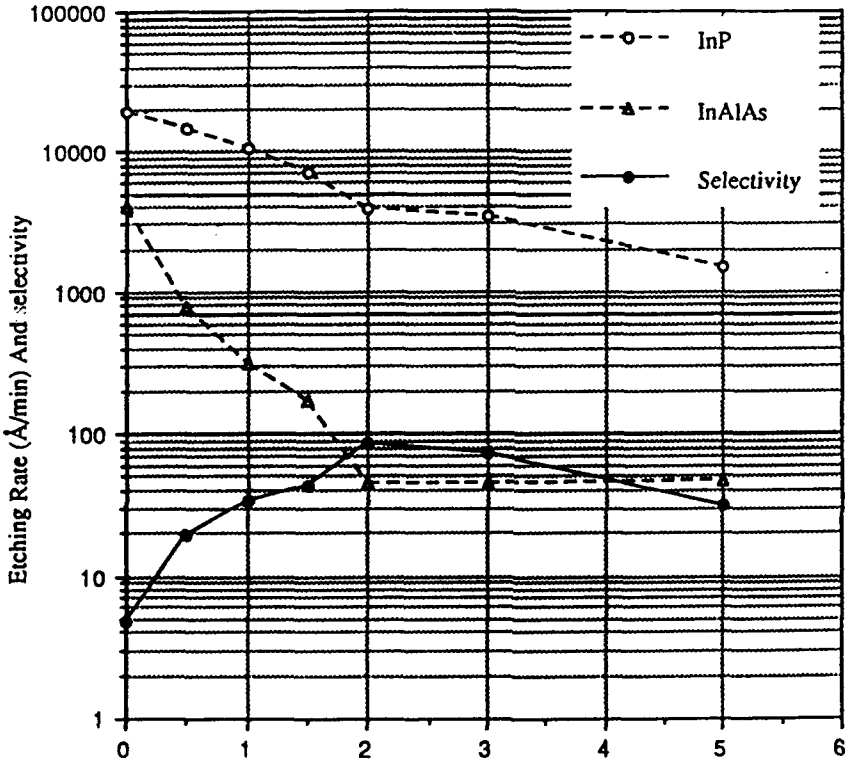
100000
10000
1000
100
10
1
0
1
2
3
4
5
6
InP
InAlAs
Selectivity
Etching Rate (Å/min) And selectivity
CH3COOH Content (X) In 1:1:X of HCl:H3PO4:CH3COOH

Fig. 1.

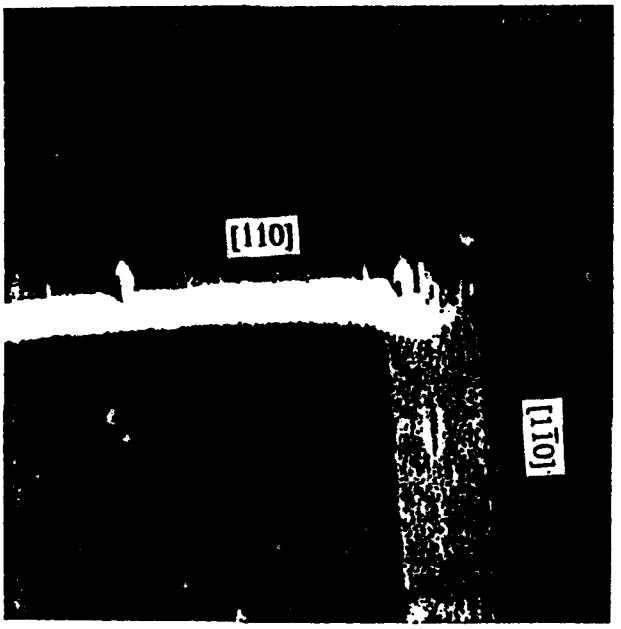

Fig. 2.

STUDY OF As AND P INCORPORATION BEHAVIOR IN GaAsP BY GAS-SOURCE MOLECULAR-BEAM EPITAXY

B. W. LIANG, H. Q. HOU, and C. W. TU
Department of Electrical and Computer Engineering, University of California at San Diego, La Jolla, CA 92093-0407

ABSTRACT

A simple kinetic model has been developed to explain the agreement between *in situ* and *ex situ* determination of phosphorus composition in $GaAs_{1-x}P_x$ ($x < 0.4$) epilayers grown on GaAs (001) by gas-source molecular-beam epitaxy (GSMBE). The *in situ* determination is by monitoring the intensity oscillations of reflection high-energy-electron diffraction during group-V-limited growth, and the *ex situ* determination is by x-ray rocking curve measurement of $GaAs_{1-x}P_x$/GaAs strained-layer superlattices grown under group-III-limited growth condition.

INTRODUCTION

Mixed group-V ternary and quaternary III-V compounds, such as GaAsP, InAsP, and InGaAsP, are important for optoelectronic applications. Hydride-, chloride-, and metalorganic vapor-phase epitaxy (MOVPE) [1-4], molecular-beam epitaxy (MBE) [5] and gas-source molecular-beam epitaxy (GSMBE) [6], including hydride-source MBE (HSMBE), metalorganic MBE (MOMBE) or chemical-beam epitaxy (CBE), have been used to grow these materials. One of the critical issues of epitaxial growth is controlling the composition of group-V elements in the compounds [7,8]. Most researchers in this area use post-growth characterization techniques, such as X-ray diffraction and photoluminescence spectroscopy, to correlate the composition with flow rates or fluxes during growth. Recently we have demonstrated an *in situ* determination of group-V composition in GSMBE (or HSMBE) of $GaAs_{1-x}P_x$ ($x < 0.4$), using group-V hydrides, arsine and phosphine, and elemental group-III sources [8]. The group-V composition of epilayers grown under normal MBE growth condition, where the growth rate is controlled by the group-III flux, can be obtained easily from the intensity oscillations of reflection high-energy-electron diffraction (RHEED) under the group-V-limited growth condition at the same flow rates and growth temperature. Obviously, there is a competition between As and P during growth of GaAsP [7] and understanding this competition is the key point to determination of group-V composition. Even though several models have been proposed in recent years for composition determination of mixed-group-V ternary or quaternary compounds grown by MOVPE and (GS)MBE, they can not explain the agreement between the *in situ* composition determination of mixed-group-V compounds by RHEED intensity and *ex situ* composition determination by X-ray rocking curves [2,3,5]. In this paper we take into account this competition process and propose a simple kinetic model for GSMBE of $GaAs_{1-x}P_x$ to understand the relationship between the group-III-limited and the group-V-limited growth modes.

A KINETIC MODEL

In GSMBE, the growth rate and composition may be controlled by four different kinetic processes, mass transfer (i.e., beam fluxes), adsorption, desorption, and surface reaction. For binary compounds like GaAs, under normal growth conditions (T_s in the 450 - 650°C range and R_g in the order of 1 monolayer/s), the growth rate is expected to be limited by mass transfer, which means that surface reaction rates are much faster than that of mass transfer. In this case the growth rate does not depend on the substrate temperature. On the other hand, in very low temperature or very high beam flux range, the growth rate may be controlled by surface reaction. The growth rate then will be sensitive to temperature variation. For mixed group-III ternary compounds such as AlGaAs, the situation is almost the same as that of GaAs. The growth rate and composition are controlled simply by Al and Ga beam fluxes. For mixed group-V ternary compounds, however, the situation is quite different. Even though the growth rate is still

Mat. Res. Soc. Symp. Proc. Vol. 222. ©1991 Materials Research Society

controlled by the group-III element beam flux, the composition is controlled by chemical reactions between group-III atoms and group-V species and thermal desorptions of group-V species on the growth front surface.

On a Ga-rich surface, the growth rate (R_g) of GaAsP is limited by the incorporation rates of As_2 and P_2 [8]. We can write

$$R_{g(GaAsP)} = R_{g(GaAs)} + R_{g(GaP)} \qquad (1)$$

Because Ga atoms are abundant on the surface, it is reasonable to assume that As_2 or P_2 can easily react with two Ga atoms at one time. In other words, we assume that the following elementary chemical reactions occur on the surface during growth of GaAs and GaP,

$$V_2\,(g) \xrightarrow{(FS)_V} V_2\,(ad)$$

$$V_2\,(ad) + 2\,Ga\,(ad) \xrightarrow{K_V} 2\,GaV$$

$$V_2\,(ad) \xrightarrow{D_V} V_2\,(g)$$

where V stands for As or P; F, the beam flux; S, the sticking probability; K_V, reaction rate coefficient; and D_V, desorption rate coefficient. Then, the growth rates can be written in terms of reaction rate coefficients and surface activities a_i (i = Ga or As or P),

$$R_{g(GaAs)} = K_{As}\, a_{Ga}^2\, a_{As} \qquad (2)$$

$$R_{g(GaP)} = K_P\, a_{Ga}^2\, a_P \qquad (3)$$

$$R_{dV} = D_V\, a_V \qquad (4)$$

where R_{dV} is desorption rate of group-V dimers. The total flux at growth front is then the sum of the growth rate and desorption rate.

$$(FS)_V = R_{gV} + R_{dV} \qquad (5)$$

The phosphorus composition (x) in the epilayer can be written as

$$x = \frac{R_{g(GaAsP)} - R'_{g(GaAs)}}{R_{g(GaAsP)}}$$

where (') stands for the situation where only As_2 molecules are deposited. In principle, the As incorporation rate into GaAsP will change upon injection of P_2 due to displacement of As by P. Foxon *et al.* reported a slight decrease of As_4 sticking coefficient when P_4 was injected during MBE of GaAsP [7]. The situation is similar if dimers are used. In our case, however, excess Ga atoms are deposited on the surface before the group-V-limited RHEED oscillation measurements. Therefore, we can expect the displacement of As by P is negligible. In addition, As has much higher sticking coefficient than P, especially when both are present [7]. In short, for group-III-rich surface, the As incorporation rate is independent of whether P is present or not, at least for low x range. Therefore, $R_{g(GaAs)}$ and $R'_{g(GaAs)}$ conceal out with each other, i.e.,

$$x = \frac{\frac{(FS)_P}{A_P}}{\frac{(FS)_P}{A_P} + \frac{(FS)_{As}}{A_{As}}} \qquad (6)$$

where

$$A_V \equiv 1 + \frac{D_V}{K_V} = \left(1 + \frac{1}{\alpha}\right) \text{ for As and } \left(1 + \frac{1}{\beta}\right) \text{ for P}$$

Because of high vapor pressure and short surface lifetime of the group-V elements, if we assume that at the growth temperature considered, the desorption probability of group-V species is much greater than incorporation probability , i.e., $D_V/K_V >> 1$, then

$$x \approx \frac{1}{1 + \frac{F_{As}}{F_P}\frac{S_{As}}{S_P}\frac{\alpha}{\beta}} \qquad (7)$$

Since As_2 and P_2 beam fluxes are proportional to the AsH_3 and PH_3 flow rates, respectively [9], we can write

$$x \approx \frac{1}{1 + C\frac{f_{AsH_3}}{f_{PH_3}}} = \frac{1}{1 + C\frac{(1 - X_f)}{X_f}} \qquad (8)$$

where f's are hydride flow rates; X_f, the phosphine flow-rate fraction; and

$$C \equiv \frac{\alpha}{\beta}\frac{S_{As}}{S_P}\sqrt{\frac{M_{P_2}}{M_{As_2}}}$$

Now we consider normal GSMBE growth condition (group-V rich), where not so many Ga atoms are available as in the Ga-rich condition. The following elementary surface reactions involving dimers are assumed,

$V_2\,(g) \rightarrow V_2\,(ad)$

$V_2\,(ad) + Ga\,(ad) \rightarrow GaV + V\,(ad)$

$V\,(ad) + Ga\,(ad) \rightarrow GaV$

$V\,(ad) + V\,(ad) \rightarrow V_2\,(ad)$

$V_2\,(ad) \rightarrow V_2\,(g)$

The growth rate equation of GaAsP in this case is similar to equation (1), but it is limited by the Ga-beam flux.

$$R_{g(GaAsP)} = R_{g(GaAs)} + R_{g(GaP)}$$

$$= K_{As}\, a_{Ga}\, a_{As} + K_P\, a_{Ga}\, a_P = \lambda F_{Ga} \qquad (9)$$

where λ is a constant relating the Ga flux and the growth rate, $R_{g(GaAsP)} = \lambda F_{Ga}$. Therefore,

$$x = \frac{R_{g(GaP)}}{R_{g(GaAsP)}} = \frac{K_P\, a_{Ga}\, a_P}{\lambda F_{Ga}}$$

Using equation (4), we have

$$x = \frac{(FS)_P}{(FS)_P + (FS)_{As}\frac{\alpha}{\beta} + R_{g(GaAsP)}} \qquad (10)$$

$$x = \frac{1}{1 + \frac{F_{As}}{X_F F_{(As+P)}}\left(\frac{S_{As}}{S_p}\right)\left(\frac{\alpha}{\beta}\right) + \frac{\lambda F_{Ga}}{X_F S_P F_{(As+P)}}} \qquad (11)$$

where X_F is group-V beam flux fraction of P_2. Since V/III > 1 in term of beam flux and $D_V/K_V \gg 1$, in low x range, $F_{As}S_{As} \gg \lambda F_{Ga}$. Also since As incorporation is more efficient than P incorporation at the growth temperature considered, i.e., $\alpha/\beta \geq 1$, we can have

$$x = \frac{1}{1 + \frac{F_{As}}{F_P}\frac{S_{As}}{S_P}\frac{\alpha}{\beta}}$$

$$= \frac{1}{1 + C\frac{f_{AsH_3}}{f_{PH_3}}} = \frac{1}{1 + C\frac{(1 - X_f)}{X_f}} \qquad (12)$$

which is identical to equation (8).

COMPARISON WITH EXPERIMENTAL RESULTS AND DISCUSSION

Equations (8) and (12) reveal the relationship between phosphorus composition (x) in the epilayer and flow-rate fraction of PH_3 (X_f) as well as other parameters included in the parameter C. The interesting and important point is that under the physically reasonable assumptions we made above, they are applicable for two different growth modes, group-III-limited and group-V-limited, in the low x range. If we know these parameters, such as S, K and D, we can obtain the parameter C and calculate the growth rates under different conditions. Since K and D obey an Arrhenius relation, the phosphorus composition depends on the growth temperature. Unfortunately, experimental data of these parameters are not available. However, since in equation (12) x and X_f are determined experimentally at a given growth temperature, we can calculate C for different temperatures. For T_s = 500°C, the average of C equals 2.48. Then, we obtain the phosphorus composition as a function of phosphine flow rate for the same growth temperature, as shown in Fig.1.

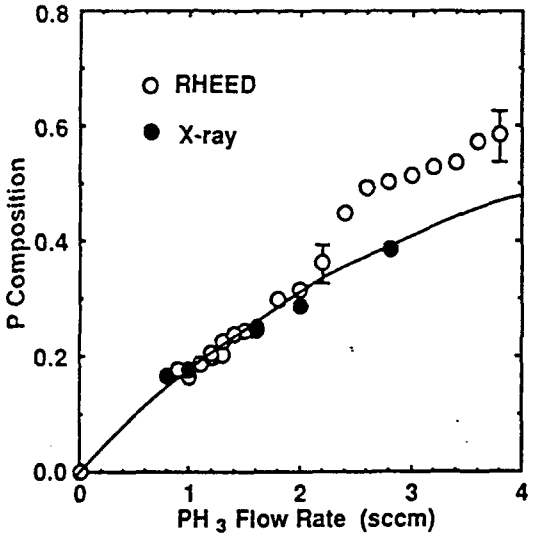

Fig.1 P composition in GaAsP on GaAs (001) as a function of PH_3 flow rate at AsH_3 flow rate of 1.6 sccm and growth temperature of 500°C. Closed circles are from X-ray diffraction study of GaAsP /GaAs SLS's. Open circles indicate RHEED oscillations results, and the line is calculation result based on equation (8), once C is determined from one data point.

Figure 1 also compares the P composition determined *in situ* by RHEED, shown by open circles. Obviously, the *in situ* and *ex situ* determinations agree well with each other in low x range ($x < 0.4$). For other growth temperatures, C= 2.73 for 420°C, 1.3 for 580°C and 0.96 for 700°C. According to equation (12) phosphorus composition in GaAsP epilayers is independent of V/III ratio in the temperature range considered now. This has been verified by our experimental results [8].

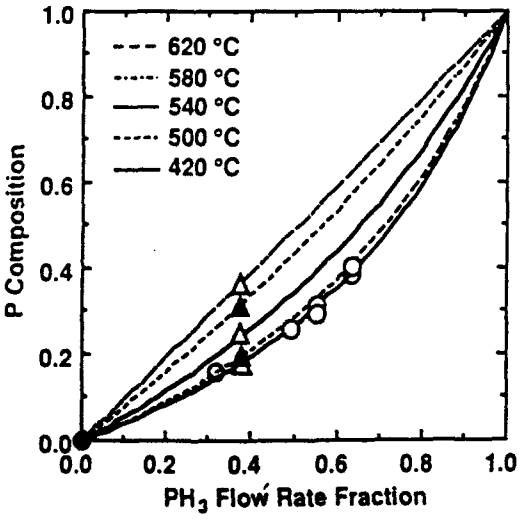

Fig. 2 P composition in GaAsP on GaAs (001) as a function of PH_3 flow rate fraction at different growth temperatures. The closed circles are from X-ray diffraction of GaAsP /GaAs SLS's grown at 500°C. Other symbols indicate SLS's grown at different substrate temperatures.The lines are calculations from the kinetic model.The triangles were used to get C.

In high x range, however, the results from the *in situ* determination does not agree with that from the *ex situ* ones. The reasons are believed to be (1) it is difficult to obtain reasonably good RHEED oscillation because of high strain; (2) the SLS structure may be partially relaxed because of strain; and (3) the assumptions in equation (6) that As and P incorporation being independent on a Ga-rich surface may not hold any more because of the existence of unnegligible amount of phosphorus on the growth front.

Figure 2 shows the P composition as a function of flow-rate fraction in gas phase at different growth temperatures. The lines come from our model. It is interesting to notice the similarity between results from GSMBE and those from MOVPE. It is well known that in MOVPE the growth rate are limited by diffusion of group-III species through the boundary layer above the susceptor under normal growth conditions. However, the group-V composition is controlled by competing reaction rates between group-V species and group-III's and desorptions of group-V species on the substrate surface. This is because that the group-V overpressure is very high and diffusion rates are much higher than surface reaction rates. In this aspect MOVPE is similar to the situation of GSMBE. Because GSMBE is carried out in high vaccum, the corresponding temperatures are lower than those in MOVPE. Also, it is interesting to notice that $C \approx 1$, when growth temperature is about 620°C. In this case the phosphorus composition is almost equal to the flow-rate fraction of PH_3. The composition control then is easier than at low temperatures.

CONCLUSIONS

A simple kinetic model has been proposed to explain the arsenic and phosphorus incorporation behavior in $GaAs_{1-x}P_x$ grown on GaAs (001) by GSMBE. For $GaAs_{1-x}P_x$ ($x < 0.4$) epilayers, one can use the *in situ* determination by RHEED to obtain the phosphorus composition. At a growth temperature of about 620°C, a simple relation exists between phosphorus composition in epilayers and flow-rate fraction.

ACKNOWLEDGEMENTS

We wish to thank T. P. Chin and M. C. Ho for assistance in GSMBE growth. This work is partially supported by the Office of Naval Research.

REFERENCES

[1] A. D. Huelsman, J. Electron. Mater. **18**, 91 (1989).

[2] L. Samuelson, P. Omling and G. Grimmeiss, J. Cryst. Growth **61**, 425 (1983).

[3] H. Seki and A. Koukitu, J. Cryst. Growth **74**, 172 (1986).

[4] G. B. Stringfellow, J. Cryst. Growth **70**, 133 (1984).

[5] T. Nomura, H.Ogasawara, M. Miyao and M. Hagino, J. Cryst. Growth (1991).

[6] M. B. Panish and S. Sumski, J. Appl. Phys. **55**, 3571 (1984).

[7] C. T. Foxon, B. A. Joyce and M. T. Norris, J. Cryst. Growth **49**, 132 (1980).

[8] H. Q. Hou, B. W. Liang, T. P. Chin and C. W. Tu, Appl. Phys. Lett. (1991).

[9] T. P. Chin, B. W. Liang, H. Q. Hou, M. C. Ho, C. E. Chang, and C. W. Tu, Appl. Phys. Lett. **58**, 254 (1991).

[10] K. Woodbridge, J. P. Gowers and B. A. Joyce, J. Cryst. Growth **60**, 21 (1982).

MRS-S91

Mat. Res. Soc. Symp. Proc. (1991) Spring Mtg.

MODULATOR STRUCTURE USING In(As,P)/InP STRAINED MULTIPLE QUANTUM WELLS GROWN BY GAS-SOURCE MBE

H. Q. HOU, T. P. CHIN, B. W. LIANG, and C. W. TU
Department of Electrical and Computer Engineering, University of California at San Diego, La Jolla, CA 92093-0407

ABSTRACT

In(As,P)/InP strained multiple quantum wells (SMQW's) were grown with gas-source molecular-beam epitaxy (GSMBE). A successful control of the As composition was achieved over a wide range by using two techniques. High-quality samples were characterized structurally and optically by x-ray diffractometry, transmission electron microscopy (TEM), photoluminescence (PL) and absorption measurements. Excitonic emission energy and the critical layer thickness of In(As,P)/InP SMQW's are calculated as a function of the As composition. The results show that 1.06, 1.3 and 1.55 μm excitonic emission can be achieved at room temperature using this material system. We also discuss the perspective of using In(As,P)/InP SMQW's for modulator application.

INTRODUCTION

$In_{1-y}Ga_yAs_xP_{1-x}$ grown on InP is promising for long-wavelength optoelectronic devices because its fundamental band gap is suitable for infrared emitters and detectors operated between 0.9 to 2.0 μm.[1] Extensive studies of the growth and characterization as well as device applications have been presented based on this material system.[2-4] In contrast, $InAs_xP_{1-x}$/InP, a special case of the quaternary $In_{1-y}Ga_yAs_xP_{1-x}$/InP, has received little attention from various advanced crystal growth techniques, such as organometallic vapor phase epitaxy (OMVPE)[5,6] or molecular beam epitaxy (MBE).[7] The growth of $InAs_xP_{1-x}$ reduces difficulties in the composition control of quaternary $In_{1-y}Ga_yAs_xP_{1-x}$, and provides a new degree of freedom for device design by tailoring the band structure with built-in biaxial strain. More importantly, an independent control of the layer thickness and alloy composition can be achieved in GSMBE growth since the thickness is determined by the indium beam flux and the composition by the AsH_3 and PH_3 flow-rate fraction. This greatly simplifies the growth control to tune excitonic emission to a desired wavelength for optoelectronic devices. However, since arsenic incorporates with indium much more significantly than phosphorus,[8] the difficulty in obtaining a desired arsenic composition in $InAs_xP_{1-x}$ arises from the need for accurate control of the hydride flow-rate fraction, especially in the low x region. Moreover, the critical layer thickness[9,10] limits pseudomorphic growth of the $InAs_xP_{1-x}$ layer when the composition x is large. In this paper we report a successful growth of device-quality $InAs_xP_{1-x}$/InP SMQW's by GSMBE. High-quality $InAs_xP_{1-x}$ layers are obtained in SMQW structures for optical modulators operated at 1.06, 1.3 and 1.55 μm. Samples with various arsenic composition and layer thickness are characterized structurally and optically. The viability of modulator application by using $InAs_xP_{1-x}$/InP SMQW's will be discussed based on the emission wavelength and critical layer thickness calculations of the SMQW structure.

GROWTH DETAILS

The $InAs_xP_{1-x}$/InP SMQW structures were grown on (100) Fe-doped semi-insulating and S-doped n^+ InP substrates in a modified Varian Modular GEN-II MBE machine. The

growth was performed with elemental indium and thermally cracked hydrides, AsH_3 and PH_3, at a substrate temperature of 460 °C. The gas-source supplies (100% arsine and 100% phosphine) were introduced into the growth chamber through a single Varian four-channel hydride injector, which was operated nominally at 1000 °C. The growth chamber was equipped with a 2200 l/s cryopump. The typical working pressure was $1X10^{-5}$ Torr. The indium flux was set such that the growth rate was about 1 μm/hr. The growth rate, therefore, the thickness of $InAs_xP_{1-x}$, is constrained only by the indium beam flux at a group-V overpressure, so the layer thickness of $InAs_xP_{1-x}$ can be controlled independently of the composition, which is related to only the AsH_3 and PH_3 flow-rate fraction. Instead of using the usual run-vent technique, the growth was interrupted at each interface. The interruption allows switching the gas flow and stabilization on beam fluxes.

Previous growth studies show that arsenic incorporates into $InAs_xP_{1-x}$ much more significantly than phosphorus when both are present.[8,11] We, therefore, used a relatively large PH_3 flow rate, compared to AsH_3, to *dilute* the arsenic fraction in the flux on the growth front so as to achieve a proper control of x. The AsH_3 flow rate was typically fixed at 0.6 sccm, and PH_3 flow rate was varied from 3 to 5 sccm; correspondingly, the x in $InAs_xP_{1-x}$ was varied from 0.65 to 0.20. Another method is alternatingly introducing AsH_3 flow during InP growth so that the As composition in the $InAs_xP_{1-x}$ quantum well layer was averaged to a smaller value by these short-period (2 to 5 monolayers per period) In(As,P)/InP superlattices. By using this technique, we could control x easily with the ratio of the open and close durations of AsH_3. Employing these two techniques, we grew a series of SMQW samples with x ranging from 0.20 to 0.65 and $InAs_xP_{1-x}$ layer thickness 75 to 100 Å. The modulator structure consists of 30-period $InAs_xP_{1-x}$(93 Å)/InP(138 Å) SMQW's grown on an n^+ InP substrate and capped with a 5000 Å p-InP layer. High resolution x-ray rocking curves taken from SMQW samples indicate a very good periodicity of the quantum well layers, and allow determination of structural parameters by simulation using dynamical diffraction theory.[8] Structural parameters for the samples used in the present study are listed in Table I.

Table I. Description of the sample structures.

Sample No.	x	$L_{In(As,P)}$ (Å)	L_{InP} (Å)	Period No.	Structure
6	0.60	78	144	15	SMQW's
11	0.50	76	162	16	SMQW's
35	0.40	92	138	30	Modulator
32	0.20	92	138	30	Modulator

PL MEASUREMENTS AND ENERGY LEVEL CALCULATION

PL spectra were measured at ~10 K with a closed-cycle cryostat. The luminescence was excited by an Ar^+ laser, and dispersed by a 50 cm monochromator. The signal was detected by a cooled Ge photodetector, and measured by a lock-in amplifier. The spectral resolution was 2 Å. Fig. 1 shows a typical PL spectrum measured from sample #35, a modulator structure. Very sharp and intense emission is attributed to free heavy-hole excitons confined in $InAs_xP_{1-x}$ quantum wells. The full widths at half maximum are 4, 5.5 and 7 meV for samples #32,35, and 6, respectively. This result is among the best ever reported for $InAs_xP_{1-x}$/InP SMQW's,[12] and even for lattice-matched $In_{1-y}Ga_yAs_xP_{1-x}$/InP quantum wells.[3]

To tune the emission wavelength of a modulator structure to desired values, we calculated confined energy levels in In(As,P)/InP quantum wells using an envelope-function

model. [13] The strain was assumed to exist only in In(As,P) layers since their thickness is much smaller than that of InP. Following the standard elastic theory, we also took into account the effect that the biaxial strain in In(As,P) layer enlarges the band gap and splits the light-hole band apart from the heavy-hole band. The unstrained band gap of $InAs_xP_{1-x}$ was taken as [14] $E_g(x)=1.351-1.315x+0.32x^2$ (eV) at 300K, and $1.417-1.36x+0.36x^2$ (eV) at 10 K, respectively. The valence band offset fraction, $\Delta E_v/\Delta E_g$, was taken as 0.3, and the exciton binding energy was assumed to be 8 meV for all of these quantum wells. Since the optimum thickness of the quantum well layer in a modulator structure is usually considered to be 100 Å, our calculation is, therefore, performed for 100 Å quantum wells with various arsenic compositions. Shown in Fig. 2 is the wavelength of the first subband heavy-hole exciton transition at room temperature as a function of In(As,P) quantum-well thickness. As read from Fig. 2, the As composition should be tuned to about 0.20, 0.40, and 0.60 to obtain 1.06, 1.3 and 1.55 μm excitonic emissions. The arrows shown in Fig. 1 indicate the calculated photon energy of the heavy-hole excitonic emissions. An excellent agreement is found between experimental and theoretical results.

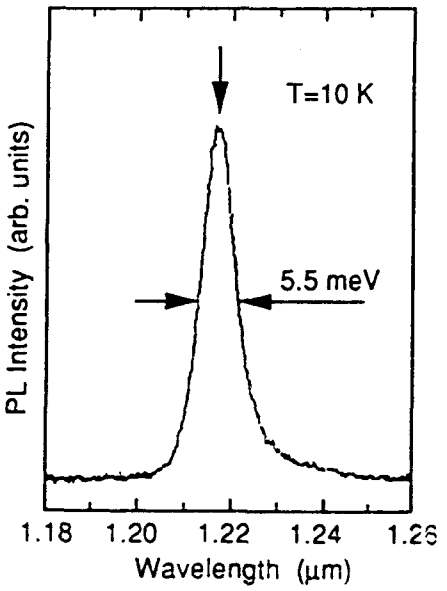

Fig. 1. A typical PL spectrum measured at 10 K for an $InAs_xP_{1-x}$/InP modulator structure, samples #35. The arrow indicates the photon energy of heavy-hole excitonic emission from the calculation.

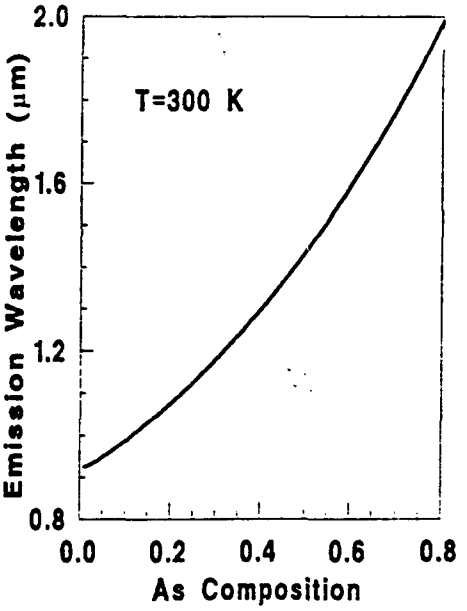

Fig. 2. Calculated photon energies of room-temperature heavy-hole excitonic emission based on the envelope-function model, as a function of arsenic compositions for $InAs_xP_{1-x}$/InP quantum wells.

CRITICAL LAYER THICKNESS

In principle, we can obtain a desired excitonic emission, even at 1.55 μm, by using $InAs_xP_{1-x}$/InP SMQW's as shown in Fig. 2. However, it is important to limit the thickness of the In(As,P) layer so as to accommodate the large strain coherently. Matthews and Blakeslee, and People and Bean proposed a mechanical equilibrium model,[9] and an energy equilibrium model,[10] respectively, to calculate the critical layer thickness (CLT), within which a pseudomorphic layer can be grown. The lower and upper curves in Fig. 3 are calculation

results from these two models, respectively, for the In(As,P)/InP system. A sample composed of five 95 Å quantum wells with different compositions grown on the same substrate was used to examined the CLT. The emission energy from a strained quantum well should agree with the transition energy calculation as described above, while a relaxed quantum well gives a smaller emission energy and a broader peak.[15] By theoretically fitting the photon energy of the low-temperature PL emissions from different-depth quantum wells, the strained and relaxed quantum wells can be identified. Open and full squares in Fig. 3 represent strained and relaxed In(As,P) layers identified from the PL spectra, respectively. It appears that pseudomorphic layers were achieved even when the layer thickness exceeded the mechanical equilibrium limit. Most favorably, the CLT determined from PL measurements agrees with the energy equilibrium limit. Therefore, we took People and Bean's limit as a reference for epitaxial growth, and we should be able to obtain a pseudomorphic 100 Å $InAs_xP_{1-x}$ single quantum well with arsenic composition as high as 0.78 [12] as shown in Fig. 3.

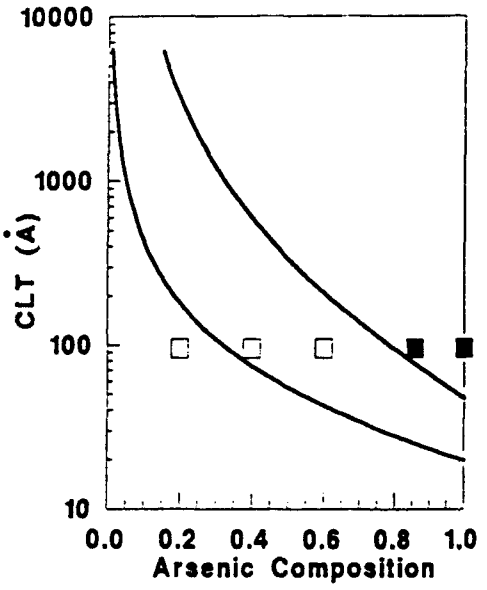

Fig. 3. The critical layer thickness of $InAs_xP_{1-x}$ pseudomorphically grown on InP as a function of the As composition calculated from mechanical (lower curve) and energy (upper curve) equilibrium models. The open and full squares represent strained and relaxed quantum by wells examined by PL measurements.

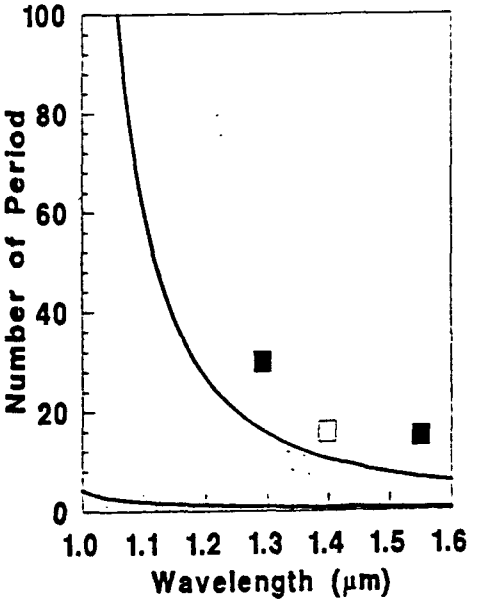

Fig. 4. Number of periods for pseudomorphic growth of In(As,P)/InP SMQW's as a function of the room-temperature emission wavelength, calculated based on mechanical (lower curve) and energy (upper curve) equilibrium models, respectively. The open and full squares represent In(As,P) quantum-well layers, examined TEM images, without and with dislocations.

Another aspect of the critical layer thickness should be considered is the upper limit of the number of periods of multiple quantum wells. The strained multiple quantum wells, as a whole, have an average free lattice constant, which is given by

$$a_{SMQW} = \frac{a_1 d_1 + a_2 d_2}{d_1 + d_2},$$

where the subscripts 1 and 2 refer to In(As,P) and InP layers, respectively; a is the lattice constant; and d is the layer thickness. This SMQW is also lattice-mismatched to InP substrate.

Thus the total thickness of the quantum well, or the number of periods, must be constrained within a limit. For a typical modulator structure consisting of 100 Å In(As,P) and 100 Å InP, the number of period was calculated as a function of room-temperature emission wavelength. The results were plotted in Fig. 4. TEM images were also taken for some SMQW samples (#6, 11, and 35).[8] The image from sample #11 shows very sharp, flat and dislocation-free In(As,P)/InP interfaces. In the picture for sample #6 some dislocation nets were observed at the interface of the SMQW and the InP buffer layer. For sample #35 some dislocations and stacking faults appear in the quantum well layers. The number of periods and emission wavelength of these three samples are plotted in Fig. 4. Open and full squares represent SMQW's without and with dislocations respectively. A relative good agreement with the energy equilibrium model can be seen.

DISCUSSION OF THE PERSPECTIVE OF In(As,P)/InP MODULATORS

As we can see in Fig. 4, for 1.06 μm modulator consisting of 100 Å In(As,P) and 100 Å InP, the pseudomorphic SMQW's can be grown with periods as many as 100. Hence, In(As,P)/InP seems the best material system for this spectral region because of the ease of growth (independent layer thickness and composition control) and much smaller strain (0.6%) than In(Ga,As)/GaAs (1.7%) quantum wells while using the same layer thickness.[16] However, to achieve 1.3 and 1.55 μm emission wavelength at room temperature, pseudomorphic SMQW's can have only 15 and 8 periods, respectively. Therefore, a better way may be using lattice-matched (In,Ga)(As,P)/InP quantum wells. Fig. 5 shows room-temperature absorption spectra measured for samples #32, 35 and 6. It can be seen that well resolved absorption peaks appear at about 1.06, 1.3 and 1.55 μm. Absorption between higher excited states can be also seen, which suggests that reasonably good quality samples were obtained even with the period number exceeding the critical value. However, the linewidth broadens with increasing As composition owing to partial strain relaxation. We have succeeded in fabricating 1.06 and 1.3 μm optical modulators from samples #32 and #35, and device performance will be reported elsewhere.

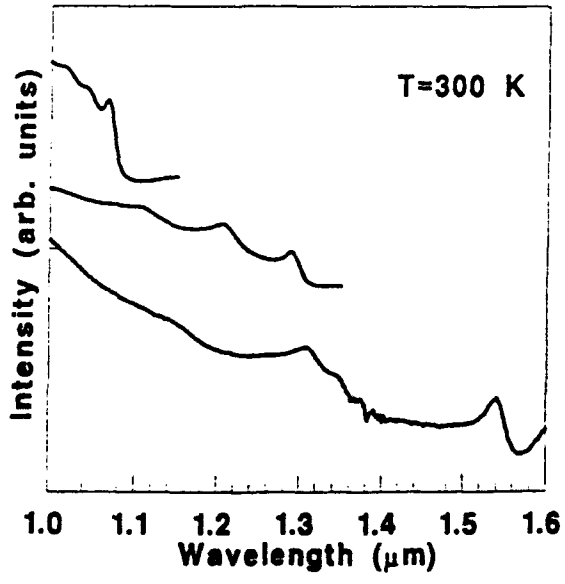

Fig. 5. Absorption spectra taken from In(As,P)/InP SMQW sample #32, 35 and 6 at room temperature. First-subband heavy-hole excitonic absorptions were obtained at 1.06, 1.3 and 1.55 μm, respectively.

CONCLUSION

$InAs_xP_{1-x}$/InP multiple quantum well structures have been grown by gas-source molecular-beam epitaxy with successful control of the arsenic composition ranging from 0.20 to 0.65. Highly strained samples are characterized by photoluminescence, absorption, x-ray rocking curve and transmission electron microscopy. Device-quality 1.06 and 1.3 μm modulator structures were obtained. Calculations of room-temperature emission energy from the quantum well and of the critical layer thickness allow a discussion of the viability of modulator application using $InAs_xP_{1-x}$/InP multiple quantum wells.

ACKNOWLEDGEMENT

The authors are delighted to acknowledge Dr. S. N. G. Chu at AT&T Bell Labs for TEM measurements. This work is partially supported by the Office of Naval Research and the DARPA Optoelectronic Technology Center.

REFERENCES

1. H. C. Casey, Jr. and M. B. Panish, Heterostructure Lasers, (Academic Press, New York, 1978).
2. M. B. Panish and S. Sumski, J. Appl. Phys. 55, 3571 (1984).
3. B. Soucail, P. Voisin, M. Voos, D. Rondi, J. Nagle, and B. de Cremoux, Superlattices and Microstructures 8, 279 (1989).
4. H. K. Tsang, J. B. D. Soole, H. P. LeBlanc, R. Bhat, M. A. Koza, and I. H. White, Appl. Phys. Lett. 57, 2285 (1990).
5. K. H. Huang and B. W. Wessels, J. Cryst. Growth 92, 547 (1988).
6. R. P. Schneider, Jr., D. X. Li, and B. W. Wessels, J. Electrochem. Soc. 136, 3490 (1989).
7. T. K. Woodward, T. Sizer, and T. H. Chiu, Appl. Phys. Lett. 58, 1366 (1991).
8. H. Q. Hou, C. W. Tu, and S. N. G. Chu, Appl. Phys. Lett. 58, (1991), (to be published).
9. J. W. Matthews and A. E. Blakeslee, J. Cryst. Growth 27, 118 (1974).
10. R. People and J. C. Bean, Appl. Phys. Lett. 47, 322 (1985); 49, 229(E) (1986).
11. T. Fukui and N. Kobayashi, J. Cryst. Growth 71, 9 (1985).
12. R. P. Schneider, Jr. and B. W. Wessels, Superlattices and Microstructures 6, 287 (1989); and Mat. Res. Soc. Symp. Proc. 145, 145 (1989).
13. G. Bastard and J. A. Brum, IEEE J. Quantum Eletron. QE-22, 1625 (1986).
14. Landolt-Bornstein New Series, Group III, vol. 22a, edited by O. Madelung, (Springer-Verlag, Berlin, 1988).
15. T. G. Andersson, Z. G. Chen, V. D. Kulakovskii, A. Uddin, and J. T. Vallin, Appl. Phys. Lett. 51, 752 (1987).
16. T. K. Woodward, T. Sizer, D. L. Sivco, and A. Y. Cho, Appl. Phys. Lett. 57, 548 (1990).

Gas-source molecular beam epitaxy growth of highly strained device quality InAsP/InP multiple quantum well structures

H. Q. Hou and C. W. Tu
Department of Electrical and Computer Engineering, University of California at San Diego, La Jolla, California 92093-0407

S. N. G. Chu
AT&T Bell Laboratories, Murray Hill, New Jersey 07974

(Received 1 March 1991; accepted for publication 28 March 1991)

$InAs_xP_{1-x}$/InP strained multiple quantum wells with strain as high as 2.5% were grown by gas-source molecular beam epitaxy. Successful control of the arsenic composition over a wide range was achieved by two different growth techniques. Structural and optical studies, such as high-resolution x-ray rocking curve, cross-sectional transmission electron microscopy, photoluminescence, and absorption measurement, indicate that we have obtained high quality multiple quantum wells that are suitable for optoelectronic applications.

$In_{1-x}Ga_xAs_yP_{1-y}$ grown on InP is a promising material for optoelectronic applications because its fundamental band gap is suitable for infrared emitters and detectors operated between 0.9 and 2.0 μm.[1] Extensive studies of the growth and characterization as well as device applications have been presented based on this material system.[2–4] In contrast, $InAs_xP_{1-x}$/InP, a special case of quaternary $In_{1-x}Ga_xAs_yP_{1-y}$/InP, has received little attention from various advanced crystal growth techniques, such as organometallic vapor phase epitaxy (OMVPE)[5,6] or molecular beam epitaxy (MBE). The growth of $InAs_xP_{1-x}$ reduces difficulties in the composition control of quaternary $In_{1-x}Ga_xAs_yP_{1-y}$ and provides a new degree of freedom for device design by tailoring the band structure with built-in biaxial strain. Moreover, an independent control of the layer thickness and alloy composition can be achieved since the former is determined only by the indium beam flux, while the latter can be controlled properly by adjusting the AsH_3 and PH_3 flow-rate fraction in gas-source MBE (GSMBE) growth. However, the difficulty in obtaining pseudomorphic growth of $InAs_xP_{1-x}$ arises from the accurate control of the hydride flow-rate fraction since As incorporates with In much more significantly than P does.[7] In this letter we report a successful growth of device quality $InAs_xP_{1-x}$/InP strained multiple quantum wells (SMQWs) by GSMBE. High quality materials were characterized by high-resolution x-ray rocking curves, transmission electron microscopic (TEM) images. Photoluminescence (PL) and absorption spectra show the application possibility of optoelectronic devices, such as modulator or laser, based on such a material system.

The $InAs_xP_{1-x}$/InP SMQW structures were grown on (100) Fe-doped semi-insulating InP substrates in a modified Varian Modular Gen-II MBE machine. The growth was performed with elemental indium and thermally cracked hydrides, AsH_3 and PH_3, at a substrate temperature of 460 °C. The gas-source supplies (100% arsine and 100% phosphine) were introduced into the growth chamber through a single Varian four-channel hydride injector, which was operated nominally at 1000 °C. The growth chamber was equipped with a 2200 ℓ/s cryopump and a 220 ℓ/s ion pump. The typical working pressure was 1×10^{-5} Torr. The indium flux was set such that the growth rate was about 1 μm/h as determined by intensity oscillations of reflection high-energy electron diffraction (RHEED).

Our previous growth studies of $GaAs_{1-x}P_x$ grown on GaAs[8] show that arsenic incorporates into $GaAs_{1-x}P_x$ much more significantly than phosphorus when both are present. This is especially true for $InAs_xP_{1-x}$ growth with AsH_3 and PH_3 because the effective adsorption rate of As to P is higher in InAsP than in GaAsP.[9] Therefore, it is necessary to use a relatively large PH_3 flow rate, compared to AsH_3, to *dilute* the arsenic fraction in the flux on the growth front so as to achieve a proper control of the arsenic composition. We fixed the AsH_3 flow rate at 0.6 sccm, varied PH_3 flow rates from 3 to 5 sccm, and grew a series of SMQW samples with a typical structure of 15-period $InAs_xP_{1-x}$(80 Å)/InP(150 Å). Correspondingly, the arsenic composition in $InAs_xP_{1-x}$ was varied from 0.65 to 0.20.

Instead of using the usual run-vent technique, the growth was interrupted at each interface. Shown in Fig. 1 is a diagram of the shutter operation sequence. The interruption duration t_1 was 20 s typically to allow switching the AsH_3 and to stabilize the beam flux of arsenic. t_2, t_3, t_4, varying from 3 to 10 s, are interruption durations for recovering the growth front and purging the residual gas. However, achieving an $InAs_xP_{1-x}$ layer with a very small As composition by this growth method is limited by the stability of the mass flow controller at very low flow rate. Therefore, an alternative method was employed. As shown at the lower part of Fig. 1, AsH_3 was alternatingly introduced during InP growth so that the As composition in the $InAs_xP_{1-x}$ quantum well layer was averaged to a smaller value by these short-period (2–5 monolayers per period) InAsP/InP superlattices. The x can be controlled with the ratio of open and close durations of AsH_3 easily by using this technique.

The growth rate, therefore, the thickness of $InAs_xP_{1-x}$ is constrained only by the indium beam flux at a group-V overpressure, so the layer thickness of

 0003-6951/91/252954-03$02.00

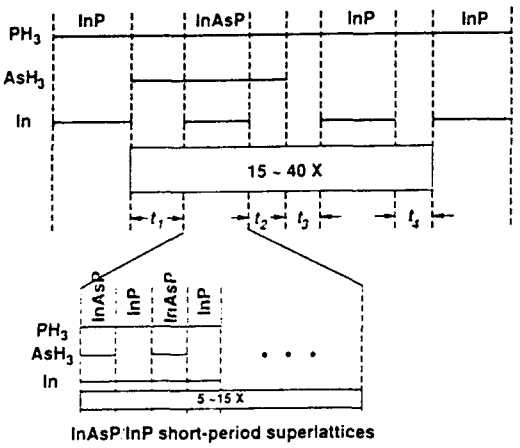

FIG. 1. Diagram of the growth sequence of multiple quantum well structures. The lower part indicates the growth of $InAs_xP_{1-x}$ layer by short-period superlattices.

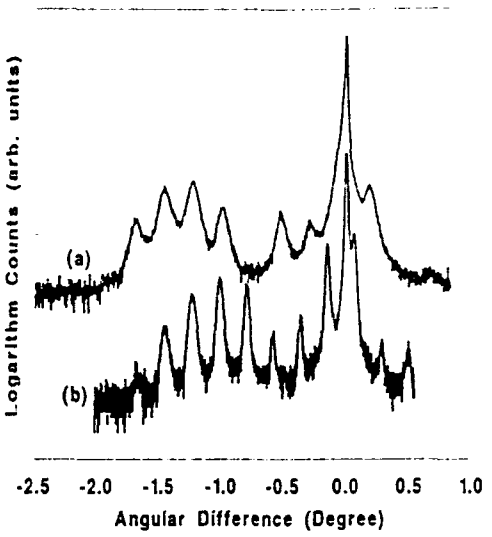

FIG. 2. High-resolution x-ray rocking curves with (004) diffraction taken from (a) sample 1 and (b) sample 2, SMQW structures grown by different methods.

$InAs_xP_{1-x}$ can be controlled independently of the composition, which is related to only the AsH_3 and PH_3 flow-rate fraction. Featureless surface morphology was obtained for all the samples over a wide composition range grown with both techniques. Two SMQW samples grown with the two different methods, respectively, were used in the present studies. Sample 1 was grown with 0.6 sccm AsH_3 and 4 sccm PH_3, and it consists of 16-period $InAs_{0.6}P_{0.4}$(78 Å)/InP(144 Å) quantum wells. Sample 2 was grown with a continuous supply of 3 sccm PH_3 and an alternating supply of 2 sccm AsH_3, and it consists of 15-period $InAs_{0.5}P_{0.5}$(76 Å)/InP(162 Å) quantum wells. In sample 2 the $InAs_{0.5}P_{0.5}$ layer was composed of 5 periods of 2.5 -monolayer $InAs_yP_{1-y}$ (y is greater than 0.5) and 2.5 monolayer InP. The V/III ratio on the substrate surface during growth was typically 4:1 as determined from the group-V- and group-III-induced RHEED oscillations.[8,10]

High-resolution x-ray rocking curves were recorded with symmetric (004) diffraction from a monochromatic Cu $K\alpha_1$ line through four Ge crystals for the two samples, as shown in Figs. 2(a) and 2(b). Satellite peaks, resulting from diffraction of SMQWs, can be observed up to the seventh order, and they are sharp and distinct. This suggests that good periodicity of these multilayered structures was obtained, even with strain as high as 2.3%. The slight broadening of the peaks in Fig. 1(b) is attributed to the partial relaxation of the strain and As carryover into the InP layer at the interface during the growth interruption.[6] By assuming an abrupt interface in the quantum well structure and a strain-free InP layer, a simulation based on the dynamic theory was carried out. It turns out that the structural parameters determined from the growth condition agree with those determined from x-ray diffraction. Furthermore, the ratio of layer thicknesses of InAsP to InP is exactly the same as the ratio of growth durations of these two layers, because the growth rates of both InAsP and InP are determined only by the indium flux. Moreover, it appears that little phosphorus was incorporated in the $InAs_yP_{1-y}$ during short-period superlattice growth with 2 sccm AsH_3 present since the As composition in $InAs_{0.5}P_{0.5}$ layer is the average of InP and InAs.

Figures 3(a) and 3(b) show the cross-sectional TEM images taken from samples 1 and 2, respectively. It is shown that SMQW interfaces are very flat and abrupt. However, as shown in Fig. 3(a), there is a contrast change in the InP buffer layer, adjacent to the epitaxial SMQWs. The appearance of these dislocation nets results from the large lattice mismatch (2.3%) of the InP substrate and the quantum well structure. These dislocations are located in the buffer layer and terminated at the first InAsP layer as the strained-layer superlattices can work as a threading dislocation barrier due to the alternating compressive and tensile strain in the strained epilayers.[11] In Fig. 3(b), no dislocation is observed in the quantum well layers, and the short-period superlattice structure in the $InAs_{0.5}P_{0.5}$ layer can be seen clearly.

PL measurements were carried out at 10 K with 0.5 mW argon ion laser excitation. The luminescence was dispersed with a 50 cm monochromator and detected by a cooled Ge photodiode. The sharp and intense peaks are observed with the full widths at half maximum (FWHM) of 9 and 5 meV for these two samples respectively, attributable to emissions from heavy-hole excitons confined in the quantum wells. These are among the best results which have been reported so far for this material system.[6] Figures 4(a) and 4(b) show absorption spectra taken from samples 1 and 2 at room temperature using a broadband halogen lamp. Very sharp and significant absorption can be seen at 1.55 and 1.4 μm, respectively. The absorption structures appearing at high energy side are from the transitions between higher subbands. It is interesting to note that sample 1 has a sharper PL peak but broader absorption peak, compared with sample 2. This is understood that a miniband was formed in the short-period superlattice composing the $InAs_xP_{1-x}$ quantum well layer in sample 2.

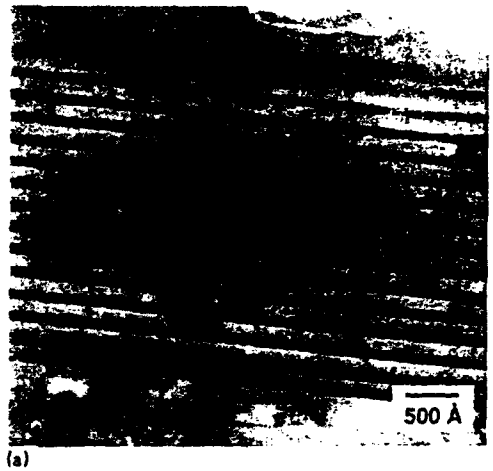

(a)

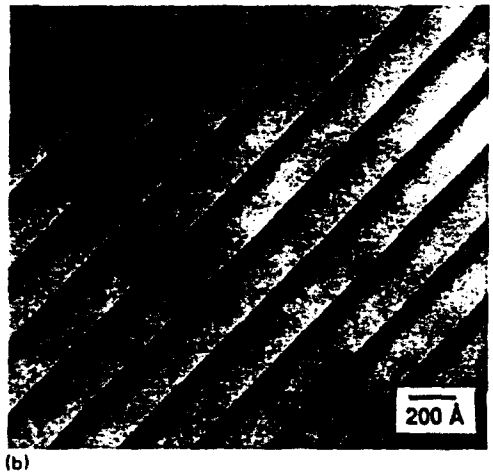

(b)

FIG. 3. TEM images taken from (a) sample 1 and (b) sample 2. Note that in (a) the misfit dislocations lie in the buffer layer and that in (b) fine structures corresponding to the short-period superlattice in the InAsP layer can be well resolved.

Hence, the absorption peak, reflecting the density-of-state of the relatively broad miniband, is broader than that from sample 1, while the PL spectrum suggests that better periodicity of the SMQW structures was obtained for sample 2. These excitonic transitions from the confined heavy hole levels are extremely useful for optoelectronic device applications. Currently we are working on 1.3 and 1.55 μm modulator fabrications that are promising for fiber communications, and device results will be reported elsewhere.

In summary, $InAs_xP_{1-x}/InP$ strained multiple quantum wells with strain as high as 2.5% were grown with the GSMBE technique. The arsenic composition was successfully controlled either by using a high PH_3 flow rate to

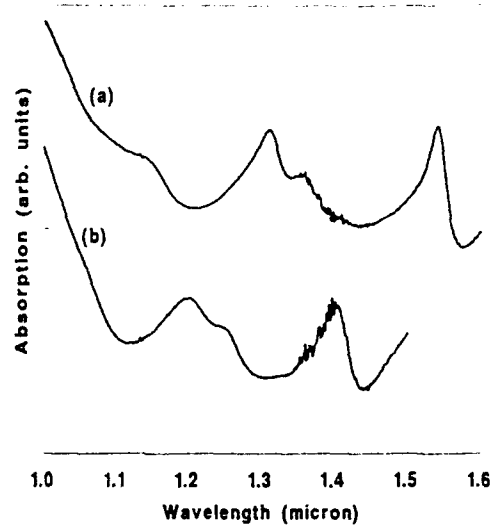

FIG. 4. Absorption spectra taken at room temperature by using a broadband halogen lamp for (a) sample 1 and (b) sample 2. The significant absorption peaks are from the excitonic transitions in the quantum wells.

dilute the As to P incorporation ratio, or by using a short-period InAsP/InP superlattice to average the arsenic composition. Structural and optical studies, by high-resolution x-ray rocking curve, cross-sectional TEM, PL, and absorption measurements, indicate that we have achieved high quality SMQWs that are suitable for optoelectronic applications.

This work is partially supported by the Powell Foundation, DARPA Optoelectronic Technology Center, and the Office of Naval Research. The authors (H.Q.H. and C.W.T.) wish to acknowledge T. P. Chin, B. W. Liang, and M. C. Ho for helpful discussions of MBE growth.

[1] H. C. Casey, Jr. and M. B. Panish, *Heterostructure Lasers* (Academic, New York, 1978).
[2] T. P. Pearsall, *GaInAsP Alloy Semiconductors* (Wiley, New York, 1982).
[3] W. T. Tsang, M. C. Wu, T. Tanbun-Ek, R. A. Logan, S. N. G. Chu, and A. M. Sergent, Appl. Phys. Lett. **57**, 2065 (1990).
[4] H. Asonen, K. Rakennus, K. Tappura, M. Hovinen, and M. Pessa, J. Cryst. Growth **105**, 101 (1990).
[5] K. H. Huang and B. W. Wessels, J. Cryst. Growth **92**, 547 (1988).
[6] R. P. Schneider, Jr., D. X. Li, and B. W. Wessels, J. Electrochem. Soc. **136**, 3490 (1989).
[7] C. T. Foxon, B. A. Joyce, and M. T. Norris, J. Cryst. Growth **49**, 132 (1980).
[8] H. Q. Hou, B. W. Liang, T. P. Chin, and C. W. Tu, Appl. Phys. Lett. **59**, (to be published, 1991).
[9] T. Fukui and N. Kobayashi, J. Cryst. Growth **71**, 9 (1985).
[10] T. P. Chin, B. W. Liang, H. Q. Hou, M. C. Ho, C. E. Chang, and C. W. Tu, Appl. Phys. Lett. **58**, 254 (1991).
[11] M. Yamaguchi, T. Nishioka, and M. Sugo, Appl. Phys. Lett. **54**, 24 (1989).

In situ determination of phosphorus composition in $GaAs_{1-x}P_x$ grown by gas-source molecular beam epitaxy

H. Q. Hou, B. W. Liang, T. P. Chin, and C. W. Tu
Department of Electrical and Computer Engineering, University of California at San Diego, La Jolla, California 92093-0407

(Received 27 December 1990; accepted for publication 15 April 1991)

We report for the first time an *in situ* determination of phosphorus compositions in a mixed group-V compound, such as $GaAs_{1-x}P_x$, grown by gas-source molecular beam epitaxy. Reflection high-energy electron diffraction intensity oscillations from As-limited and (As + P)-limited growth are observed on a Ga-rich GaAs surface. The phosphorus composition is therefore deduced from the different growth rates. Viability of this technique is strongly confirmed by the good agreement with the phosphorus compositions determined *ex situ* by x-ray rocking curve measurements on GaAs/GaAsP strained-layer superlattice structures.

Phosphide-based semiconductors, such as $In_{1-x}Ga_xAs_yP_{1-y}$, as well as the end ternary alloys $GaAs_{1-x}P_x$ and $InAs_xP_{1-x}$, are useful materials for optoelectronic applications because their fundamental band gaps are suitable for both visible and infrared emitters and detectors operated between 0.7 and 2.0 μm.[1] Arthur and Lepore pioneered molecular beam epitaxy (MBE) growth of GaAsP by using a solid effusion source of red phosphorus.[2] However, it is difficult to achieve the necessary control over the ratio of As to P by using solid phosphorus. Panish *et al.* greatly improved the flux control by using phosphorus and arsenic from thermally cracked phosphine and arsine, respectively, in gas-source MBE (GSMBE).[3] The precise composition control in alloys with mixed group-V elements, nevertheless, remains a difficult issue since As and P have different sticking coefficients with group-III metals,[3-7] and there is no simple relation between gaseous flows and solid-phase compositions of the group-V elements. The phosphorus composition reported so far has been determined by the calibration of the composition with x-ray diffraction, optical and other *ex situ* measurements for thick as-grown layers.[3-7] To determine the composition of mixed group-III alloys, on the other hand, intensity oscillations of reflection high-energy electron diffraction (RHEED)[8] are extensively used. This technique, however, can not be applied in a normal way to determine the composition of mixed group-V compounds because the growth rate is limited by the group-III metal fluxes when the growth is performed under an arsenic and/or phosphorus *over pressure*.

In this letter we present an *in situ* phosphorus-composition determination method by measuring the group-V-limited growth rate in $GaAs_{1-x}P_x$ grown on GaAs by GSMBE. The results of this calibration technique agree with an *ex situ* composition determination by x-ray rocking curve measured for strained-layer superlattice (SLS) structures.

Our experiment was carried out in a modified Varian Modular GEN-II MBE machine equipped with a 2200 *l*/s (H_2) cryopump and a 220 *l*/s ion pump in the growth chamber. Two separate gas cabinets house two gas-source supplies (100% arsine and 100% phosphine) as well as the scrubbers. The hydride gas sources for As and P were introduced into the growth chamber through a single Varian four-channel hydride injector, which was operated nominally at 1000 °C. The growth was achieved with elemental group-III metals and thermally cracked hydrides AsH_3 and PH_3. The typical working pressure in the growth chamber was 1×10^{-5} Torr. $GaAs_{1-x}P_x$ was grown at 580 °C since this temperature was reported to be optimum for both GaAs and GaP growth,[9] and the Ga flux was set such that the growth rate is about 0.7 monolayer per second. The intensity of the RHEED specular beam was detected by an optical-fiber-coupled photodiode, and the signal was recorded by a computer after it was enhanced with a dual-channel differential amplifier.

It is well known that the RHEED intensity will oscillate when the Ga flux is introduced onto a GaAs surface, and one period of oscillation corresponds to the growth of one monolayer.[8] The same concept is adopted in the present investigation, but the oscillation is induced by the group-V injection. A Ga-rich surface is intentionally formed by stopping the hydride injection and opening the Ga shutter only; thus, Ga atoms accumulate on the GaAs surface. When the AsH_3 and/or PH_3 shutters are opened, the excess Ga on the surface reacts with cracked AsH_3 and/or PH_3, causing RHEED intensity oscillations.[9] Figures 1(a) and 1(b) illustrate typical group-V-limited RHEED oscillations for GaAs and $GaAs_{1-x}P_x$ growth, respectively. The AsH_3 flow rate was fixed at 1.6 sccm in both cases, whereas PH_3 was also introduced with a flow rate of 2.4 sccm for the oscillation shown in Fig. 1(b). The (As + P)-limited growth rate was found to be higher than the As-limited growth rate. Such measurements were performed at a fixed AsH_3 flow rate (1.6 sccm) and various PH_3 flow rates ranging from 0 to 4.0 sccm.

Generally speaking, the As incorporation rate into $GaAs_{1-x}P_x$ might change upon the injection of P due to the displacement of As by P. Foxon *et al.*[4] reported a slight decrease of As_4 sticking coefficient when P_4 was injected during $GaAs_{1-x}P_x$ MBE growth under a limited Ga supply (8×10^{13} atoms $cm^{-2}s^{-1}$), where As_4 was 50 times more effective at displacing P_4 than vice versa. In our case, excess Ga atoms are deposited on the surface before the group-V-limited RHEED oscillation measurements, hence the displacement of As by P may be negligible. It is very

 0003-6951/91/290292-03$02.00

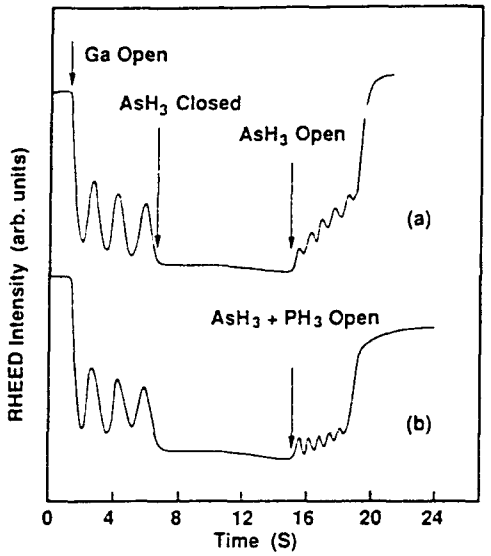

FIG. 1. Typical group-V-limited RHEED intensity oscillations on a Ga-rich GaAs surface. The oscillation is induced by (a) As, and (b) As + P.

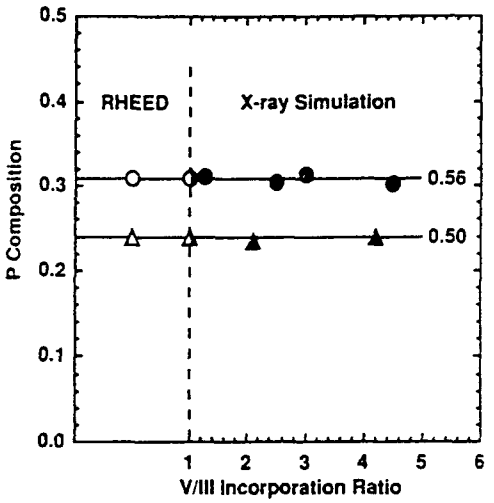

FIG. 3. The phosphorous composition as a function of the V/III incorporation ratio at different phosphine flow-rate fractions, 0.05 and 0.56. The solid marks represent the data *ex situ* determined; the open marks indicate the *in situ* determinations at the same corresponding phosphine flow fractions.

reasonable to assume that the increase in the growth rate shown in Fig. 1(b) is uniquely due to the addition of P. Therefore, the difference in the group-V growth rates gives the net incorporation rate of phosphorus from which the phosphorus composition, x, can be deduced.

The RHEED-determined phosphorus composition in $GaAs_{1-x}P_x$ .ted in Fig. 2 (indicated by open circles) versus the PH_3 flow-rate fraction (PH_3 flow rate over the total flow rate). Typical errors in determining x from the RHEED oscillations are indicated with error bars for $0.3 < x < 0.6$. This uncertainty is significant when the phosphorus composition is greater than 0.3 since the relatively large surface strain reduces the number of oscillations, which causes errors in reading the time scale. As shown in Fig. 2, the composition of phosphorus incorporated in the solid is different from the PH_3 flow-rate fraction in the gas phase. This is attributed to different sticking coefficients and arrival rates (a factor of square root of the As_2 to P_2 molecule mass ratio) of arsenic and phosphorus.[3,4] However, x is not proportionally dependent on the PH_3 flow-rate fraction over the whole flow-rate fraction range.

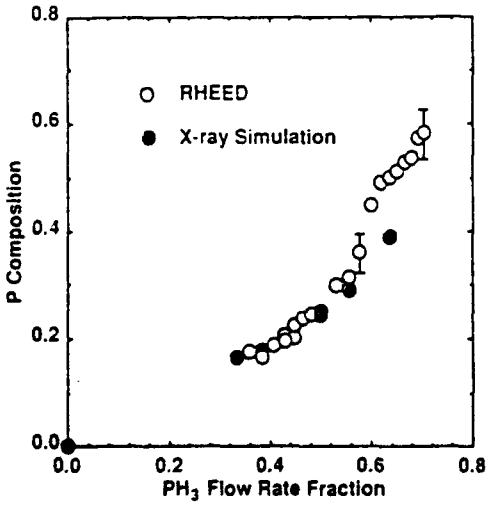

FIG. 2. Phosphorus composition in $GaAs_{1-x}P_x$ as a function of the PH_3 flow-rate fraction. The data shown by open circles are determined from the RHEED oscillations, and the full circles represent the x-ray simulation data.

The *in situ* determined composition is examined by x-ray rocking curve measurements of SLS structures. Five samples, typically consisting of 15-period GaAs(95 Å)/$GaAs_{1-x}P_x$(95 Å) superlattices, were grown with the same fixed AsH_3 flow rate (1.6 sccm) and substrate temperature (580 °C) as RHEED measurements and PH_3 flow rates ranging from 0.8 to 2.8 sccm. The thickness of the $GaAs_{1-x}P_x$ layer is less then the critical layer thickness so that pseudomorphic $GaAs_{1-x}P_x$ growth is expected. In such a case, by assuming Vegard's law the structural parameters can be determined accurately from the x-ray diffraction simulation based on the dynamic theory.[10] X-ray results for these five samples are shown in Fig. 2 with full circles. It is remarkable that RHEED oscillation and x-ray diffraction data are in very good agreement for $x < 0.3$. However, a significant deviation in the compositions exists for the sample with the highest phosphorus composition.

In order to understand the viability of this *in situ* determination of the phosphorus composition, several more 15-period GaAs(95 Å)/$GaAs_{1-x}P_x$(95 Å) SLS samples were grown with the same phosphine flow fraction, but different V/III incorporation ratios. Here, the *incorporation ratio* refers to the ratio of the group-V and group-III incorporation rates determined by group-V- and group-III-limited RHEED oscillations, respectively.[9] Shown in Fig. 3 by solid circles and triangles represents phosphorus compositions versus V/III incorporation ratios when the phosphine flow-rate fractions are fixed at 0.50 (by triangles)

and 0.56 (by circles), respectively. The open marks indicate the *in situ* determined composition from RHEED oscillations at the same flow-rate fraction and substrate temperature as those prepared for above SLS samples. As seen in Fig. 3, the phosphorus composition is almost independent of the V/III incorporation ratio in the current ratio range as long as the phosphine flow-rate fractions are the same. In other words, the phosphorus compositions are the same when the samples are grown with V/III incorporation ratio greater or close to unity. On the other hand, when the V/III ratio is unity, the phosphorus composition determined by the group-V-limited RHEED oscillation is naturally the same as that for group-III-limited growth. Therefore, the *in situ* derived composition (V/III < 1) agrees with the x-ray *ex situ* determination (V/III > 1). A dynamic growth model[11] by Seki *et al.* proposed that the phosphorus composition depends on the V/III beam-flux ratio for metalorganic chemical vapor deposition (MOCVD) growth of $GaAs_{1-x}P_x$. It is important to note that the V/III incorporation ratio is different from the beam-flux ratio, since the incorporation rate is a function of the beam flux and the sticking coefficient, which is different for arsenic and phosphorus. Therefore, the incorporation ratio is more relevant to growth studies. Our data also show that the phosphorus composition depends on the substrate temperature. However, the *in situ* method is still viable provided that the *in situ* calibration and real growth are carried out at the same substrate temperature. Results of a systematic study on the phosphorus composition incorporated in the solid phase as functions of the substrate temperature, V/III flux ratio and strain will be reported elsewhere.[12]

In conclusion, a simple, *in situ* approach to determine the phosphorus composition in $GaAs_{1-x}P_x$ grown by gas-source molecular beam epitaxy has been presented. The different incorporation rates of As and As + P, hence, the composition in the alloy layer, were deduced by observing the RHEED intensity oscillations of the group-V-limited growth on a Ga-rich surface (V/III < 1). The results agree favorably with the x-ray examination of as-grown (V/III > 1) superlattice samples. It is viable provided the same substrate temperature and phosphine flow-rate fraction are used for RHEED oscillation calibration and real growth.

This work is partially supported by the Office of Naval Research and Powell Foundation. The authors are delighted to acknowledge assistance of M. C. Ho and C. E. Chang, the critical reading of this manuscript by Professor H. H. Wieder, and valuable comments by the reviewer.

[1] H. C. Casey, Jr. and M. B. Panish, *Heterostructure Lasers* (Academic, New York, 1978).
[2] J. R. Arthur and J. J. Lepore, J. Vac. Sci. Technol. 6, 545 (1969).
[3] For reviews, see M. B. Panish, Prog. Cryst. Growth Charact. 12, 1 (1986); M. B. Panish and H. Temkin, Annu. Rev. Mater. Sci. 19, 209 (1989).
[4] C. T. Foxon, B. A. Joyce, and M. T. Norris, J. Cryst. Growth 49, 132 (1980).
[5] T. Fukui and N. Kokayashi, J. Cryst. Growth 71, 9 (1985).
[6] T. Nomura, H. Ogasawara, M. Miyao, and M. Hagino, J. Cryst. Growth 111, 61 (1991).
[7] L. Samuelson, P. Omling, and H. G. Grimmeiss, J. Cryst. Growth 61, 425 (1983).
[8] J. H. Neave, B. A. Joyce, P. J. Dobson, and N. Norton, Appl. Phys. A31, 1 (1983).
[9] T. P. Chin, B. W. Liang, H. Q. Hou, M. C. Ho, C. E. Chang, and C. W. Tu, Appl. Phys. Lett. 58, 254 (1991).
[10] H. Q. Hou, Y. Huang, and J. M. Zhou, J. Cryst. Growth 99, 306 (1990).
[11] H. Seki and A. Koukitu, J. Cryst. Growth. 74, 172 (1986).
[12] B. W. Liang, H. Q. Hou, and C. W. Tu, Mat. Res. Soc. Symp. Proc. 222 (to be published).

Journal of Electronic Materials, Vol. 21, No. 2, 1992

Growth of $GaAs_{1-x}P_x/GaAs$ and $InAs_xP_{1-x}/InP$ Strained Quantum Wells for Optoelectronic Devices by Gas-Source Molecular Beam Epitaxy

H. Q. HOU and C. W. TU

Department of Electrical and Computer Engineering,
University of California at San Diego, La Jolla, CA 92093-0407

In this paper we show that pseudomorphically strained heterostructures of $InAs_xP_{1-x}/InP$ may be an alternative to lattice-matched heterostructures of $In_{1-x}Ga_xAs_yP_{1-y}/InP$ for optoelectronic applications. We first studied the group-V composition control in the gas-source molecular beam epitaxy (GSMBE) of the $GaAs_{1-x}P_x/GaAs$ system. Then we studied GSMBE of strained $InAs_xP_{1-x}/InP$ multiple quantum wells with the ternary well layer in the composition range $0.15 < x < 0.75$. Structural and optical properties were characterized by high-resolution x-ray rocking curves, transmission electron microscopy, absorption and low-temperature photoluminescence measurements. High-quality multiple-quantum-well structures were obtained even for highly strained (up to 2.5%) samples. The achievement of sharp excitonic absorptions at 1.06, 1.3 and 1.55 μm at room temperature from $InAs_xP_{1-x}/InP$ quantum wells suggests the possibility of long-wavelength optoelectronic applications.

Key words: Gas-source molecular beam epitaxy, strained quantum wells, $GaAs_{1-x}P_x/GaAs$, $InAs_xP_{1-x}/InP$

I. INTRODUCTION

$In_{1-x}Ga_xAs_yP_{1-y}$ quaternary material lattice-matched to InP is promising for long-wavelength emitter and detector applications[1] since the room-temperature excitonic emission from the quantum well can be tuned from 0.9 to 1.8 μm. Extensive studies on the growth, characterization and device applications have been reported on this material system.[2-4] However, the compositions of both group-III and group-V elements have to be properly controlled. As an alternative to $In_{1-x}Ga_xAs_yP_{1-y}$, the ternary compound $InAs_xP_{1-x}$ has received some attention since the fundamental bandgap of $InAs_xP_{1-x}$ can also cover the same long-wavelength region as $In_{1-x}Ga_xAs_yP_{1-y}$. Epitaxial layers of this ternary have been grown by organometallic vapor phase epitaxy (OMVPE)[5] and molecular beam epitaxy (MBE).[6,7] Moreover, there are several advantages in growing this ternary compound, compared to the quaternary compound. First of all, the composition control is made easier because only one composition parameter is involved. Second, the layer thickness and alloy composition can be controlled independently in gas-source MBE (GSMBE). The thickness is governed only by the group-III beam flux under a group-V overpressure, and the composition is adjusted by arsine (AsH_3) and phosphine (PH_3) flow rates. This property of growing $InAs_xP_{1-x}$ can greatly simplify the growth control when a certain excitonic emission wavelength is desired for the intended optoelectronic application. Furthermore, tailoring the band structure by the biaxial strain in $InAs_xP_{1-x}/InP$ heterostructures offers an additional degree of freedom for device design. Finally, when the InAs molar fraction x in $InAs_xP_{1-x}$ is larger than about 0.7, the room-temperature electron mobility is above 10,000 cm^2/Vs.[8] Therefore, $InAs_xP_{1-x}$ may also be important for electronic device applications.

The proper composition control for growing this mixed group-V ternary compound, however, is still a difficult issue because As is more readily incorporated than P, as demonstrated in OMVPE[9,10] and MBE growth (using As_4 and P_4).[11] To understand the sticking behavior of As and P in mixed group-V ternary compounds grown by GSMBE, we first studied the growth of $GaAs_{1-x}P_x$ on GaAs. An *in situ* method for determining the phosphorus composition in $GaAs_{1-x}P_x$ was developed by observing both As- and (As + P)-induced intensity oscillations of reflection high-energy electron diffraction (RHEED). The phosphorus composition incorporated in the solid phase was found to be less than the PH_3 flow-rate fraction (PH_3 flow rate over the total hydride flow rate) in the gaseous phase.[11] This phenomenon was observed to be especially pronounced for growing $InAs_xP_{1-x}$. Special concerns were therefore used to control properly the arsenic composition in $InAs_xP_{1-x}$ over a wide composition range from $x = 0.15$ to 0.75. Strained multiple quantum well (SMQW) samples of $InAs_xP_{1-x}/InP$ were evaluated by x-ray rocking curves and dynamical simulations, transmission electron microscopy (TEM), absorption, and low-temperature photoluminescence (PL) measurements. All of these characterizations show that device-quality samples were obtained even for highly-strained structures.

II. COMPOSITION CALIBRATION OF MIXED GROUP-V COMPOUNDS

Epitaxial growth was accomplished in a Varian Modular Gen-II MBE machine by using high-purity

(Received June 19, 1991; revised September 10, 1991)

0361-5235/1992/1401-13755.00©92 TMS

elemental group-III sources and dimers of arsenic and phosphorus from thermally cracked hydrides. Cylinders containing 100% AsH_3 and 100% PH_3 were housed in separate cabinets. Arsine and phosphine were introduced into the growth chamber through a Varian four-channel injector, which was operated at a nominal temperature of 1000° C. The growth chamber was evacuated by a 2200 *l/s* cryopump. Typical working pressure was 1×10^{-5} Torr. Heterostructures of $GaAs_{1-x}P_x$/GaAs and $InAs_xP_{1-x}$/InP were grown at 580 and 460° C, respectively. The intensity of the RHEED specular beam was measured with an optical-fiber-coupled phototransistor, and the signal was enhanced with a dual-channel differential amplifier, then recorded by a computer. The growth procedure has been described in more detail elsewhere.[7,12,13]

We have used an *in situ* method to determine the phosphorus composition in $GaAs_{1-x}P_x$ by observing group-V-limited RHEED oscillations.[12-15] A Ga-rich surface was intentionally formed by stopping the hydride injection and opening only the Ga shutter. The excess Ga atoms accumulated on the GaAs surface reacted with As_2 and/or P_2 when the appropriate valves were opened, causing RHEED intensity oscillations. The (As + P)-limited growth rate was found to be higher than the As-limited growth rate. Such measurements were performed at a fixed AsH_3 flow rate (1.6 sccm) and different PH_3 flow rates ranging from 0 to 4.0 sccm. Although the sticking coefficients of As and P may change when both As and P are present, we assume that because of the abundance of Ga on the surface, the amounts of As and P incorporated are independent of each other. We then can determine the phosphorus composition by attributing the difference between the (As + P)-limited growth rate and the As-limited growth rate to the incorporation of phosphorus.[12] Shown in Fig. 1(a) by open circles are phosphorus compositions deduced from these RHEED oscillation measurements. This *in situ* determined composition was calibrated by x-ray rocking curve measurements of $GaAs/GaAs_{1-x}P_x$ strained-layer superlattice samples, grown under the same substrate temperature and hydride flow rates as were used in the RHEED oscillation experiment. Structural parameters can be determined accurately from the x-ray diffraction by comparison with rocking curves calculated using dynamical theory.[16] Compositions from the simulation are shown in Fig. 1(a) with closed circles. It is remarkable that RHEED oscillation and x-ray diffraction data are in very good agreement when the phosphorus composition is less than 0.3.

Based on a thermodynamic equilibrium model, Seki *et al.*[17] predicted that the incorporation of GaAs and GaP is comparable, whereas InAs would be preferentially incorporated as compared to InP. Shown in Fig. 1(b), plotted against the AsH_3 flow-rate fraction, is the arsenic composition in $InAs_xP_{1-x}$ determined from simulations to x-ray rocking curves taken from $InAs_xP_{1-x}$/InP SMQW samples. As can be seen, the As composition in the solid phase is much greater than the AsH_3 flow-rate fraction in the gas phase. Therefore, the phosphorus sticking coefficient can change drastically when an AsH_3 flow is introduced. Thus, we cannot apply the above *in situ* RHEED method for composition calibration of $InAs_xP_{1-x}$ on InP.

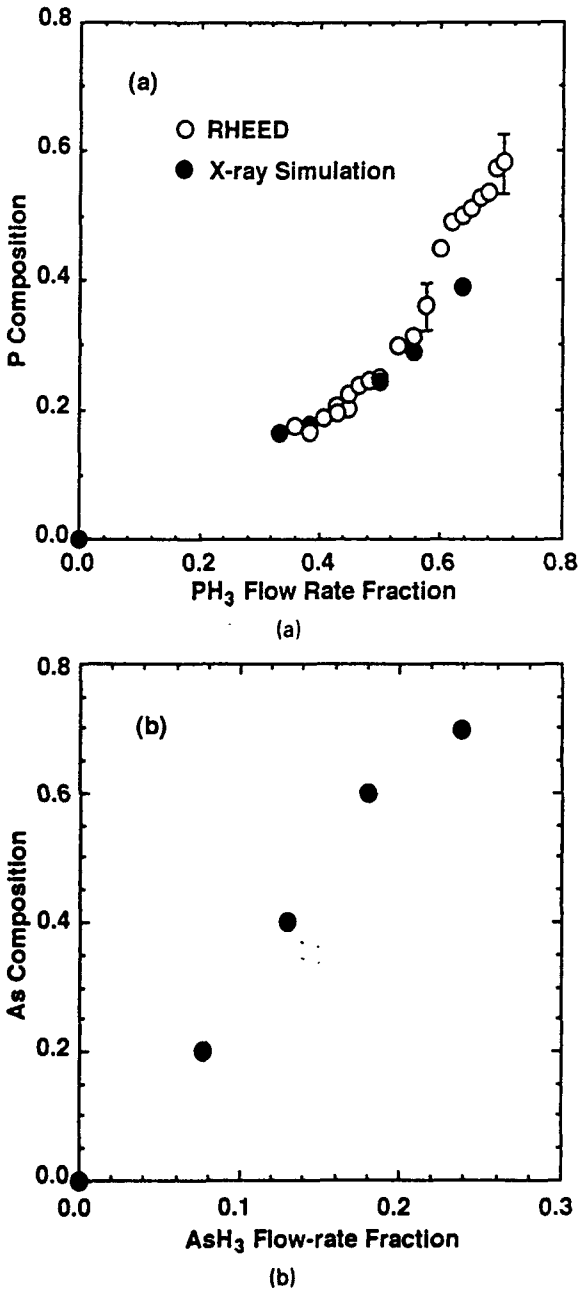

Fig. 1 — (a) Shows the phosphorus composition incorporated in $GaAs_{1-x}P_x$ on GaAs vs the PH_3 flow-rate fraction; (b) shows the arsenic composition incorporated in $InAs_{1-x}P_x$ on InP vs the AsH_3 flow-rate fraction. Closed circles represent the compositions determined from x-ray rocking curves, and open circles are from RHEED oscillations.

III. GROWTH AND CHARACTERIZATION

In order to obtain layers of $InAs_xP_{1-x}$ with small x, it is necessary to use a small flow rate of AsH_3.

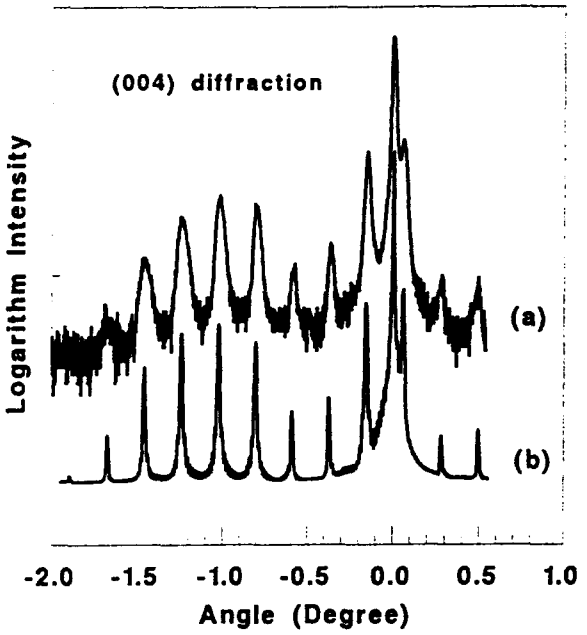

Fig. 2 — (a) High-resolution x-ray rocking curve and (b) a dynamical-theory simulation for a 16-period $InAs_{0.5}P_{0.5}$(76Å)/InP(162Å) SMQW structure.

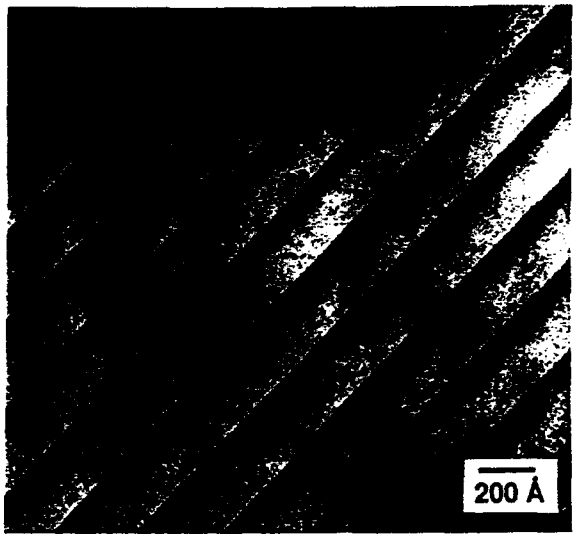

Fig. 3 — A cross-sectional TEM microimage of an $InAs_{0.5}P_{0.5}/InP$ SMQW sample, in which the $InAs_{0.5}P_{0.5}$ layer was grown with SPSL, as shown by the fine structure in the dark region of the picture.

However, our ability to do this is limited by the stability of the mass-flow-controller output when a small setting (<0.5 sccm) is chosen. We therefore used a relatively large PH_3 flow rate (ranging from 3 to 5 sccm), compared to AsH_3 (0.6 sccm), in order to *dilute* the arsenic fraction on the growth front. Instead of using the usual run-vent technique, we interrupted the growth at each interface to wait for the beam fluxes to become stabilized, to recover the growth front, and to purge the residual gas. An alternative to the random alloy $InAs_xP_{1-x}$ is an $InAs_yP_{1-y}/InP$ short-period superlattice (SPSL). In this case the AsH_3 and PH_3 flow rates can be comparable and the As composition in $InAs_xP_{1-x}$ is controlled by the time intervals of growing $InAs_yP_{1-y}$ and InP. With these two growth techniques, the high PH_3 flow rate and the SPSL approach, the arsenic composition x could be successfully controlled from $x = 0.15$ to 0.75. The surface morphology was examined under a Nomarski contrast optical microscope. Featureless surface was obtained for all the SMQW samples.

Figure 2(a) shows the x-ray rocking curve taken from a 16-period $InAs_{0.5}P_{0.5}/InP$ SMQW structure, in which the $InAs_{0.5}P_{0.5}$ layers consist of 5 periods of 2.5 monolayers of $InAs_yP_{1-y}$ (here y is greater than 0.5) and 2.5 monolayers of InP. The nominal thicknesses of $InAs_{0.5}P_{0.5}$ and InP were 73Å and 158Å, respectively. The PH_3 flow was continuous at 3 sccm, whereas the AsH_3 flow was alternating at 2 sccm. High-resolution x-ray rocking curves from SMQW samples were recorded with symmetric (004) diffraction from a monochromatic Cu $K\alpha_1$ line through four Ge crystals. Well resolved satellite peaks from diffraction of the SMQW's can be observed up to the seventh order. This suggests that this highly-strained (1.6%), multi-layered structure possesses good periodicity and crystalline quality. The critical layer thickness for this sample is about 55Å based on the Matthews-Blakeslee model,[18] and 210Å based on the People-Bean model.[19] Assuming an abrupt interface in the quantum well structure and a perfectly coherent tetragonal distortion in the $InAs_xP_{1-x}$ layer (with strain-free InP layers), we carried out a simulation based on dynamical theory. The result is shown in Fig. 2(b). The best fit suggests that the SMQW consists of 16 periods of $InAs_{0.5}P_{0.5}$(76Å)/InP(162Å), in excellent agreement with the nominal parameters given by the growth condition. The ratio of the layer thicknesses of $InAs_{0.5}P_{0.5}$ to InP is the same as the ratio of the growth durations of these two layers, because growth rates of both $InAs_{0.5}P_{0.5}$ and InP are determined only by the indium flux. Moreover, it appears that little phosphorus was incorporated in the $InAs_yP_{1-y}$ layer during SPSL growth with an AsH_3 flow of 2 sccm because the As composition in the $InAs_{0.5}P_{0.5}$ layer is the average of 2.5 monolayers of InP and 2.5 monolayers of InAs. The slight broadening of the actual rocking curve shown in Fig. 2(a) may be attributed to As carryover into the InP layer at the interface during growth interruption. Another possibility is the random incorporation of residual As in the InP layer either from the cracker or the chamber.

A typical cross-sectional transmission electron microscopy image taken from this SMQW sample is shown in Fig. 3. It appears that the SMQW interfaces are very flat and abrupt. No dislocation was observed. Furthermore, five SPSL structure in the $InAs_{0.5}P_{0.5}$ layer can be seen clearly, suggesting that the interdiffusion at the interface of $InAs_{0.5}P_{0.5}/InP$ is not serious enough to degrade the SPSL structure.

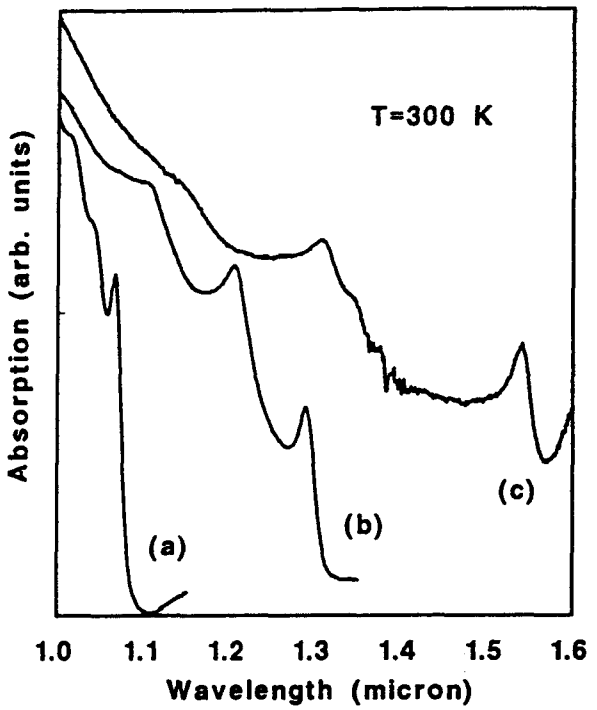

Fig. 4 — Room-temperature absorption spectra taken from three SMQW samples. The emission wavelength is located at around 1.06, 1.3 and 1.55 μm respectively.

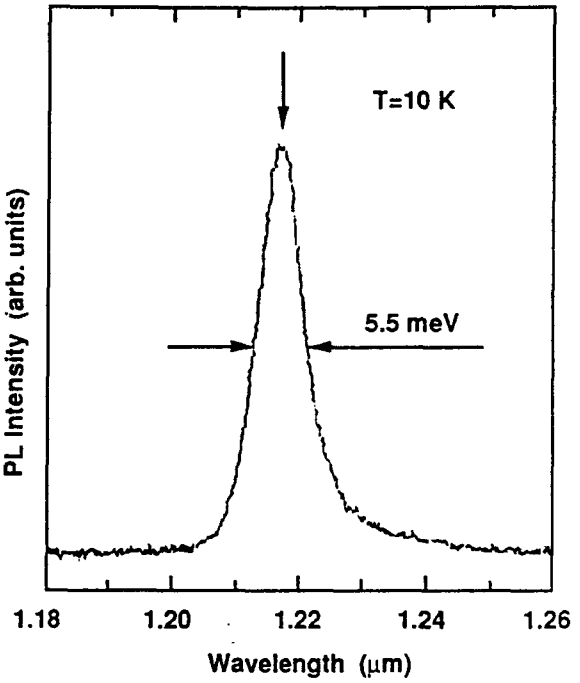

Fig. 5 — A typical PL spectrum taken at low temperature (10K) for an $InAs_{0.4}P_{0.6}$/InP SMQW structure with a FWHM of 5.5 meV. The arrow indicates the calculated energy position.

IV. ABSORPTION AND PL MEASUREMENTS

A series of SMQW samples were grown using the two techniques mentioned above. A typical sample structure consists of 15 ~ 30 periods of $InAs_xP_{1-x}$(80Å)/InP(150Å) SMQW's. Absorption measurements were performed using a broadband halogen tungsten lamp at room temperature. Absorption spectra taken from three samples are shown in Fig. 4. The arsenic compositions were determined by x-ray rocking curves to be about 0.2, 0.4 and 0.6, respectively. Very sharp and significant absorption can be seen at 1.06, 1.3 and 1.55 μm from these three samples, respectively. These transitions are assigned as the absorption from the first-subband heavy-hole excitons confined in the quantum well according to the energy-level calculation based on an envelope-function model.[20] It is also notable that transitions between higher subbands appear clearly at the high energy side of the absorption spectra. Moreover, the linewidth of the absorption peak shows an increase with increasing As composition (or strain). This is considered to result from the gradual degradation of the quantum well quality due to the large strain. Room-temperature excitonic transitions at these wavelengths are extremely useful for optoelectronic device applications, such as waveguide modulator, used in fiber optical communication. It is interesting to see in Fig. 4(c) that the second heavy-hole interband transition, located at around 1.3 μm, is also rather strong. Therefore it may be possible to fabricate a single waveguide modulator that can be operated near both 1.55 and 1.3 μm.

Photoluminescence measurements were carried out at 10 K with argon-ion laser excitation. The luminescence was dispersed with a 50 cm monochromator, detected by a cooled Ge photodiode, and measured by lock-in technique. Sharp and intense peaks were observed from these three SMQW samples. The full widths at half maximum (FWHM) of these excitonic emissions are 4, 5.5 and 9 meV, respectively. These results, among the best that have ever been reported for this material system,[6,7,21] indicate that very good interlayer uniformity, intralayer periodicity and crystal perfection were obtained in these samples. Figure 5 shows a typical spectrum from a 30-period $InAs_{0.4}P_{0.6}$(92Å)/InP(138Å) SMQW sample with 1.3 μm absorption at room temperature. The arrow indicates the calculated emission energy of the heavy-hole exciton. An excellent agreement was achieved.

Another interesting aspect lies in the $InAs_xP_{1-x}$/InP SMQW structure grown with SPSL's. Two samples were prepared, with SPSL (#11) and uniform (#6) ternary $InAs_xP_{1-x}$, respectively. Sample #11 exhibits a sharper PL, but broader absorption peak, as compared to Sample #6. We believe that a miniband is formed in the SPSL in Sample #11. Hence, the absorption peak, reflecting the density of states of the relatively broad miniband, is broader than that from Sample #6. On the other hand, the narrower PL peak suggests that Sample #11 possesses better periodicity. If an electric bias is applied to a modulator structure, the quantum well potential will

be titled. Therefore, a reduced coupling of the wavefunction, and even breakdown of the miniband, in the SPSL can be expected. As a result, a sharper absorption peak from the SMQW's grown with SPSL may appear, which is an interesting issue in modulator studies. Currently we are working on waveguide modulators based on the $InAs_xP_{1-x}$/InP SMQW's, and device results will be reported elsewhere.

V. CONCLUSION

In summary, the incorporation behavior of As and P in mixed group-V compounds, $GaAs_{1-x}P_x$ on GaAs and $InAs_{1-x}P_x$ on InP was studied. Methods for proper, even *in situ*, composition control were developed. $InAs_xP_{1-x}$/InP strained multiple quantum wells with strain as high as 2.5% were grown with the GSMBE technique. The arsenic composition was successfully controlled either by using a high PH_3 flow rate to dilute the As to P flux ratio, or by using a short-period $InAs_yP_{1-y}$/InP superlattice to average the arsenic composition. Structural and optical studies, by high-resolution x-ray rocking curve, cross-sectional TEM, absorption, and PL measurements, indicate that high-quality $InAs_xP_{1-x}$/InP SMQW's can be grown by GSMBE. Further studies are underway to assess their potential for optoelectronic device applications.

ACKNOWLEDGMENTS

This work is partially supported by the Office of Naval Research and the DARPA Optoelectronic Technology Center. The authors gratefully acknowledge Dr. S. N. G. Chu at AT&T Bell Laboratories for TEM measurements, B. W. Liang, T. P. Chin, and M. C. Ho for discussions on GSMBE growth, and the reviewer for critical reading of the manuscript.

REFERENCES

1. H. C. Casey, Jr. and M. B. Panish, Heterostructure Lasers, (Academic, New York, 1978).
2. M. B. Panish and S. Sumski, J. Appl. Phys. *55*, 3571 (1984).
3. W. T. Tsang, M. C. Wu, T. Tanbun-Ek, R. A. Logan, S. N. G. Chu and A. M. Sergent, Appl. Phys. Lett. *57*, 2065 (1990).
4. H. K. Tsang, J. B. D. Soole, H. P. LeBlanc, R. Bhat, M. A. Koza and I. H. White, Appl. Phys. Lett. *57*, 2285 (1990).
5. R. P. Schneider, Jr., D. X. Li and B. W. Wessels, J. Electrochem. Soc. *136*, 3490 (1989).
6. T. K. Woodward, T. Sizer and T. H. Chiu, Appl. Phys. Lett. *58*, 1366 (1991).
7. H. Q. Hou, C. W. Tu and S. N. G. Chu, Appl. Phys. Lett. *58*, 2954 (1991).
8. P. J. Wang and B. W. Wessels, Appl. Phys. Lett. *44*, 766 (1984).
9. T. Fukui and N. Kobayashi, J. Cryst. Growth *71*, 9 (1985).
10. K. H. Huang and B. W. Wessels, J. Cryst. Growth *92*, 547 (1988).
11. C. T. Foxon, B. A. Joyce and M. T. Norris, J. Cryst. Growth *49*, 132 (1980).
12. H. Q. Hou, B. W. Liang, T. P. Chin and C. W. Tu, Appl. Phys. Lett. *59*, 292 (1991).
13. T. P. Chin, B. W. Liang, H. Q. Hou, M. C. Ho, C. E. Chang and C. W. Tu, Appl. Phys. Lett. *58*, 254 (1991).
14. J. H. Neave, B. A. Joyce, P. J. Dobson and N. Norton, Appl. Phys. *A31*, 1 (1983).
15. B. F. Lewis, R. Fernandez, A. Madhukar and F. J. Grunthaner, J. Vac. Sci. Technol. *B4*, 560 (1986).
16. B. K. Tanner, Adv. X-ray Anal. *33*, 1 (1990).
17. H. Seki and A. Koukitu, J. Cryst. Growth *74*, 172 (1986).
18. J. W. Matthews and A. E. Blakeslee, J. Cryst. Growth *32*, 265 (1976).
19. R. People and J. C. Bean, Appl. Phys. Lett. *47*, 322 (1985).
20. H. Q. Hou, T. P. Chin, B. W. Liang and C. W. Tu, Mat. Res. Soc. Symp. Proc. *228*, (to be published).
21. R. P. Schneider, Jr. and B. W. Wessels, Appl. Phys. Lett. *54*, 1142 (1990).

Appl. Phys. Lett. 1992

In situ control of As composition in InAsP and InGaAsP grown by gas-source molecular beam epitaxy

H. Q. Hou and C. W. Tu

Department of Electrical and Computer Engineering,
University of California at San Diego, La Jolla, California 92093-0407

(Received)

Group-III- and group-V-induced intensity oscillations of reflection high-energy electron diffraction are observed for InAsP in gas-source molecular beam epitaxial growth. The As incorporation rate is found to be dominant, independent of the presence of P when the phosphine flow rate is reasonably low. This observation suggests a simple method for controlling the As composition in InAsP by just controlling the incorporation-rate ratio of As to In when this ratio is less than unity. This successful *in situ* composition control for InAsP, combined with the *in situ* composition calibration in GaAsP reported previously, provides a general guideline for controlling the compositions in InGaAsP.

1991 PACS numbers: 68.55.Bd, 68.55.Nq, 61.10.-i

High-quality InGaAsP and all its ternary and binary end member compounds have been routinely grown by using gas-source molecular beam epitaxy (GSMBE),[1] or chemical beam epitaxy (CBE),[2] and metalorganic chemical vapor deposition (MOCVD) techniques. Among these materials, InGaAsP/InP[3-5] and strained InAsP/InP[6-8] quantum well structures are of great importance for long-wavelength optoelectronic applications since fundamental bandgaps of $In_{1-y}Ga_yAs_xP_{1-x}$ and $InAs_xP_{1-x}$ can be tuned to achieve the bandedge emission from 0.9 to 2 μm. However, controlling the compositions, especially the As composition in the quaternary compound $In_{1-y}Ga_yAs_xP_{1-x}$, has been a difficult issue owing the different incorporation behavior of As and P. Furthermore, this incorporation behavior also depends on group-III elements since As incorporation is different for GaAsP and InAsP.[9,10] Previously, two composition parameters in $In_{1-y}Ga_yAs_xP_{1-x}$ have to be determined, after the samples are grown, by at least two independent methods[3,4] (x-ray diffraction, photoluminescence, electron probe, etc.). The data are then fed back to fine tune the growth parameters to obtain desired compositions. Therefore, it would be very useful if an *in situ* composition control can be achieved.

However, the intensity oscillation of reflection high-energy electron diffraction (RHEED) cannot be simply applied to determine the As composition in InAsP since its growth rate is governed by only the In beam flux under normal growth conditions (group-V rich). Recently, we reported an *in situ* determination of the phosphorus composition in GaAsP[12] by measuring group-V-induced RHEED oscillations.[13,14] In this paper, we shall present an *in situ* method to control the As composition in $InAs_xP_{1-x}$ by controlling the incorporation ratio of As to In measured by As- and In-induced RHEED oscillations. The As composition in the InGaAsP quaternary compound can then be controlled based on the *in situ* composition calibration for its ternary members.

Epitaxial growth was performed in an Intevac (Varian) Modular GEN-II MBE system modified for handling arsine (AsH_3) and phosphine (PH_3)[8]. The gas cracker was operated at a nominal temperature of 1000 °C. The growth of InAs, InP and InAsP was

performed on semi-insulating InP (100) substrates at a substrate temperature around 460 °C. The In incorporation rate on InP was set to about 0.6 ML/s as determined by RHEED oscillations. As is well known, the growth rate is limited by the beam flux of the group-III elements[11] under group-V rich condition. However, if we *intentionally* create a group-III-rich surface, then the growth will be controlled by the arrival rate of group-V atoms or molecules.[13,14] Fig. 1 shows the As incorporation rate as a function of the AsH_3 flow rate calibrated at the substrate temperature of 460 °C. It appears that the As incorporation rate is proportional to the AsH_3 flow rate. This incorporation rate also has an Arrhenius dependence on the substrate temperature.[14] The inset of Fig. 1 shows group-III- ($t_1<t<t_2$) and group-V-induced ($t_3<t<t_4$) RHEED oscillations during InAs growth on InAs. The InAs was grown on a 3 μm, totally strain-relaxed thick InAs layer on InP. During $t_1<t<t_2$, the growth rate was limited by the arrival rate of the In flux as normally applied.[11] However, the growth rate was limited by the As arrival rate during $t_3<t<t_4$ since excess In atoms were deposited on the InAs surface during $t_2<t<t_3$. Therefore, the incorporation rates of In and As, R_{In} and R_{As}, at the given growth temperature can be determined from these oscillations.

When both As and P were injected onto the substrate surface at t_3, the growth rate is higher due to the addition of P. In Fig. 2 the growth rates limited by (As+P) are plotted against PH_3 flow rates at several fixed AsH_3 flow rates (0, 0.5, 0.75 and 1 sccm). The lines through the data points are drawn to guide the eyes. It appears that the incorporation rate of (As+P) has the same linear dependence on the PH_3 flow rate as the incorporation rate of only P itself (calibrated for InP grown on InP). The only difference is a constant offset corresponding to the additional incorporation of As. (The jump in the incorporation rate for the results grown with 0.5 sccm AsH_3 may be due to the change of the RHEED pattern for a highly strained InAsP surface). We can, therefore, conclude that the As incorporation into $InAs_xP_{1-x}$ is independent of the presence of P under the In-rich growth conditions. This behavior agrees with the prediction of Seki and Koukiku.[9]

cracked hydrides, AsH_3 and PH_3, at a substrate temperature of 460 °C. The gas-source supplies (100% arsine and 100% phosphine) were introduced into the growth chamber through a single Varian four-channel hydride injector, which was operated nominally at 1000 °C. The growth chamber was equipped with a 2200 ℓ/s cryopump and a

InAsP/InP superlattices. The x can be controlled with the ratio of open and close durations of AsH_3 easily by using this technique.

The growth rate, therefore, the thickness of $InAs_xP_{1-x}$ is constrained only by the indium beam flux at a group-V overpressure, so the layer thickness of

2954 Appl. Phys. Lett. 58 (25), 24 June 1991 0003-6951/91/252954-03$02.00

Now we can assume that the As incorporation into $InAs_xP_{1-x}$ is dominant in our normal growth conditions (group-V rich but $R_{As}/R_{In}<1$) with substrate temperature at around 460 °C and small PH_3 flow rate, which is sufficient to provide a higher total group-V flux than In. In other words, phosphorus reacts with In only when there is not enough As to react with all of the In. This situation makes controlling the As composition in $InAs_xP_{1-x}$ very simple. Once we calibrate the As and In incorporation rates at a desired growth temperature by As- and In-induced RHEED oscillations, respectively, as shown in Fig. 1, the ratio of the As to In incorporation rates (*when* ≤ 1) is basically the As composition in $InAs_xP_{1-x}$.

Based on this idea of *in situ* controlling the As composition in InAsP, a series of InAsP/InP strained-layer superlattice (*SLS*) structures were grown at 2 *sccm* PH_3 flow rates and different R_{As}/R_{In} ratios. High-resolution x-ray rocking curves were measured from (004) diffraction of the Cu $K\alpha_1$ line for these samples. Computer simulations based on a dynamical theory yield a precise determination of the As composition in $InAs_xP_{1-x}$. Shown in Fig. 3 is the *ex situ* determined As composition versus the R_{As}/R_{In} ratio. An excellent agreement can be seen when $x<0.5$. This implies that our assumption of As being dominantly incorporated in InAsP under the normal growth conditions is correct, and this *in situ* method to determine the composition is viable. The discrepancy for $x>0.5$ is not well understood presently. A possible reason is that the large surface strain may affect the incorporation behavior of As and P. Chang *et al.* reported a similar result of composition control in MBE grown GaAsSb.[15] They found that the control of the Sb composition can best be achieved by maintaining the ratio of Sb/Ga when below unity. They attributed this behavior to the higher sublimation energy (longer surface lifetime), and lower atomization energy (more reactions with Ga surface atoms) of Sb_4 than As_4.[15]

The SLS samples used for *ex situ* composition determination by x-ray rocking curves and simulations, shown in Fig. 3, were all grown at a PH_3 flow rate of 2 sccm (except 1.5 sccm for the sample with x~0.1). However, when the PH_3 flow rate is much

higher than the AsH_3 flow rate, the As flux concentration may be greatly diluted on the substrate surface.[8] As a result, the As composition in InAsP would be dependent on the PH_3 flow rate. Therefore, a series of InAsP/InP SLS samples were grown with a fixed AsH_3 flow rate (0.25 and 0.5 sccm, respectively) and various PH_3 flow rates ranging from 1.25 to 4 sccm. Shown in Fig. 4 is the normalized As composition determined from x-ray rocking curves to the As/In incorporation-rate ratio as a function of the PH_3/AsH_3 flow-rate ratio. The full and open circles represent the respective cases with AsH_3 flow rate of 0.25 and 0.4 sccm. The As composition decreases when the PH_3 flow rate is about 5 times as much as the AsH_3 flow rate. The corresponding surface concentration ratio is even enhanced by a factor of $(m_{As_2}/m_{P_2})^{1/2}$, where m_{As_2} and m_{P_2} are the molecular mass of As_2 and P_2, respectively. In this case, the *ex situ* determined As composition is no longer consistent with the *in situ* calibration. Therefore, to keep this *in situ* method valid it is important to use as small V/III incorporation ratio as possible. Although the As composition in InAsP is dependent on the substrate temperature, the *in situ* calibrated composition should be correct as long as the calibration (RHEED oscillations) and real growth are performed at the same substrate temperature within a reasonable range.

Previously, we succeeded in an *in situ* calibration of the phosphorus composition in GaAsP[12] by measuring the difference in the incorporation rate of (As+P) and As with group-V-induced RHEED oscillations. Because of the metal-rich condition on the surface, this difference was inferred to be due to the addition of P. The P compositions determined from RHEED oscillations agreed with the *ex situ* measurements for the samples grown under the same PH_3 flow-rate fractions (PH_3 flow rate over the total hydride flow rate) and at the same substrate temperature. Therefore, the As and P incorporation behavior is somewhat different for InAsP and GaAsP growth.

A direct *in situ* composition determination for the quaternary compound InGaAsP will be very difficult because no simple binary compound can be chosen as a reference.[5] We can, nevertheless, control the composition in InGaAsP by combining the knowledge

of the *in situ* determination for GaAsP and InAsP. The growth rates of Ga and In are calibrated first by measuring group-III-induced RHEED oscillations on GaAs and InP substrates, respectively. The Ga composition in $In_{1-y}Ga_yAs_xP_{1-x}$ is then obtained as normally done for $III_yIII_{1-y}V$ compounds. It is reasonable to assume that the respective distribution of As flux to In and Ga is $(1-y)F_{As}$ and yF_{As}, where F_{As} denotes the As beam flux. Since the As composition in $In_{1-y}Ga_yAs_xP_{1-x}$ derives from As incorporation with both In and Ga, it can be estimated individually for InAsP and GaAsP as discussed above. The As incorporates with In with almost 100% efficiency, but incorporates with Ga with an efficiency p, which depends on the presence of P. Once p is determined for a given substrate temperature and PH_3 flow rate,[12] the As composition in $In_{1-y}Ga_yAs_xP_{1-x}$ can be found from $(1-y)R_{As}/R_{In}+ypR_{As}/R_{Ga}$. By using this method, we achieved a proper control of $In_{0.7}Ga_{0.3}As_{0.65}P_{0.35}$ lattice-matched to InP. High-resolution x-ray rocking curve, low-temperature photoluminescence and absorption spectra of this InGaAsP/InP multiple quantum well structure all indicate high quality.[5] The compositions calculated from these measurements agree with those determined from *in situ* control.

In summary, an *in situ* control of the As composition in $InAs_xP_{1-x}$ was achieved in GSMBE growth by controlling the ratio (when less than unity) of the incorporation rates of As to In as determined from As- and In-induced RHEED oscillations, respectively. The composition determination for as-grown InAsP/InP strained-layer superlattice structures by x-ray rocking curve measurements verified the viability of this *in situ* method when the PH_3 flow rate is not too large. The compositions in $In_{1-y}Ga_yAs_xP_{1-x}$ can therefore be controlled by considering the *in situ* composition calibration for GaAsP and InAsP.

This work was supported by the Office of Naval Research and the DARPA Optoelectronic Technology Center.

References:

1. For reviews, see M. B. Panish, Prog. Cryst. Growth Charact. **12**, 1 (1986), and M. B. Panish and H. Temkin, Annu. Rev. Mater. Sci. **19**, 209 (1989).
2. For a review, see W. T. Tsang, J. Cryst. Growth **105**, 1 (1990), and references therein.
3. M. B. Panish, H. Temkin, R. A. Hamm, and S. N. G. Chu, Appl. Phys. Lett. **49**, 164 (1986).
4. H. K. Tsang, J. B. D. Soole, H. P. LeBlanc, R. Bhat, M. A. Koza, and I. H. White, Appl. Phys. Lett. **57**, 2285 (1990).
5. H. Q. Hou and C. W. Tu, J. Cryst. Growth, (to be published).
6. R. P. Schneider, Jr., D. X. Li, and B. W. Wessels, J. Electrochem. Soc. **136**, 3490 (1989).
7. T. K. Woodward, T. Sizer, and T. H. Chiu, Appl. Phys. Lett. **58**, 1366 (1991).
8. H. Q. Hou, C. W. Tu, and S. N. G. Chu, Appl. Phys. Lett. **58**, 2954 (1991).
9. H. Seki and A. Koukitu, J. Cryst. Growth, **74**, 172 (1986).
10. T. Fukui and N. Kobayashi, J. Cryst. Growth **71**, 9 (1985).
11. J. H. Neave, B. A. Joyce, P. J. Dobson, and N. Norton, Appl. Phys. **A31**, 1(1983).
12. H. Q. Hou, B. W. Liang, T. P. Chin, and C. W. Tu, Appl. Phys. Lett. **59**, 292 (1991).
13. B. F. Lewis, R. Fernandez, A. Madhukar, and F. J. Grunthaner, J. Vac. Sci. Tech. **B4**, 560 (1986).
14. T. P. Chin, B. W. Liang, H. Q. Hou, M. C. Ho, C. E. Chang, and C. W. Tu, Appl. Phys. Lett. **58**, 254 (1991).
15. C. A. Chang, R. Ludeke, L. L. Chang, and L. Esaki, Appl. Phys. Lett. **31**, 759 (1977).

Figure Captions

Fig. 1. The As incorporation rate as a function of the AsH_3 flow rate calibrated at the substrate temperature of 460 °C for InAs grown on a thick InAs layer. The inset shows RHEED oscillations induced by In ($t_1<t<t_2$) and As ($t_3<t<t_4$). Note that the As-induced oscillations occurred on an In-rich surface caused by depositing In during $t_2<t<t_3$.

Fig. 2. The incorporation rate of (As+P), determined by group-V-induced RHEED oscillations during InAsP growth, as a function of the PH_3 flow rate at several fixed AsH_3 flow rates (0, 0.5, 0.75, 1 sccm). The lines through the data points are drawn to guide the eyes.

Fig. 3. The As composition in $InAs_xP_{1-x}$ determined from x-ray rocking curve measurements versus the incorporation ratio of As to In obtained from RHEED oscillations.

Fig. 4. The normalized As composition in $InAs_xP_{1-x}$ (ex-situ/in-situ) as a function of the flow-rate ratio of PH_3 to AsH_3 at fixed AsH_3 flow rates, 0.25 (full circles) and 0.4 sccm (open circles).

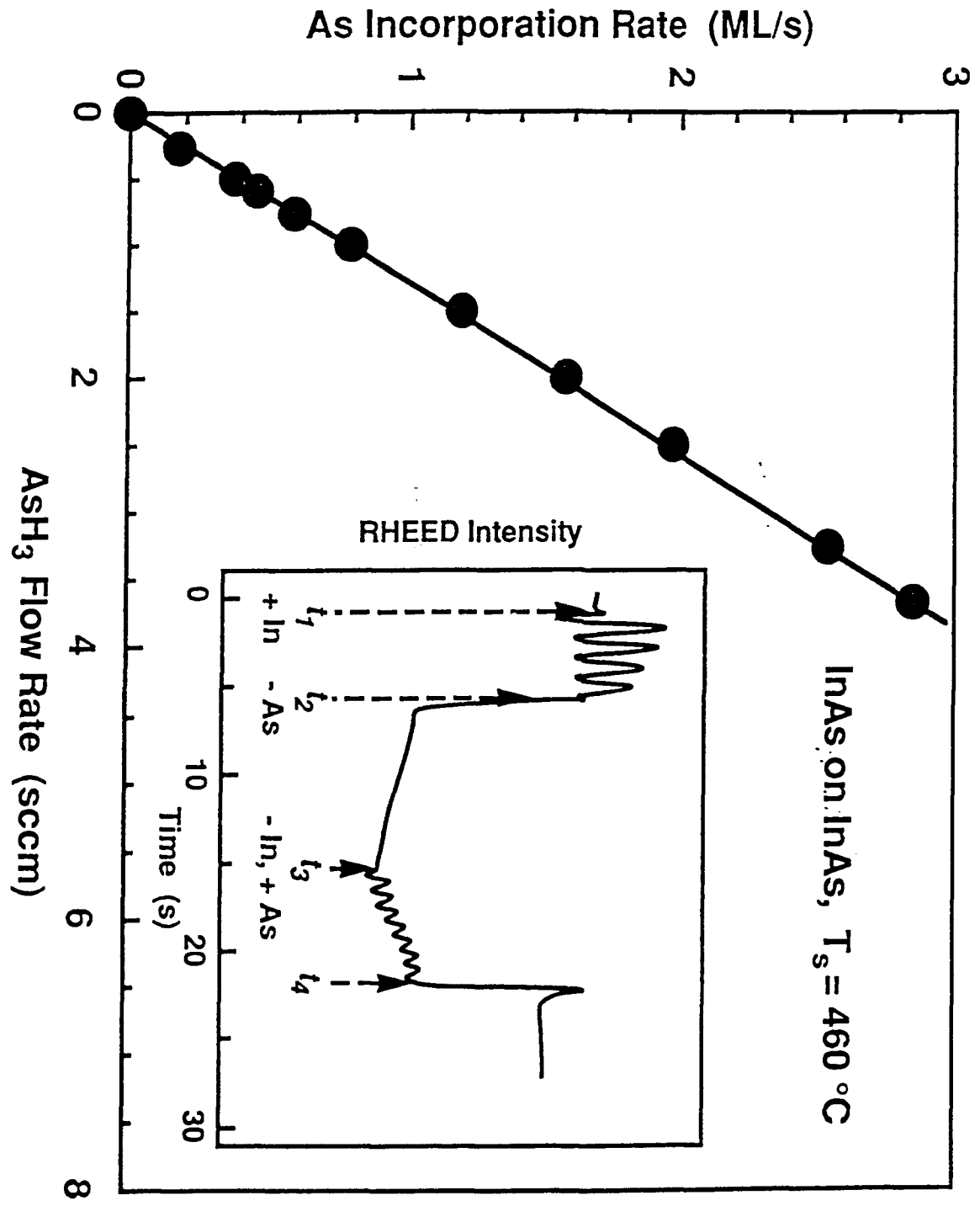
As Incorporation Rate (ML/s)
0
1
2
3
0
2
4
6
8
AsH3 Flow Rate (sccm)
InAs on InAs, Ts = 460 °C
RHEED Intensity
t1
+ In
t2
- As
t3
- In, + As
t4
0
10
20
30
Time (s)

Fig. 1

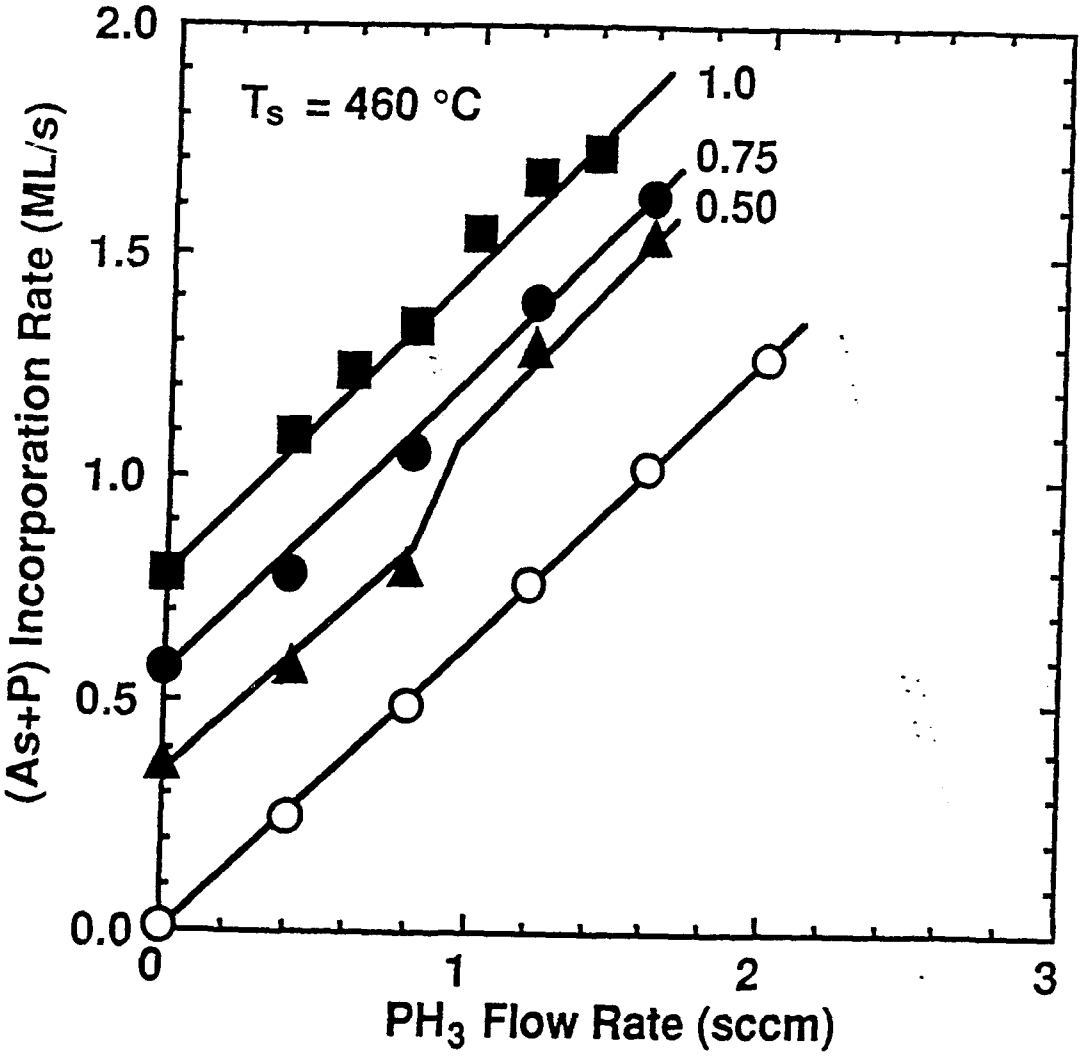
2.0
1.5
1.0
0.5
0.0
0
1
2
3
T_s = 460 °C
1.0
0.75
0.50
(As+P) Incorporation Rate (ML/s)
PH_3 Flow Rate (sccm)

Fig. 2

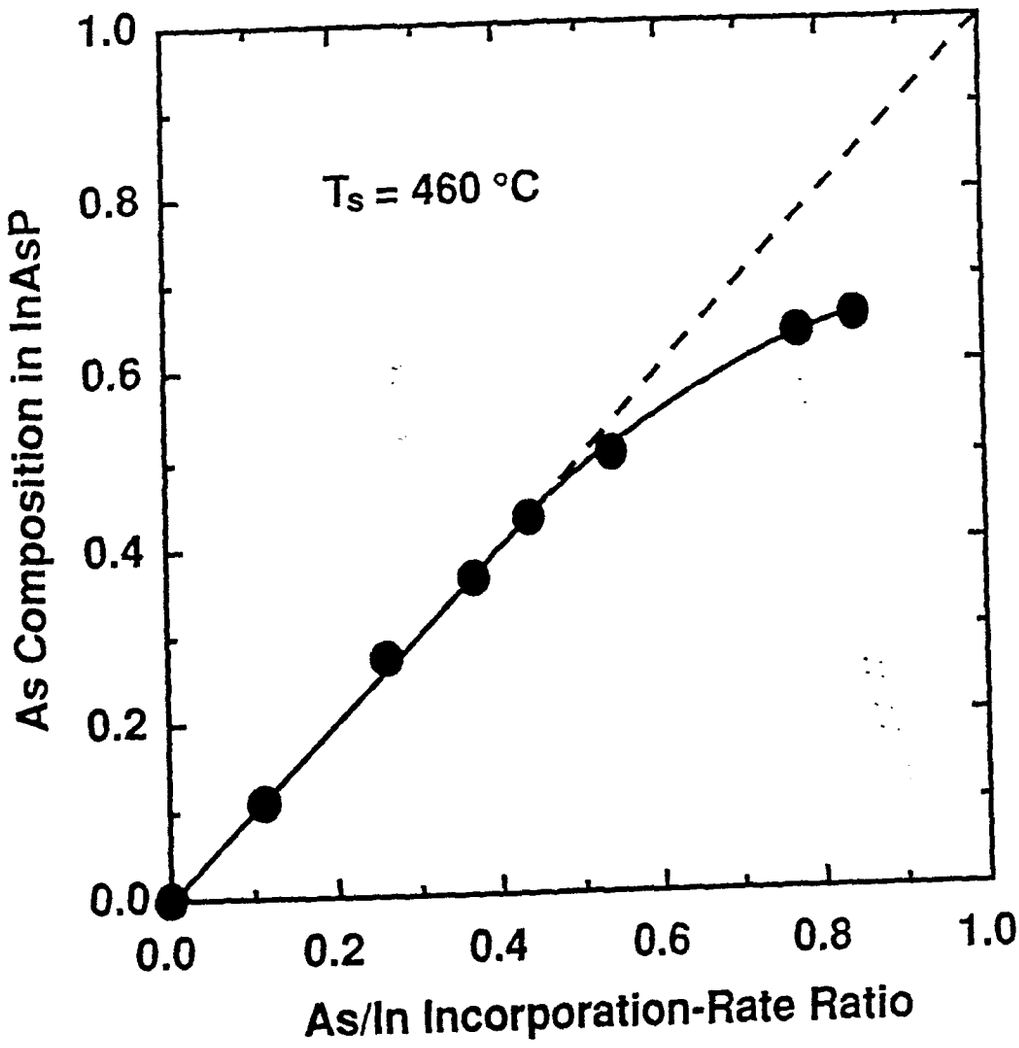
1.0
0.8
0.6
0.4
0.2
0.0
T_s = 460 °C
As Composition in InAsP
0.0
0.2
0.4
0.6
0.8
1.0
As/In Incorporation-Rate Ratio

Fig. 3

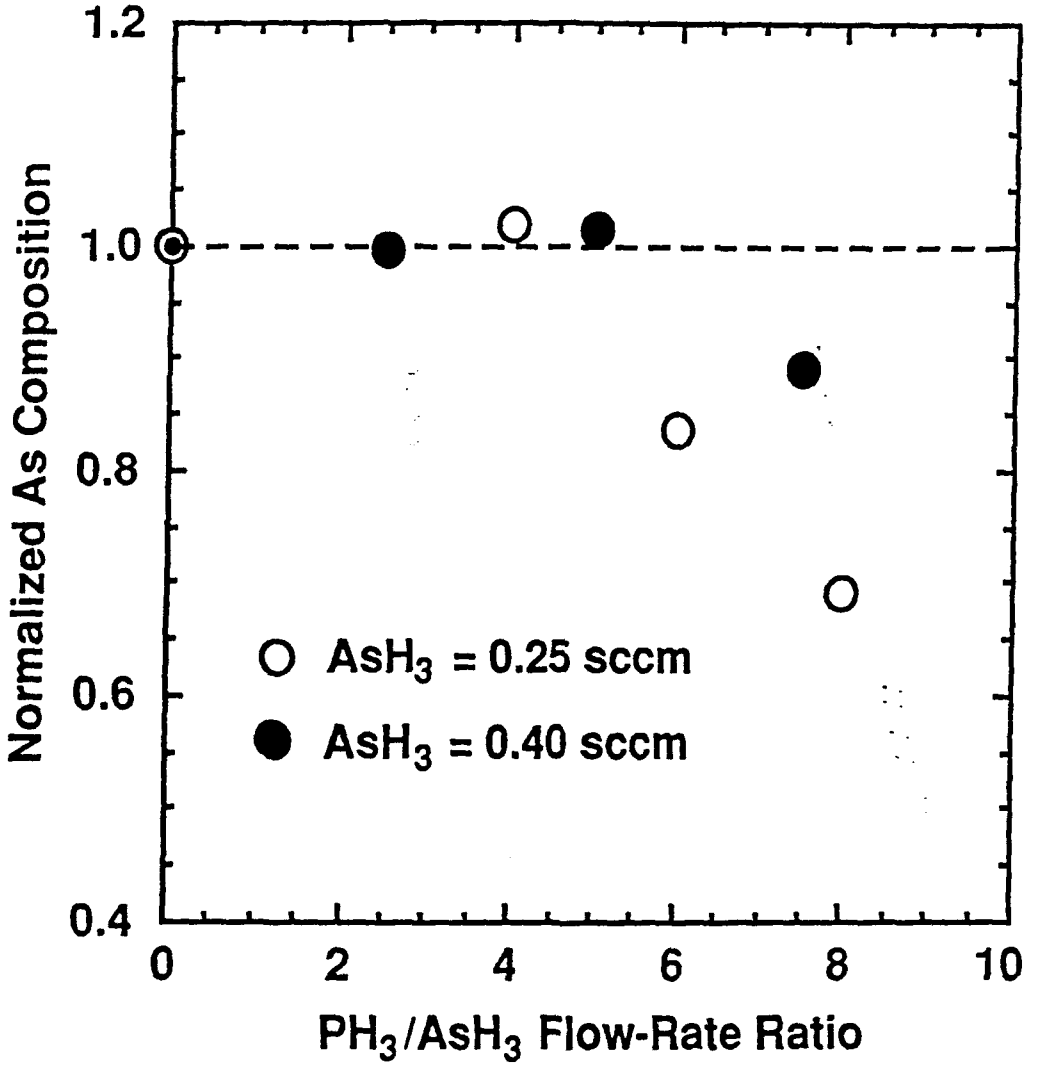
1.2
1.0
0.8
0.6
0.4
Normalized As Composition
0
2
4
6
8
10
PH3/AsH3 Flow-Rate Ratio
AsH3 = 0.25 sccm
AsH3 = 0.40 sccm

Fig. 4

To be published in J. Cryst. Growth
1992

InGaAsP/InP multiple quantum wells for optoelectronics grown by gas-source molecular beam epitaxy

H. Q. Hou and C. W. Tu

Department of Electrical and Computer Engineering,

University of California at San Diego, La Jolla, CA 92093-0407, U.S.A.

(Received)

ABSTRACT:

We have grown $In_{1-x}Ga_xAs_yP_{1-y}$/InP multiple quantum well structures with 1.3 μm excitonic absorption at room temperature by gas-source molecular beam epitaxy. In-situ composition determination in $GaAs_{1-x}P_x$ and $InAs_xP_{1-x}$ was carried out by measuring group-V-induced intensity oscillations of reflection high-energy electron diffraction. Based on the in-situ composition calibration for these ternary end members, the Ga and As composition in the quaternary compound, $In_{1-x}Ga_xAs_yP_{1-y}$, was controlled successfully. Measurements by x-ray rocking curve, low-temperature photoluminescence and absorption spectroscopy indicate that high-quality $In_{1-x}Ga_xAs_yP_{1-y}$/InP multiple quantum well samples were obtained.

I. INTRODUCTION

$In_{1-x}Ga_xAs_yP_{1-y}$ lattice-matched on InP is very important for long-wavelength optoelectronic applications.[1,2] Extensive studies on the material growth, characterization and device applications have been reported during the last decade.[3-5] Excitonic absorption at 1.06 μm can be achieved by growing strained InAsP/InP [6,7] or InGaAs/GaAs [8] multiple quantum wells (MQW's), and at 1.55 μm by lattice-matched InGaAs/InP MQW's.[9] Previously we reported [10] the growth of highly-strained InAsP/InP MQW's for 1.3 μm absorption at room temperature. The present study focuses on the preparation of lattice-matched $In_{1-x}Ga_xAs_yP_{1-y}$/InP MQW structures for modulators or lasers. The bandgap and lattice constant in the quaternary compound $In_{1-x}Ga_xAs_yP_{1-y}$ can be changed independently.[1,2] Fig. 1 shows the calculated Ga composition and room-temperature bandgap (in wavelength) of the $In_{1-x}Ga_xAs_yP_{1-y}$ lattice-matched to InP as a function of the As composition. To achieve 1.3 μm excitonic emission from an InGaAsP/InP MQW structure with a typical well width of 100 Å, an energy-level calculation [10] suggests that the bandgap of InGaAsP should be tuned to about 1.35 μm, due to the quantum-size effect. This requires growing $In_{0.7}Ga_{0.3}As_{0.65}P_{0.35}$.

The gas source molecular-beam epitaxy (GSMBE) technology, by using group-V hydride sources and elemental group-III sources, offers a convenient way to control the group-V beam fluxes by electronic mass flow controllers.[3] One of the key issues for growing quaternary compounds by GSMBE is composition control. In this paper we shall present an in-situ procedure for controlling the composition in $In_{1-x}Ga_xAs_yP_{1-y}$ by considering As and P incorporation behavior in $GaAs_{1-x}P_x$ and $InAs_xP_{1-x}$, as studied by group-V-induced intensity oscillations of reflection high-energy electron diffraction (RHEED).[11,12] We succeeded in growing $In_{1-x}Ga_xAs_yP_{1-y}$/InP MQW's with desired structural parameters. Characterizations by x-ray rocking curve, absorption and low-

temperature photoluminescence (PL) measurements suggest that high-quality samples were obtained.

II. IN-SITU COMPOSITION DETERMINATION FOR GaAsP AND InAsP

Epitaxial growth was performed in a Varian Modular GEN-II MBE system modified for handling arsine (AsH_3) and phosphine (PH_3). The growth chamber was evacuated by two cryopumps (2200 *l*/s for H_2) and one ion pump (150 *l*/s). Arsine and phosphine were introduced into the growth chamber through a four-channel Varian injector, which was operated at a nominal temperature of 1000 °C. The growth rate was measured by monitoring RHEED oscillations. More detailed growth conditions were reported previously,[11] and will not be repeated here.

As is well known, the period of RHEED intensity oscillations corresponds to the time to grow one monolayer on the surface.[13] Under normal MBE growth condition (group-V rich), the growth rate is limited by the beam flux of the group-III elements. However, if we *intentionally* create a group-III rich surface, then the growth will be controlled by the arrival rate of group-V atoms or molecules.[14,15] The RHEED oscillation results taken from $GaAs_{1-x}P_x$ grown on a Ga-rich GaAs surface yield a faster (As+P)-limited growth rate than As-limited growth rate. The difference in these growth rates was attributed to the incorporation of phosphorus. The phosphorus composition can, therefore, be determined.[11] The in-situ determined compositions agree with those derived from an ex-situ method, which determines the compositions by dynamical-theory simulations to x-ray rocking curves taken from $GaAs/GaAs_{1-x}P_x$ strained-layer superlattice structures grown under the same hydride flow rates and substrate temperature as the RHEED measurements.[11] Shown in fig. 2 are the results of in-situ (closed circles) and ex-situ (open circles) determined composition plotted against the PH_3 flow-rate fraction (PH_3 flow rate over the total hydride flow rate). It should be mentioned that the results shown in fig. 2 were obtained for a substrate temperature of 580 °C. and

results for 460 °C can be deduced from the temperature dependence of the As incorporation behavior. [16]

The incorporation behavior of As and P in $InAs_xP_{1-x}$, however, is quite different. Shown in fig. 3 are incorporation rates of (P+As) as a function of PH_3 flow rates at various fixed AsH_3 flow rates (0, 0.5, 0.75 and 1 sccm). These incorporation rates are determined by group-V-induced RHEED oscillations of $InAs_{1-x}P_x$ grown on InAs. The lines through the data points are drawn to guide the eyes. It appears that the incorporation rate of (As+P) has the same linear dependence on the PH_3 flow rate as the incorporation rate of only P itself (calibrated for InP grown on InP). The difference between the two cases is a constant offset corresponding to the additional incorporation of As. The jump in the incorporation rate for the results grown with 0.5 sccm AsH_3 may be due to the change of RHEED pattern of a highly-strained InAsP surface. We can, then, conclude that the As incorporation into $InAs_xP_{1-x}$ is independent of the presence of P under In-rich growth conditions. From a calculation of Gibbs free energies based on a thermodynamic model, Seki and Koukitu [17] predicted that InAs preferentially incorporates into $InAs_xP_{1-x}$, compared to InP. On the other hand, the incorporations of GaAs and GaP in $GaAs_{1-x}P_x$ are comparable. Now we can assume that the As incorporation into $InAs_xP_{1-x}$ is dominant in our normal growth conditions (group-V rich) with PH_3 flow rate < 2 sccm and substrate temperature at around 460 °C. In other word, phosphorus reacts with In only when there is not enough As to react with all of the In.[12] This situation makes controlling the As composition in $InAs_{1-x}P_x$ very simple. Once we calibrate the As and In incorporation rates at a desired growth temperature by group-V and group-III-induced RHEED oscillations, respectively, the ratio of the As to In incorporation rates (*when* ≤ 1) is basically the As composition in $InAs_xP_{1-x}$. Based on this idea of in-situ controlling the As composition, a series of InAsP/InP strained-layer superlattice structures were grown. The ex-situ determination by x-ray rocking curve measurements gives an excellent agreement with the in-situ results. This implies our assumption that As is dominantly

incorporated in InAsP under the normal growth conditions is correct, and the in-situ method to determine the composition is viable.

III. GROWTH OF InGaAsP/InP

It should be noted that the in-situ composition determination for these ternary compounds requires that the incorporation rate of As is not changed by adding P. Therefore, the compositions of GaAsP and InAsP are calculated with respect to the As-limited growth rates of GaAs and InAs, respectively. A direct in-situ composition calibration for InGaAsP would be difficult because no one simple binary compound can be chosen as a reference. We can, however, control the composition in InGaAsP by combining the knowledge of the in-situ determination for GaAsP and InAsP. The growth rates of Ga and In are calibrated first by measuring group-III-induced RHEED oscillations on GaAs and InP substrates, respectively. The Ga composition in $In_{1-x}Ga_xAs_yP_{1-y}$ is then obtained as normally done for $III_xIII_{1-x}V$ compounds. It is reasonable to assume that the distribution of As flux to In and Ga is $(1-x)F_{As}$ and xF_{As}, respectively, where F_{As} denotes the As beam flux. Since the As composition in $In_{1-x}Ga_xAs_yP_{1-y}$ derives from As incorporation with both In and Ga, it can be estimated individually for InAsP and GaAsP as discussed above. The As incorporates with In with almost 100% efficiency, but incorporates with Ga with an efficiency p, which depends on the presence of P, as shown in fig. 2. Once p is determined for a given substrate temperature and PH_3 flow rate, the As composition in $In_{1-x}Ga_xAs_yP_{1-y}$ can be found from $(1-x)R_{As}/R_{In}+xpR_{As}/R_{Ga}$. Here R denotes the incorporation rate. We grew a series of InGaAsP/InP MQW structures with growth rates of 0.67 ML/s for In and 0.28 ML/s for Ga as measured on InP and GaAs substrates, respectively. The PH_3 flow rate was fixed at 2 sccm, but the AH_3 flow rate varied from 0.8 sccm to 1.2 sccm. Combining x-ray rocking curve, PL and absorption measurements with simulations and calculations, we found the As composition to be very close to what is expected, as will be described in

the next section. Thus, the in-situ composition determination procedures described here provide a general guideline for composition control in InGaAsP quaternary compounds.

IV. Structural and Optical Property

The typical structure used in the present investigation consists of 20-period $In_{0.7}Ga_{0.3}As_{0.65}P_{0.35}$(100 Å)/InP(150 Å) undoped MQW's grown on an Fe-doped semi-insulating (100) InP substrate and capped with a 300 Å InP layer. Mirror-like surface morphology was obtained. High-resolution x-ray rocking curve was recorded for the symmetric (004) diffraction from a monochromatic line of Cu $K\alpha_1$ through four Ge crystals. The full width at half maximum (FWHM) for a 2 μm thick $In_{0.7}Ga_{0.3}As_{0.65}P_{0.35}$ was as narrow as 30 arc seconds, indicating good crystalline quality. As shown in fig. 4, very sharp and distinct satellite peaks are observed, suggesting good periodicity of the multi-layered structure. The zeroth order peak from these MQW's is only 38 arc seconds away from that of the InP substrate, corresponding to a lattice mismatch of 0.1%. Assuming abrupt interfaces, we carried out a simulation based on the dynamical theory. The best fit to the rocking curve gives structural parameters of $In_{0.7}Ga_{0.3}As_{0.65}P_{0.35}$ (101.5 Å)/InP(152 Å), which are in excellent agreement with those expected by the RHEED calibrations. It is also notable that some satellite peaks are missing in the rocking curve in fig 4. This can be attributed to interdiffusion at the InGaAsP/InP interface.[18]

Low-temperature PL was excited by the 488 nm line of an Ar^+ laser, dispersed by a 50 cm monochromator, and detected by a cooled Ge detector. The sample was mounted on the cold head of a close-cycle cryostat, and the measurement temperature was about 20 K. The PL spectra taken from 20-period MQW structures show very luminescent and sharp peaks, corresponding to the emission from the first heavy-hole (HH) interband excitons. The FWHM of emission peaks from these MQW's ranges from 6 to 9 meV. The transition energies agree well with the energy-level calculation based on an envelope-

function model with the structural parameters determined by RHEED and x-ray measurements. The PL results are comparable with those obtained from InAsP/InP quantum wells at 1.3 μm (4~9 meV). However, absorption spectra taken at room temperature from InGaAsP/InP quantum wells are not as sharp as that from InAsP/InP quantum wells, as represented by fig. 5(a) and 5(b), respectively. We believe that the built-in biaxial strain in the InAsP/InP quantum well splits the valence-band degeneracy, and the absorption peak from the light-hole (LH) becomes well resolved from the HH excitonic transition. On the other hand, only a relatively small splitting between HH and LH absorption peaks is generated by the quantum size effect for lattice-matched InGaAsP/InP quantum wells. Since the absorption peak is actually an overlap of HH and LH excitonic transitions, it is a broader from quaternary quantum wells than from ternary quantum wells.

V. Conclusion

High-quality InGaAsP/InP multiple quantum well structures with room temperature excitonic absorption at 1.3 μm have been grown by gas-source molecular beam epitaxy. The compositions in the quaternary compound were successfully controlled to desired values by in-situ composition determinations for GaAsP and InAsP from group-V-induced RHEED intensity oscillations. Both InAsP/InP strained MQW's and InGaAsP/InP MQW's with the same bandgap could be used for various optoelectronic applications.

The authors wish to thank B. W. Liang and T. P. Chin for helpful discussions of GSMBE growth. This work was partially supported by the DARPA Optoelectronic Technology Center and the Office of Naval Research.

REFERENCES:

1. H. C. Casey, Jr. and M. B. Panish, *Heterostructure Lasers*, (Academic Press, New York, 1978).
2. T. P. Pearsall, *GaInAsP alloy semiconductors*, (Wiley, New York, 1982).
3. M. B. Panish and Sumski, J. Appl. Phys. 55 (1984) 3571.
4. W. T. Tsang, M. C. Wu, T. Tanbun-Ek, R. A. Logan, S. N. G. Chu, and A. M. Sergent, Appl. Phys. Letters 57 (1990) 2065.
5. H. K. Tsang, J. B. D. Soole, H. P. LeBlanc, R. Bhat, M. A. Koza, and I. H. White, Appl. Phys. Letters 57 (1990) 2285.
6. T. K. Woodward, T. Sizer, and T. H. Chiu, Appl. Phys. Letters 58 (1991) 1366.
7. H. Q. Hou, C. W. Tu, and S. N. G. Chu, Appl. Phys. Letters 58 (1991) 2954.
8. T.K. Woodward, T. Sizer, D.L. Sivco, and A.Y. Cho, Appl. Phys. Letters 57 (1990) 548.
9. For a review, see W. T. Tsang, J. Cryst. Growth 105 (1990) 1.
10. H. Q. Hou, T. P. Chin, B. W. Liang, and C. W. Tu, Mat. Res. Soc. Symp. Proc. 228, (to be published).
11. H.Q. Hou, B.W. Liang, T.P. Chin, and C.W. Tu, Appl. Phys. Letters 59 (1991) 292.
12. H. Q. Hou and C. W. Tu, (unpublished).
13. J. H. Neave, B. A. Joyce, P. J. Dobson, and N. Norton, Appl. Phys. A31 (1983) 1.
14. B. F. Lewis, R. Fernandez, A. Madhukar, and F. J. Grunthaner, J. Vac. Sci. Tech. B4 (1986) 560.
15. T. P. Chin, B. W. Liang, H. Q. Hou, M. C. Ho, C. E. Chang, and C. W. Tu, Appl. Phys. Letters 58 (1991) 254.
16. B. W. Liang, H. Q. Hou, and C. W. Tu, Mat. Res. Soc. Symp. Proc. 222, (to be published).
17. H. Seki and A. Koukitu, J. Cryst. Growth, 74 (1986) 172.
18. J. C. P. Chang, T. P. Chin, K. L. Kavanagh, and C. W. Tu, Appl. Phys. Letters 58 (1991) 1530.

FIGURE CAPTIONS

Fig. 1. The Ga composition and room-temperature fundamental bandgap of $In_{1-x}Ga_xAs_yP_{1-y}$, lattice-matched to InP, as a function of the As composition.

Fig. 2. Phosphorus composition in $GaAs_{1-x}P_x$ as a function of the PH_3 flow-rate fraction, determined in-situ by group-V-induced RHEED oscillations (open circles) and ex-situ by x-ray rocking curves (full circles).

Fig. 3. The incorporation rate of (P+As) into $InAs_xP_{1-x}$ as a function of the PH_3 flow rate at a fixed AsH_3 flow rate of 0, 0.5, 0.75, and 1 sccm. The inset shows the agreement of the As composition in $InAs_xP_{1-x}$ from in-situ and ex-situ determinations.

Fig. 4. An x-ray rocking curve of (004) diffraction from a 20-period $In_{0.7}Ga_{0.3}As_{0.65}P_{0.35}$(101.5 Å)/InP(152 Å) MQW structure. Some satellite peaks are missing because of the intermixing at the InGaAsP/InP interface.

Fig. 5. Absorption spectra taken at room temperature for (a) InGaAsP(101.5 Å)/InP(152 Å) MQW's, and (b) InAsP(92 Å)/InP(138 Å) strained MQW's.

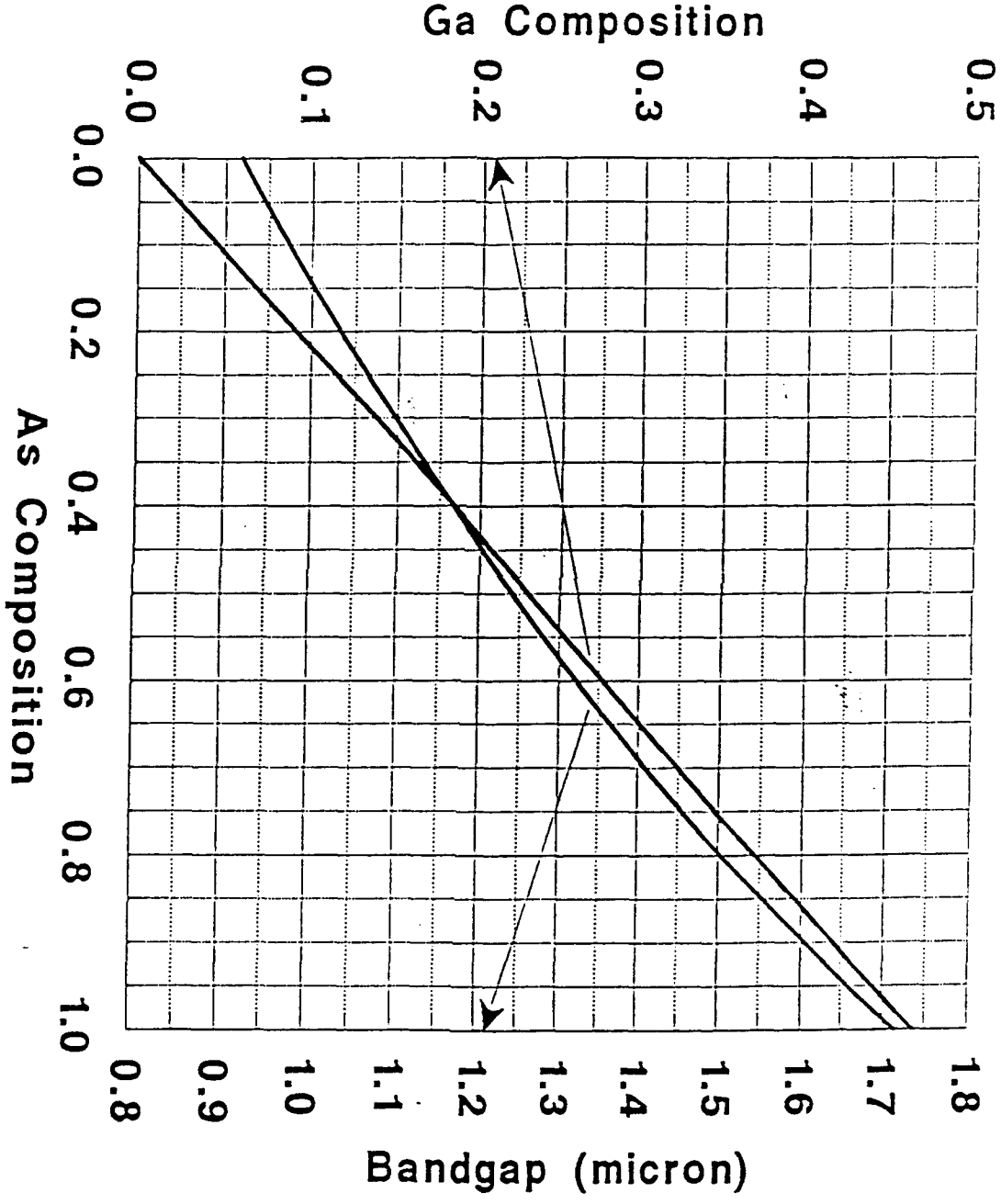
Ga Composition
0.0
0.1
0.2
0.3
0.4
0.5
As Composition
0.0
0.2
0.4
0.6
0.8
1.0
Bandgap (micron)
0.8
0.9
1.0
1.1
1.2
1.3
1.4
1.5
1.6
1.7
1.8

Fig. 1

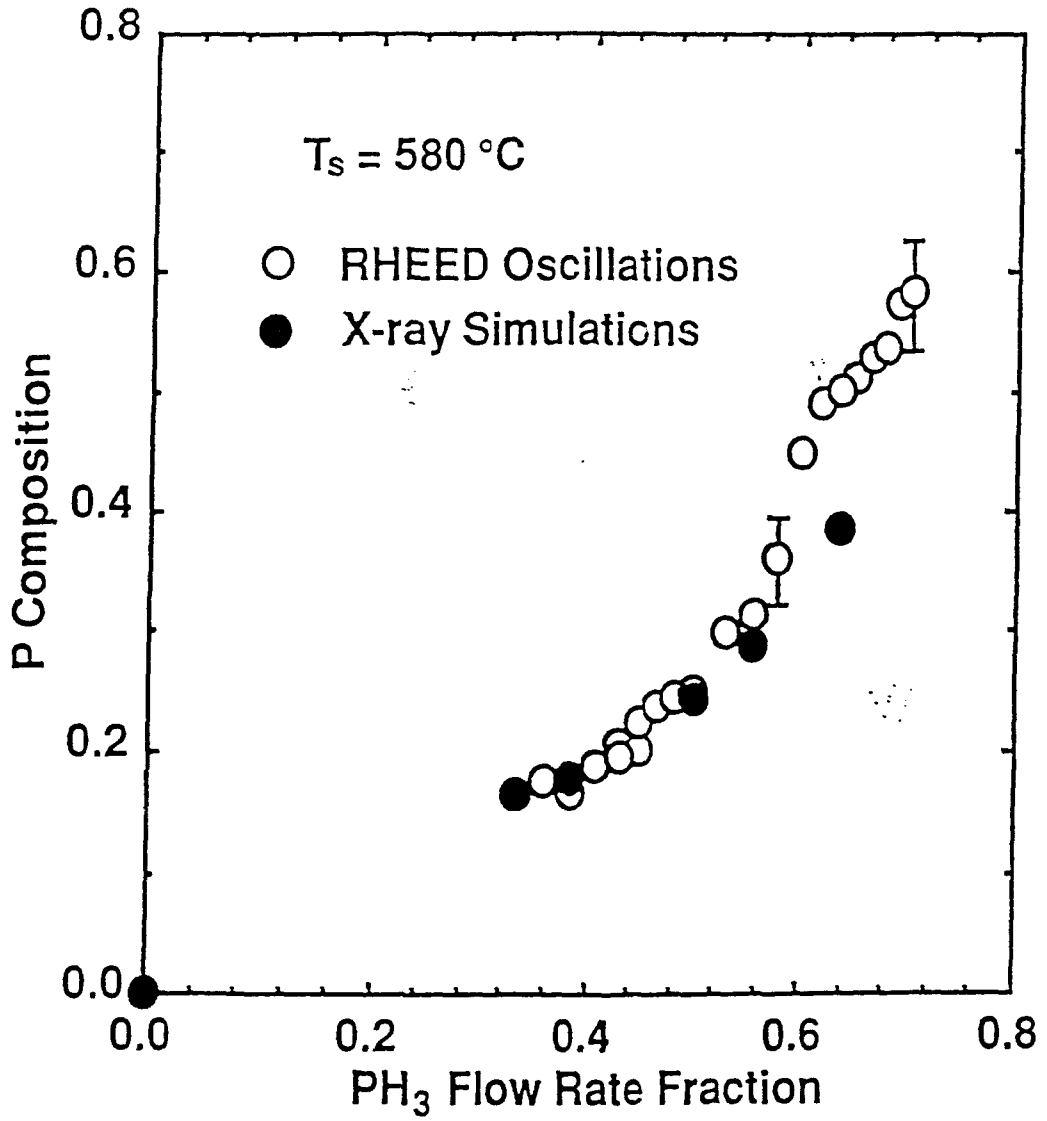
0.8
0.6
0.4
0.2
0.0
P Composition
T_S = 580 °C
RHEED Oscillations
X-ray Simulations
0.0
0.2
0.4
0.6
0.8
PH_3 Flow Rate Fraction

Fig. 2

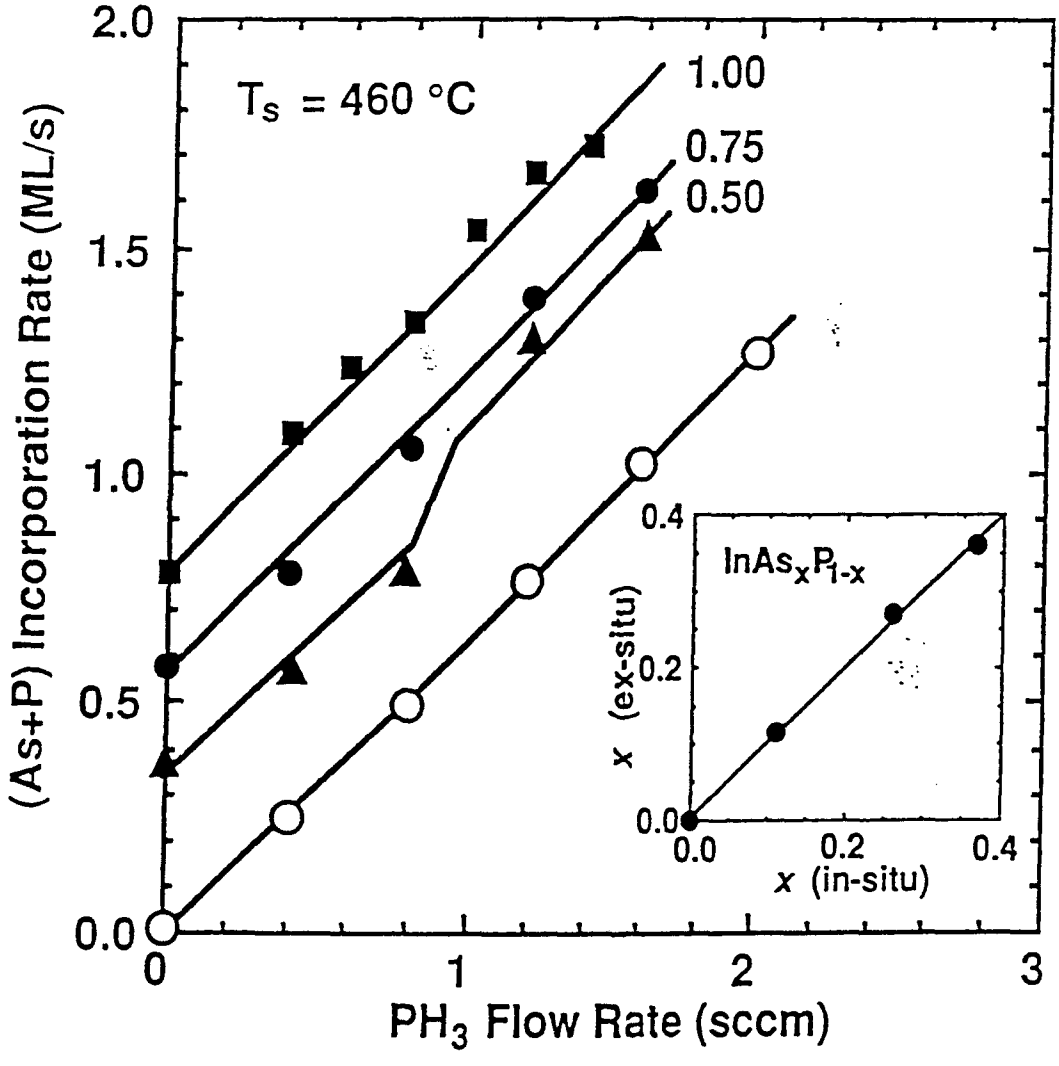
2.0
1.5
1.0
0.5
0.0
0
1
2
3
T_s = 460 °C
1.00
0.75
0.50
(As+P) Incorporation Rate (ML/s)
PH_3 Flow Rate (sccm)
$InAs_xP_{1-x}$
0.4
0.2
0.0
0.0
0.2
0.4
x (ex-situ)
x (in-situ)

Fig. 3

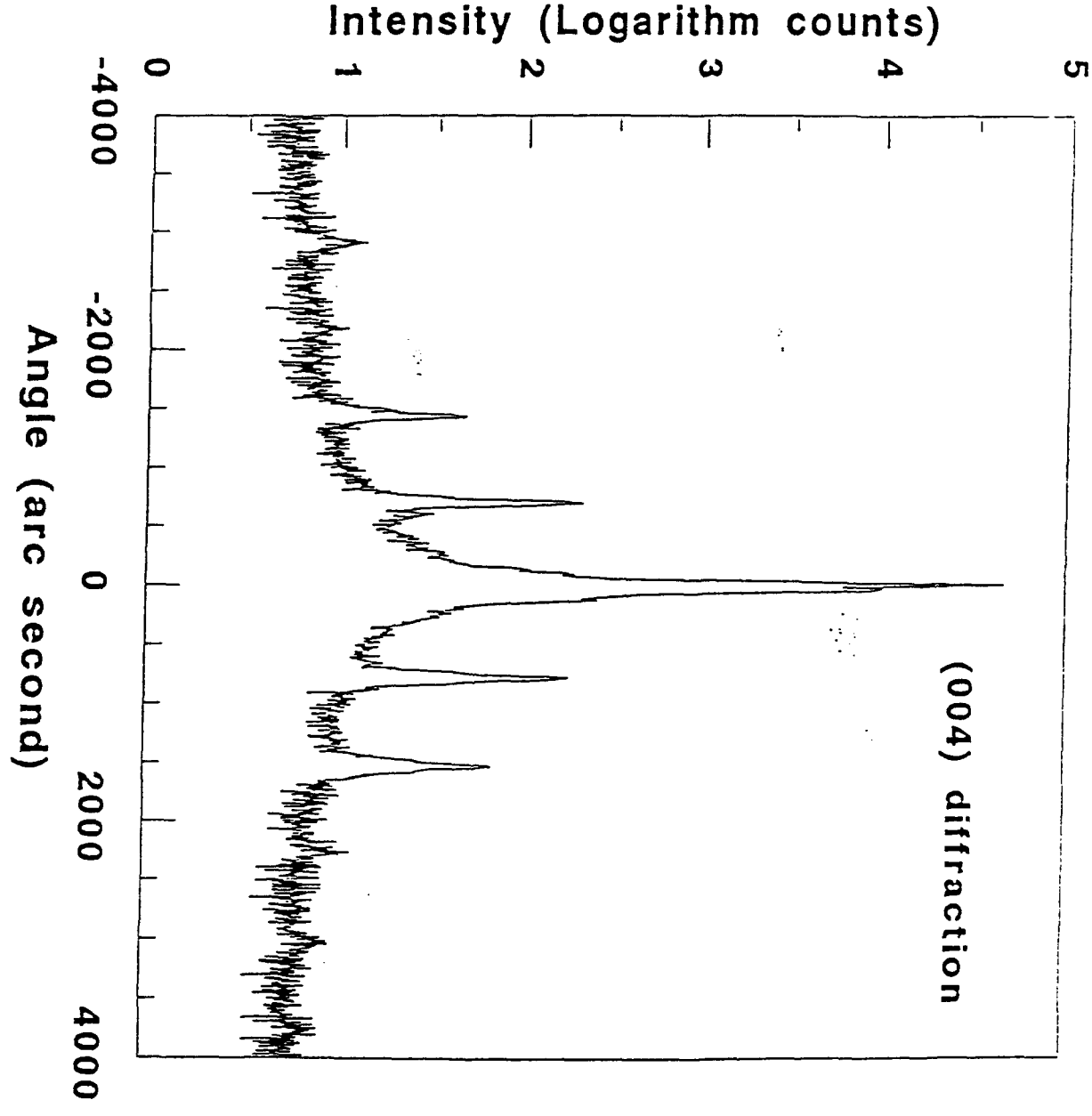
Intensity (Logarithm counts)
0
1
2
3
4
5
-4000
-2000
0
2000
4000
Angle (arc second)
(004) diffraction

Fig. 4

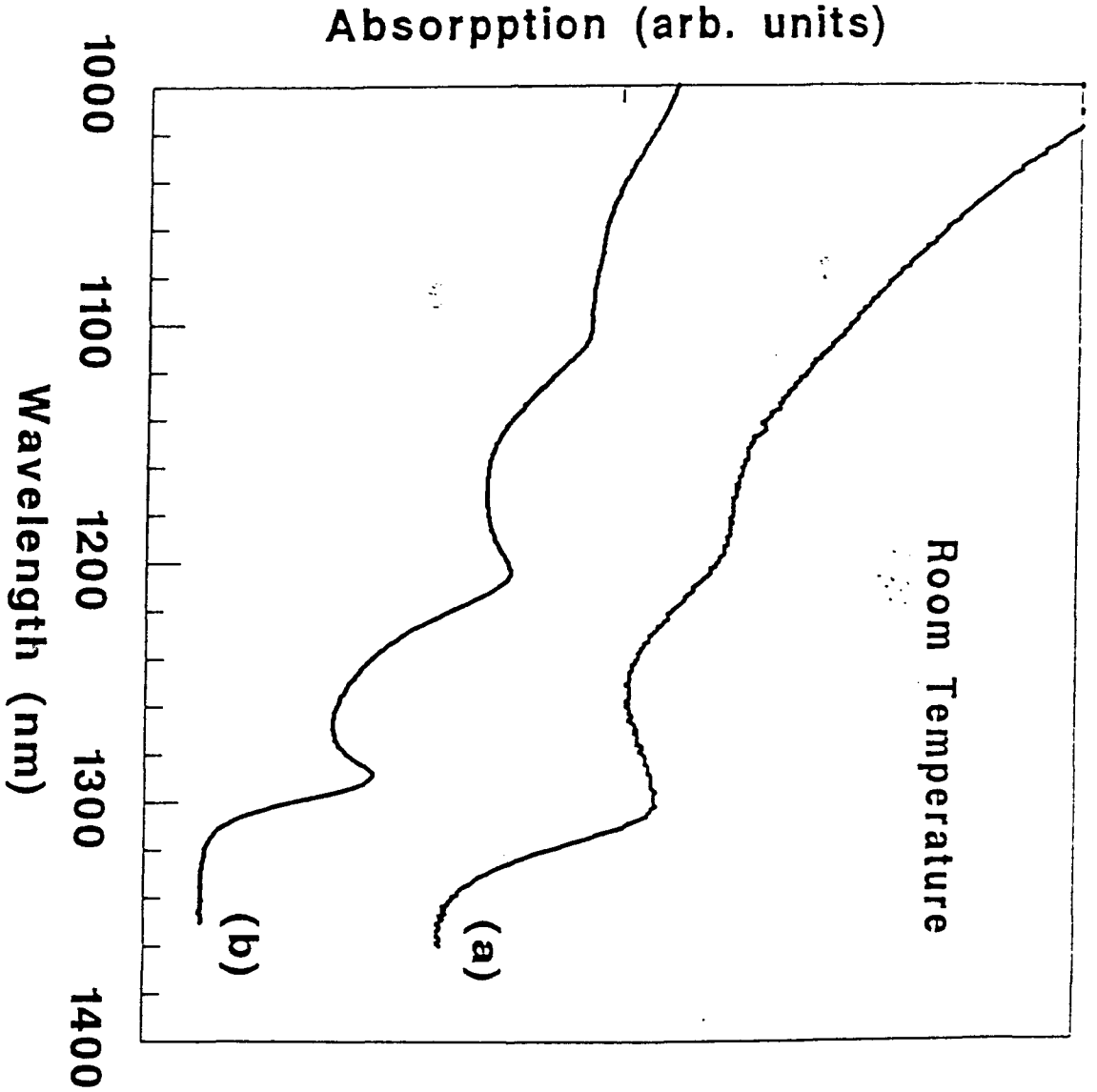
Absorpption (arb. units)
1000
1100
1200
1300
1400
Wavelength (nm)
Room Temperature
(a)
(b)

Fig. 1

12-16

A Study of Group-V Desorption from InP and InAs by Reflection High-Energy Electron Diffraction

B. W. Liang and C. W. Tu

Department of Electrical and Computer Engineering, University of California at San Diego, CA 92093-0407

Abstract

Desorption behaviors of arsenic on InAs and phosphorus on InP surface have been studied by the specular-beam intensity change of reflection high-energy electron diffraction when the group-V-cracker shutter is closed in gas-source molecular-beam epitaxy. We obtained an activation energy of 55 kcal/mole for arsenic desorption from InAs at high temperature, and 38 kcal/mole at low temperature. This difference is explained. Compared with arsenic on InAs, phosphorus on InP has a very large desorption rate constant and only one activation energy of 50 kcal/mole.

PACS numbers: 68.55.Bd, 68.45.Da, 61.50.Cj

Desorption is one of the important steps in molecular-beam epitaxy (MBE) and metalorganic MBE of III-V compound semiconductors, especially for group-V elements.[1,2] Because group-V elements, such as arsenic, have large desorption rate at normal growth temperatures, we can easily obtain stoichiometric binary compounds, such as GaAs, by using group-V overpressure. On the other hand, during the growth of mixed group-V ternary compounds, such as GaAsP, because of non-unity sticking coefficients of group-V elements, one may have difficulty in controlling the composition.[3] Therefore, desorption is an important issue.

Recently, low-temperature (LT) growth of GaAs and AlGaAs has received much attention because of their high-resistivity properties.[4-6] About 1 to 1.5% extra arsenic is found in LT GaAs. On the other hand, we have found that InP and InAs grown at LT have low resistivity.[7,8] Group-V-rich related native defects, such as group-V antisite defects, are assumed to explain the experimental results since a relatively small amount of group-V element desorbs from the growth front at LT, compared to that at normal growth temperature. Therefore, desorption plays an even more important role in LT materials.

Foxon *et al.* used modulated-beam mass spectroscopy (MBMS) to study As_4 and As_2 desorption behaviors on GaAs,[9] and Zhang *et al.* studied indium desorption from InAs.[10] Chow and Fernandez used group-V induced intensity oscillations of reflection high-energy electron diffraction (RHEED) to compare the difference in desorption behavior between As_4 and

As_2.[11] We used the same method to study phosphide materials grown by gas-source molecular-beam epitaxy (GSMBE).[12] We have also used this method to perform an *in situ* composition determination of mixed group-V ternary compounds.[13] However, the desorption obtained by the group-V-induced RHEED intensity oscillations is carried out on a group-III-rich surface, which is different from the real growth situation. In this letter, we present a simple method to study group-V desorption behaviors of arsenic on InAs and phosphorus on InP by monitoring the change of the RHEED intensity when the hydride-cracker shutter is opened or closed. Comparing the desorption rate constants in these two cases, we can obtain a better understanding of the *in situ* composition control of mixed-group-V ternary InAsP compound during GSMBE.[14]

The desorption study is performed in an Intervac Gen II MBE system, modified as GSMBE, which can handle AsH_3 and PH_3. We have described this system previously.[12] The electron energy for RHEED is 10 keV. The substrates are semi-insulating (SI) (001) InP and 1-μm thick InAs grown on SI (001) GaAs.

Since the specular-beam intensity of RHEED corresponds to the smoothness of the growing surface,[15] it is obvious that during the growth interruption, when we close the group-V cracker shutter, group-V desorption from the surface would make the surface rough at the normal growth temperature. Figs. 1 and 2 show the change of the RHEED specular-beam intensity as a function of time at different substrate

temperatures for InAs and InP, respectively. In Figs. 1(a) and 2(a), when the cracker shutter is closed, the RHEED specular-beam intensity decreases. The higher the substrate temperature is, the faster the intensity decays. However, in Figs. 1(b) and 2(b), which are obtained in a lower temperature range, when we close the cracker shutter, the RHEED specular-beam intensity increases. This indicates that during growth interruption at low temperature excess group-V species, accumulated on the growing surface,[7] desorb.

If we assume that the change of the specular-beam intensity is due to group-V species desorption, we can obtain the kinetics parameter of group-V desorption from the transition time. Because the intensity decays (or increases in the low temperature range) exponentially, it is reasonable to assume the desorption is a first-order process. From the time constant of the transition, we obtain the desorption rate constants (k's). Fig. 3 shows the desorption rate constants of arsenic from InAs and phosphorus from InP as a function of the reciprocal substrate temperature. Phosphorus desorption rate constant is much higher than that of arsenic in the high-temperature range. From Fig. 3, we can obtain the activation energy for arsenic and phosphorus desorption. The activation energy for arsenic desorption from InAs is 55 kcal/mole at high temperature, and 38 kcal/mole at low temperature. For phosphorus, it is 50 kcal/mole.

What kinds of species desorb from the growth front? Based on the experimental results obtained so far, we believe

that at high temperature they are group-V dimer molecules. The reasons are as follows: (a) cracked hydrides produce mainly dimer molecules;[16] (b) the dimer is the dominant species in the vapor phase when in equilibrium with a solid III-V compounds;[17] and (c) the desorption activation energies for arsenic and phosphorus as obtained above are comparable to the heat of vaporization of As_2 (56 kcal/mole) and P_2 (42 kcal/mole) in the same temperature ranges, respectively.[18] However, for arsenic on InAs at low temperature, the desorption activation energy is comparable to the heat of vaporization of As_4 (33 kcal/mole).[18] This may imply that at low temperature most of As_2 molecules on InAs surface combine into As_4, which desorbs faster than As_2. This kind of difference between high and low temperature ranges is similar to that found by Zhang et al., where the behavior of indium desorption from InAs at high temperature is different from that at low temperature.[10] They explained the difference to be that in the high-temperature range indium desorbs from the InAs surface, but in the low-temperature range indium desorbs from indium droplets on the InAs surface. For phosphorus desorption from InP, because there is no difference in the activation energy between the two temperature ranges, we believe that no P_4 is formed on the InP surface even at low substrate temperature.

From a thermodynamic point of view, given the same group-III element, phosphides are more stable than arsenides, and arsenides are more stable than antimonides.[19] In MBE of

mixed group-V ternary compounds the sticking coefficients of antimony, arsenic and phosphorus are in a decreasing order in the normal temperature range.[3,20] We believe this trend corresponds to the vapor pressures in an increasing order. This means that the MBE growth process is far from thermodynamic equilibrium. Therefore, kinetics controls the composition of group-V elements in a mixed-group-V compound, and the desorption plays a key role.

Under steady state conditions, the beam flux (F) of the group-V element at the growth front is the sum of three parts, reflection (R_r), desorption (R_d) and incorporation (R_g) during growth, i.e., $F = R_g + R_d + R_r$. Because the product of flux and sticking probability (S) is the flux less the reflection component, $FS = F - R_r$, then $FS = R_g + R_d$. The desorption rate $R_d = kC_v$, where k, which equals $Aexp(-E_a/kT)$, is the desorption rate constant as discussed previously, and C_v is the group-V surface concentration.[3] The arsenic composition x in $InAs_xP_{1-x}$ is $x = R_g(As)/[R_g(As) + R_g(P)]$. Because the desorption rate constant of arsenic is much smaller than that of phosphorus, when FS(As) and FS(P) are comparable, $R_g(As)$ is greater than $R_g(P)$. Therefore, arsenic incorporation is dominant in growing InAsP. When the incorporation rate of arsenic is less than that of indium, as determined by group-V- and group-III-induced RHEED oscillations, all of arsenic that adsorbs on the growing surface can be expected to combine with indium, and phosphorus then combines with the rest of indium. Therefore,

the InAs composition in $InAs_xP_{1-x}$ can be determined *in situ* simply by the ratio of the incorporation rate of arsenic to indium.[14]

In conclusion, we have studied the desorption behaviors of arsenic on InAs and phosphorus on InP by the RHEED intensity decay when the group-V shutter is closed. We found that the desorption behaviors follow the equilibrium vapor pressure curves of arsenic and phosphorus. For InAs, it is As_2 that desorbs from InAs in the high-temperature range, and probably As_4 in the low-temperature range. Compared to arsenic on InAs, phosphorus on InP has a much higher desorption-rate constant. This result can explain why arsenic is the dominant species in InAsP grown by GSMBE.

This work is partially supported by the Office of Naval Research. We wish to thank Messrs. T. P. Chin, M. C. Ho and H. Q. Hou for assistance in the GSMBE system, and Dr. W. Weiss for useful discussion.

Referencs

[1] A. Y. Cho, J. Appl. Phys. **42**, 2074 (1971).

[2] B. W. Liang and C. W. Tu, Appl. Phys. Lett. **57**, 689 (1990).

[3] B. W. Liang, H. Q. Hou and C. W. Tu, Mat. Res. Soc. Symp. Proc. **222**, 145 (1991).

[4] F. W. Smith, A. R. Calawa and C. Chen, IEEE Electron Device Letters **EDL-9**, 77 (1988).

[5] Z. L. Weber, G. Cooper, R. Mariella, Jr. and C. Kocot, J. Vac. Sci. Technol. **B9**, 2323 (1991).

[6] A. C. Warren, N. Katzenellenbogen, D. Grischkowsky, J. M. Woodall, M. R. Melloch and N. Otsuka, Appl. Phys. Lett. 58, 1512 (1991).

[7] B. W. Liang, K. Ha, J. Zhang, T. P. Chin, and C. W. Tu, SPIE Proc. **1285**, 116 (1990).

[8] B. W. Liang, Y. He and C. W. Tu, Mat. Res. Soc. Symp. Proc. **241** (1991).

[9] C. T. Foxon and B. A. Joyce, Surf. Sci. **64**, 293 (1977).

[10] J. Zhang, E. M. Gibson, C. T. Foxon and B. A. Joyce, J. Cryst. Growth **111**, 93 (1991).

[11] R. Chow and R. Fernandez, Mat. Res. Soc. Symp. Proc. **145**, 13 (1989).

[12] T. P. Chin, B. W. Liang, H. Q. Hou, M. C. Ho, C. E. Chang, and C. W. Tu, Appl. Phys. Lett. **58**, 254 (1991).

[13] H. Q. Hou, B. W. Liang, T. P. Chin, and C. W. Tu, Appl. Phys. Lett. **59**, 292 (1991).

[14] H. Q. Hou and C. W. Tu, submitted to Appl. Phys. Lett.

[15] J. H. Neave, B. A. Joyce, P. J. Dobson and N. Norton, Appl. Phys. **A31**, 1 (1983).

[16] M. Panish and S. Sumski, J. Appl. Phys. **55**, 3571 (1984).

[17] J. R. Arthur, J. Phys. Chem. Solids **28**, 2257 (1967).

[18] C. J. Smithells, Metals Reference Book, 4th. Ed. Vol.1 (Butterworths Scientific Publ., 1967) p. 264.

[19] M. Yano, H. Yokose, Y, Iwai and M. Inoue, J. Cryst. Growth **111**, 609 (1991).

[20] C. A. Chang, R. Ludeke, L. L. Chang and L. Esaki, Appl. Phys. Lett. **31**, 759 (1977).

Figure Captions

Fig.1 The RHEED specular-beam intensity of InAs as a function of time when As shutter closed and opened at different temperatures. (a), in the high-temperature range; (b), in the low-temperature range.

Fig.2 The RHEED specular-beam intensity of InP as a function of time when As shutter closed and opened at different temperatures. (a), in the high-temperature range; (b), in the low-temperature range.

Fig.3 The ln of the desorption-rate constants of arsenic on InAs (solid circles with solid fitting lines) and phosphorus on InP (open squares with a dashed fitting line) as a function of the reciprocal substrate temperatures.

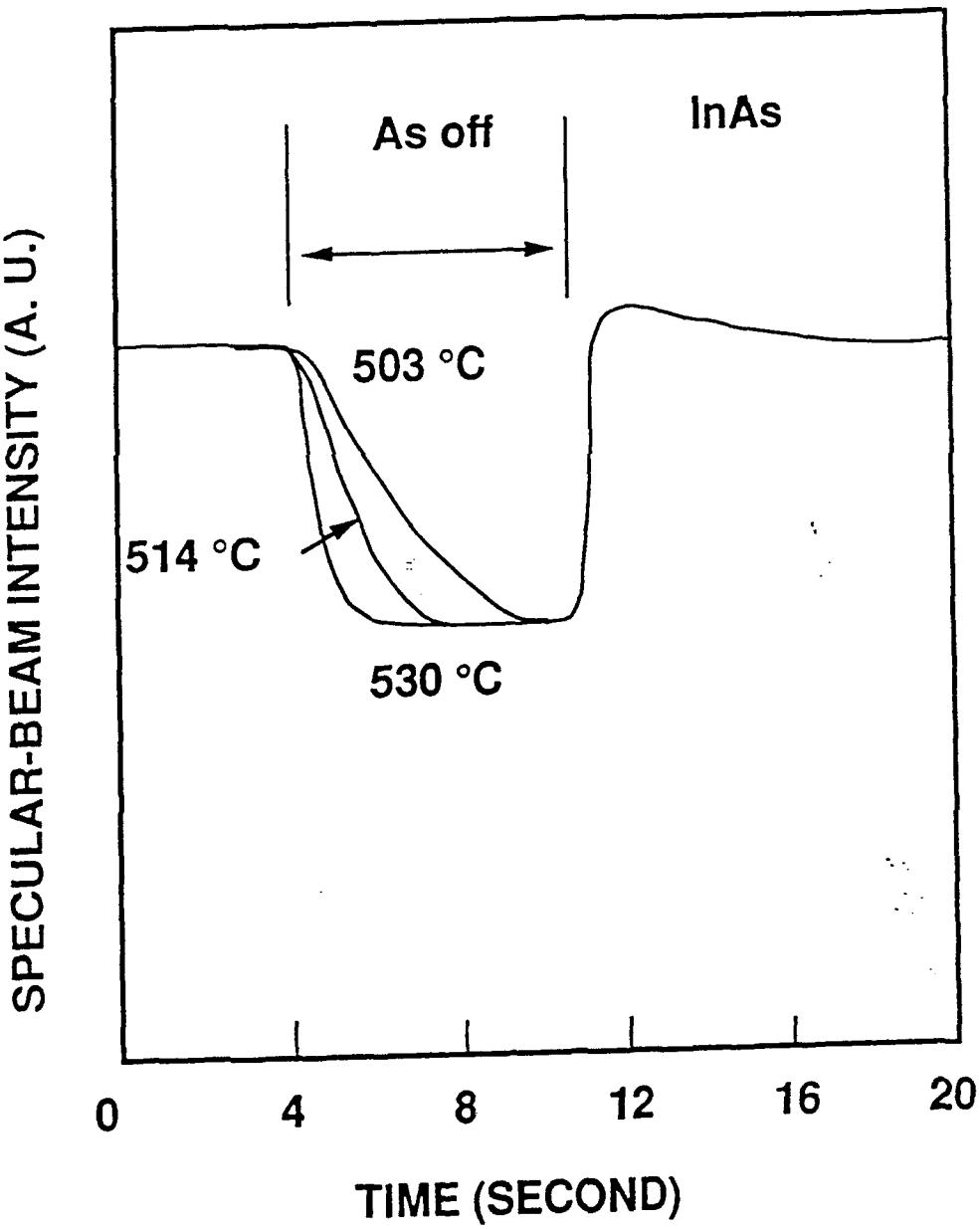
As off
InAs
503 °C
514 °C
530 °C
SPECULAR-BEAM INTENSITY (A. U.)
0
4
8
12
16
20
TIME (SECOND)

Fig. 1 (a)

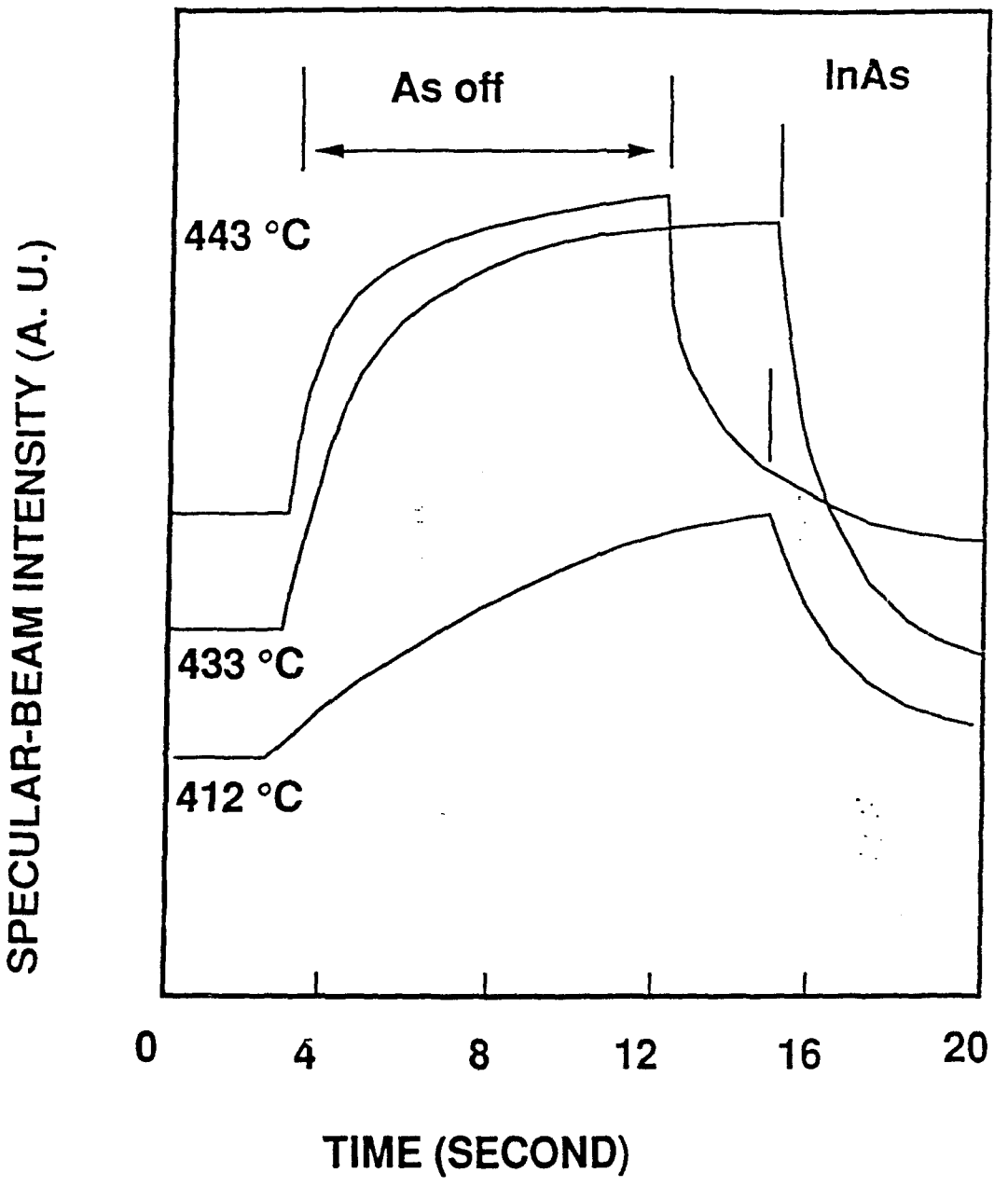
As off
InAs
443 °C
433 °C
412 °C
SPECULAR-BEAM INTENSITY (A. U.)
0
4
8
12
16
20
TIME (SECOND)

Fig. 1(b)

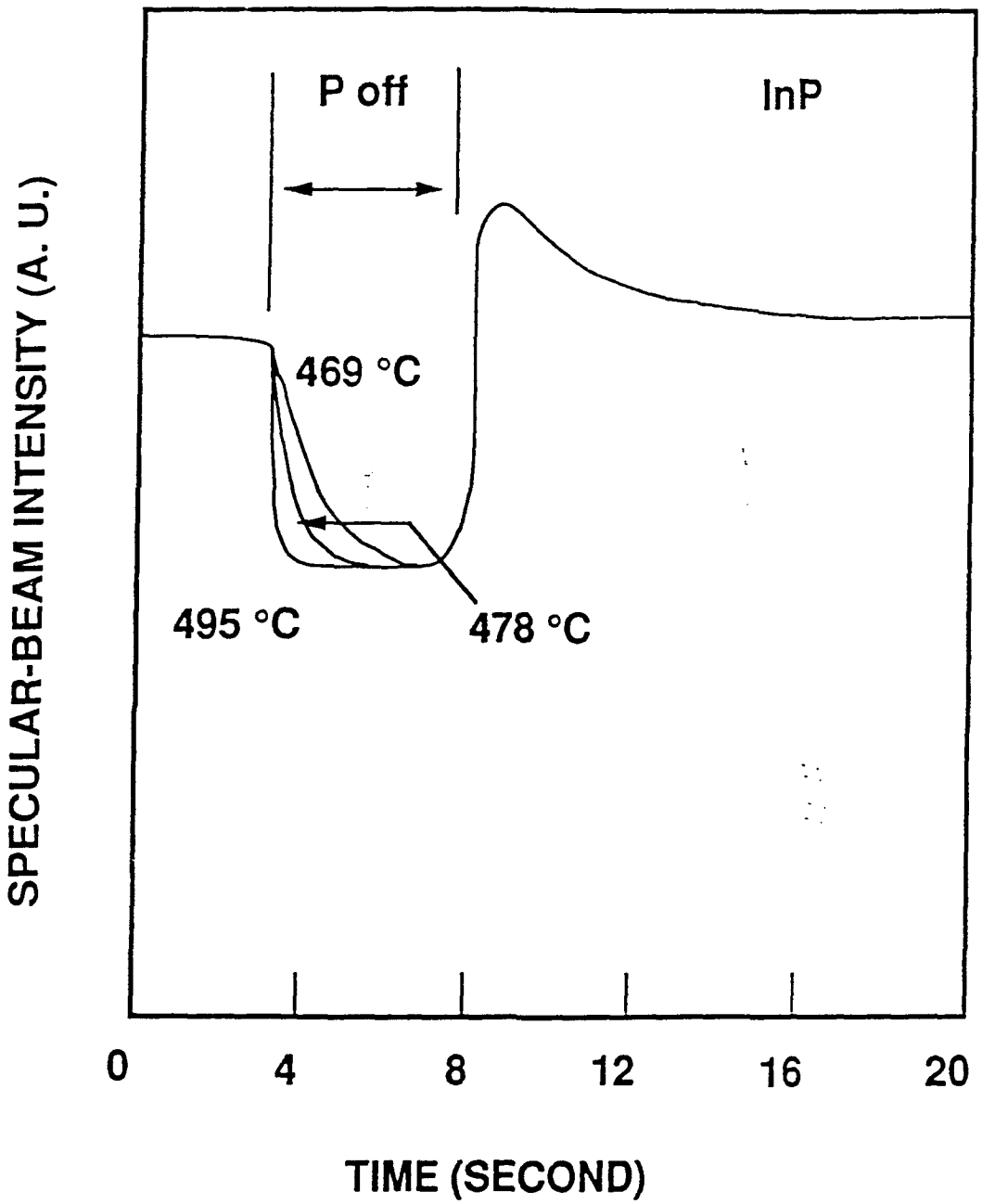
P off
InP
469 °C
495 °C
478 °C
SPECULAR-BEAM INTENSITY (A. U.)
0
4
8
12
16
20
TIME (SECOND)

Fig. 2 (a)

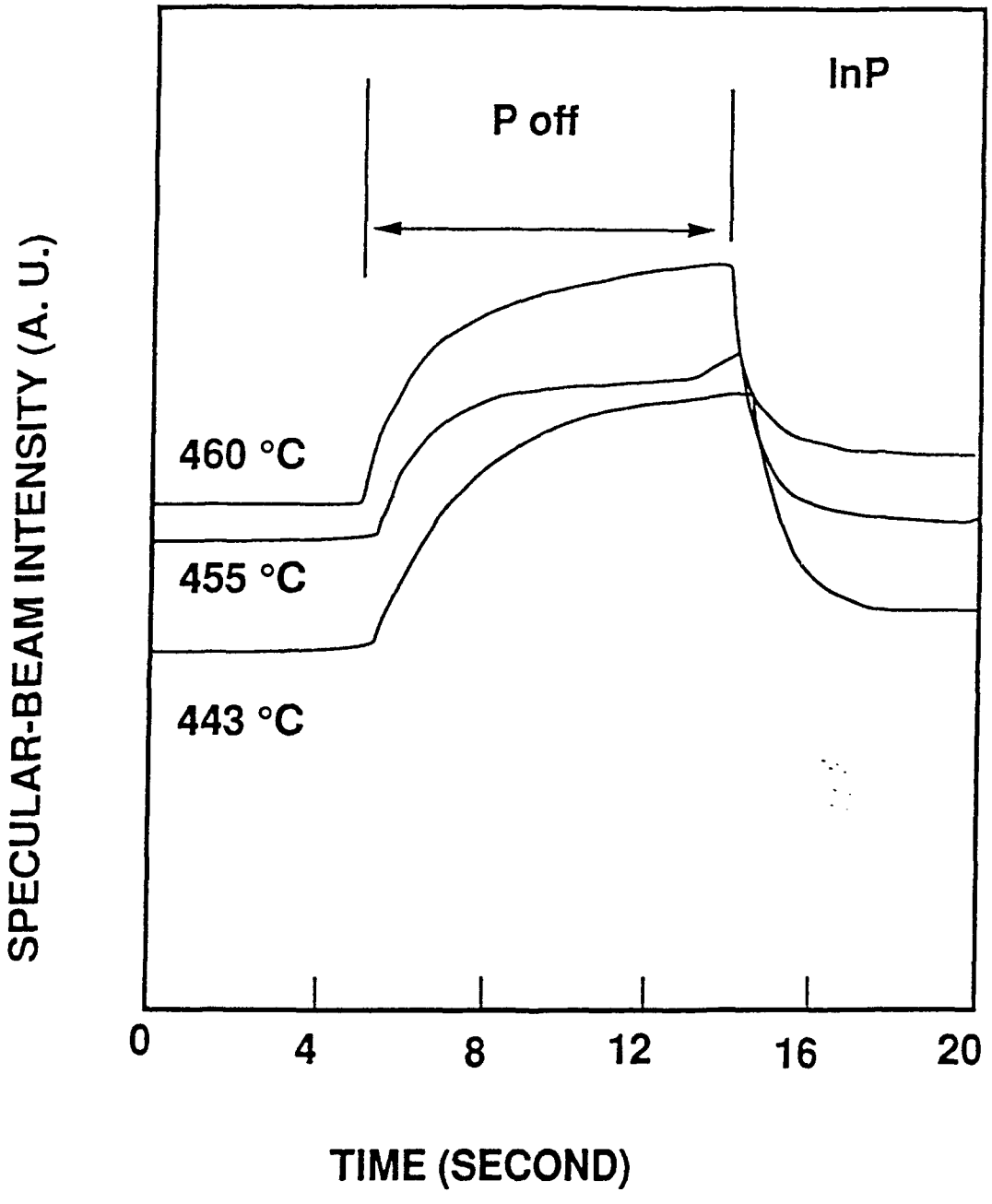
InP
P off
460 °C
455 °C
443 °C
SPECULAR-BEAM INTENSITY (A. U.)
0
4
8
12
16
20
TIME (SECOND)

Fig. 2b

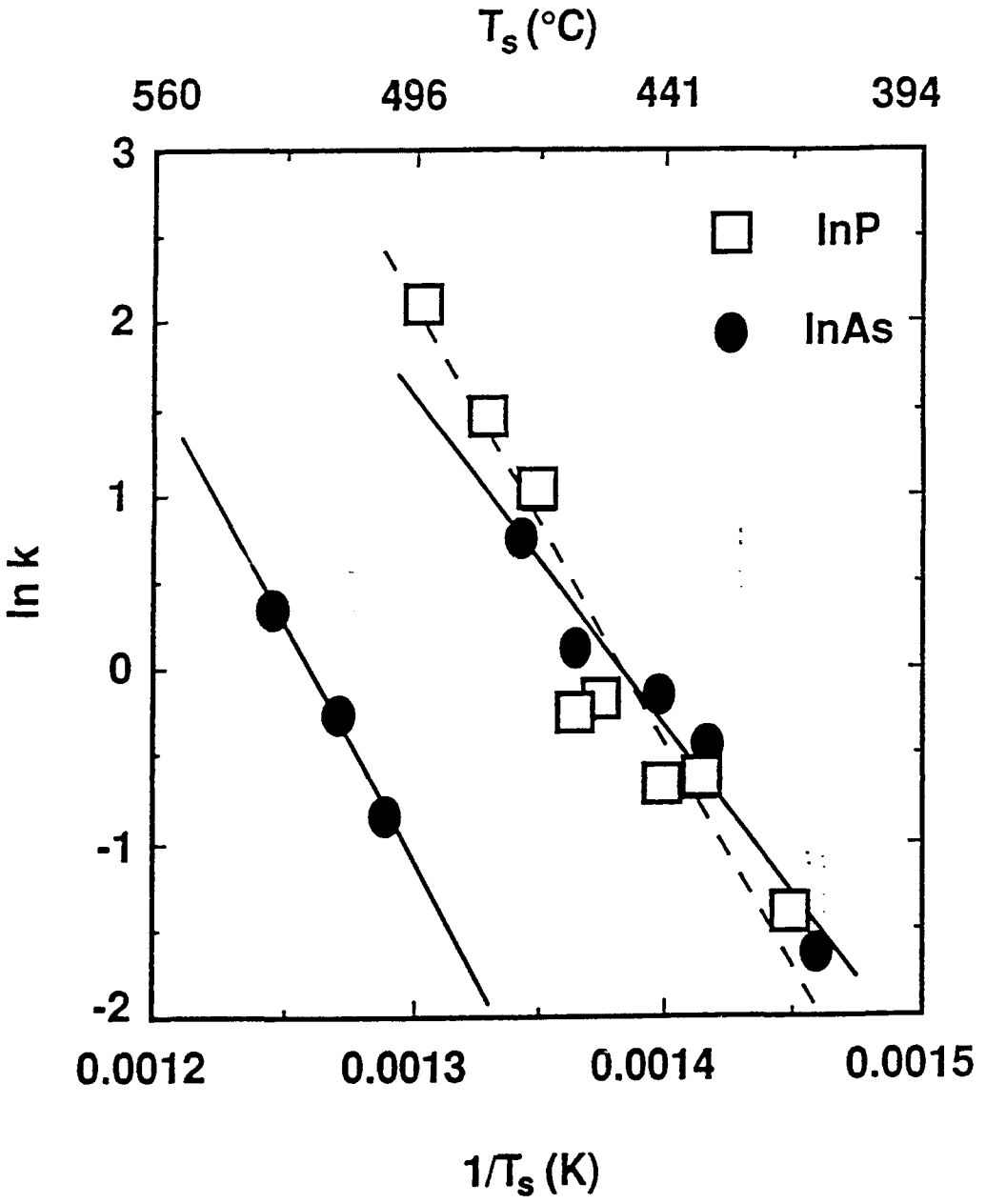
T_s (°C)
560
496
441
394
3
2
1
0
-1
-2
ln k
InP
InAs
0.0012
0.0013
0.0014
0.0015
$1/T_s$ (K)

Fig. 3

shows that the number of pulses circulating in the cavity drops from 6 to 5 at the power discontinuity. Pulses can vanish from the trains singly or a number of pulses ($n = 2, 3, 4$ ...) can disappear simultaneously (with a correspondingly larger drop in average output power). Measurements at port 2 show an abrupt increase in average output power on the disappearance of a soliton. Region C is the most interesting and controllable and the remainder of this paper deals with it exclusively.

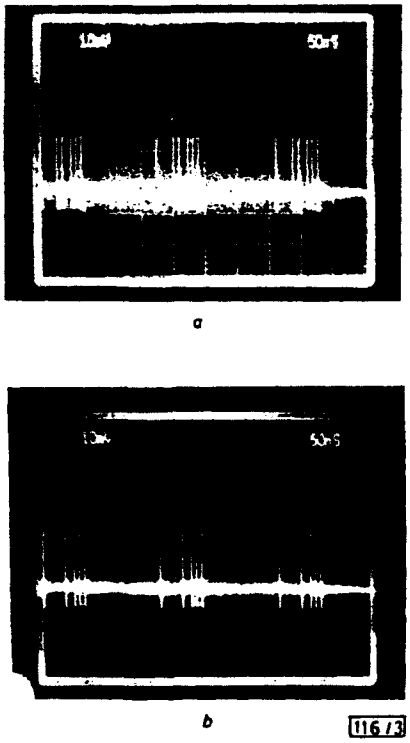

Fig. 3 *Temporal behaviour of laser output*
a At point A on inset Fig. 2
b At point B on inset Fig. 2

By measuring the change in output power $\delta P = 13\,\mu W$ (Fig. 2), we can estimate the energy of the pulses circulating within the unidirectional loop of the laser. The calculated energy $E = 12$ pJ indicates that the pulses of duration 450 fs, circulating within the isolator loop have a soliton number in the range $1{\cdot}0 < N < 1{\cdot}4$ (fibre dispersion = 3·5 ps/nm km). Optical spectra measurements at points before and after a power discontinuity reveal the appearance of additional, low level, symmetric spectral lobes on the otherwise smooth intensity spectrum at port 1. This is accompanied by the enhancement of the central wavelength component at port 2.

Discussion: The measurements are consistent with the postulate that, because of the presence of the NALM within the laser resonator, a soliton pulse experiences the lowest loss on circulation around the cavity and the laser is therefore predisposed towards operating with solitons within the cavity. Owing to intensity changes around the fibre circuit the pulse is not a perfect soliton at all points within the cavity. Non-soliton components generated within a round trip are however rejected by the NALM and are lost within the isolator. The number of pulses within the cavity is therefore quantised and determined by the pump power level. A reduction in pump power can only reduce the number of pulses by one (or an integer number) of pulses and this leads to (quantised) step discontinuities in the laser output power. Any circulating power excess above that required to support this new number of solitons is rejected from the system by the combined operation of the switch, which preferentially transmits the soliton pulse component, and the isolator. this allows for the smooth decrease in output power between jumps (inset Fig. 2). As expected, however, on dropping a pulse from the cavity, a large scale (30%) variation in the output intensity at port 2 (the NALM rejection port) is observed as the system adjusts to the new, reduced, circulating power. Further measurements indicate that the soliton pulses within groups exhibit a small pulse to pulse energy variation at port 1, of the order of a few percent. This variation, possibly due to very slight differences in polarisation states or central frequencies of the individual pulses, may facilitate the removal of a particular pulse (or a group of pulses) from the cavity as the amplifier pump power is reduced.

Conclusions: Our results demonstrate energy quantisation effects in the figure eight laser and show the mechanism by which the system is able to adapt to continuous changes in pump power. In addition, we have shown that circulating pulses within the cavity are close to being fundamental solitons. The challenge remains to control the pulse patterns in a predetermined way to generate, high bit rate, soliton sequences.

22nd October 1991

A. B. Grudinin*, D. J. Richardson and D. N. Payne (*Optoelectronics Research Centre, Southampton University, Southampton SO9 5NH, United Kingdom*)

* On leave from: Optical Fibre Department, General Physics Institute, Moscow, Russia

References

1 ZIRNGIBL, M., STULZ, L. W., STONE, J., HUGI, J., DIGIOVANNI, D., and HANSEN, P. B.: '1·2 ps pulses from passively mode-locked, diode pumped Er doped ring laser', *Electron. Lett.*, 1991, 27, pp. 1734–1735
2 DULING III, I.: 'Sub picosecond all-fibre erbium laser', *Electron. Lett.*, 1991, 27, pp. 544–545
3 RICHARDSON, D. J., LAMING, R. I., PAYNE, D. N., PHILLIPS, M. W., and MATSAS, V.: 'Self-starting passively mode-locked erbium-doped laser', *Electron. Lett.*, 1991, 27, pp. 542–544
4 RICHARDSON, D. J., LAMING, R. I., PAYNE, D. N., PHILLIPS, M. W., and MATSAS, V.: 'Pulse repetition rates in passive, selfstarting, femtosecond soliton fibre laser', *Electron. Lett.*, 1991, 27, pp. 1451–1453
5 RICHARDSON, D. J., LAMING, R. I., and PAYNE, D. N.: 'Ultra low threshold Sagnac switch incorporating an EDFA', *Electron. Lett.*, 1990, 26, pp. 1779–1781
6 NAKAZAWA, M., YOSHIDA, E., and KIMURA, Y.: 'Repetition rate control of an LD pumped femtosecond erbium doped fibre laser using a sub ring cavity'. Nonlinear Guided Wave Phenomena, 1991, PDP-9

ENHANCEMENT OF EFFECTIVE SCHOTTKY BARRIER HEIGHT ON *n*-TYPE InP

M. C. Ho, Y. He, T. P. Chin, B. W. Liang and C. W. Tu

Indexing terms: Schottky contacts, Semiconductor growth, Semiconductor devices and materials

The effective Schottky barrier height on *n*-type InP is increased by a thin heavily-doped *p*-type surface layer grown by gas-source molecular beam epitaxy. The relationships between the barrier height increment and the doping level and thickness of the surface layer have been studied. The Schottky diodes fabricated by this method show reasonably low leakage current at high reverse bias and high reverse break-down voltage.

Introduction: InP is an important material for high-speed electronic and optoelectronic application [1, 2], but it has a major disadvantage of low Schottky barrier height [3]. This inher-

ently low Schottky barrier height (0·40–0·45 eV) makes it difficult to fabricate field-effect transistors (FET) directly on InP because of the serious leakage current problem through the gate electrode. Efforts have been made to increase the barrier height by growing a high band gap material, such as InAlAs or highly strained InGaP [4, 5], as a quasi-insulating layer, or by depositing various dielectric materials on InP [6]. A simpler approach, however, was proposed by Shannon [7] and Wu [8] for Si Schottky contacts. They suggested that the effective Schottky barrier height could be controlled over a certain range (either higher or lower) with a heavily doped surface layer. This concept was proved successfully by Eglash *et al.* [9] and Pearton *et al.* [10] on GaAs by doping the surface *p*-type with respect to the *n*-type substrate. A similar structure has been reported on InP recently by Abid *et al.* [11], but the reverse leakage current density is extremely large due to poor metallisation contact. This Letter presents a study on enhancing the effective Schottky barrier height on *n*-type InP by different doping levels and thicknesses of the counterdoped surface layer.

Design and fabrication: The InP epitaxial layer was grown on an n^+ InP (001) substrate by gas-source molecular beam epitaxy (GSMBE) with elemental In and thermally cracked phosphine. The *p*-type dopant was Be. The structure, as shown in Fig. 1*a*, consists of an undoped InP buffer layer with *n*-type background doping of $8 \times 10^{15}\,cm^{-3}$, a counterdoped surface layer with doping levels of $2{\cdot}5 \times 10^{18}\,cm^{-3}$ and $5 \times 10^{18}\,cm^{-3}$, and a 150 Å thick undoped InP cap layer. The cap layer is used for protecting the surface layer in the cleaning process immediately before the metal evaporation. The thickness of the surface layer ranged from 90 to 150 Å. The surface layer thicknesses were chosen so that the layers would be completely depleted due to the built-in surface potential. Under this condition, the majority-carrier injection characteristics of the Schottky contact could be preserved. Fig. 1*b* shows a schematic band diagram for the structure. From the C–V data discussed below, the full depletion requirement was confirmed. To reduce Be diffusion during growth, the substrate temperature was kept at 450°C, which was calibrated by a pyrometer. The growth rate was 1 μm/h. After the samples were taken out of the GSMBE system, a 1500 Å thick Au film was evaporated with a thermal evaporator. Spherical diode patterns were defined by a liftoff process. The radius of the diodes, measured under an optical microscope, was 250 μm.

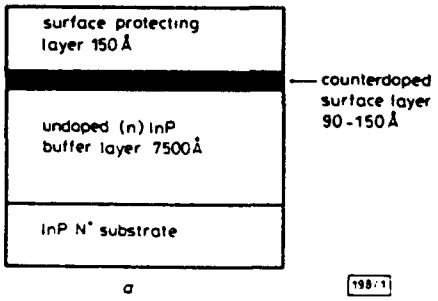

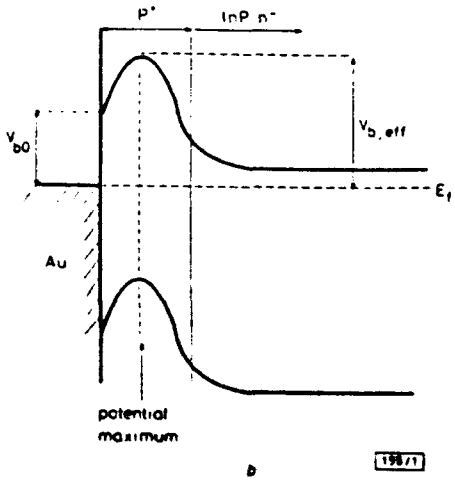

Fig. 1 *Structure of InP epi-layer and band diagram for structure used for Schottky barrier height enhancement used in this work*

a Structure of epi layer
b Band diagram

Results and discussion: The I–V characteristics of the Au-InP Schottky diode were measured by a HP4145B semiconductor parameter analyser. The effective Schottky barrier height and ideality factor were derived from the saturation current density and the current to voltage gradient. The calculation was based on the thermionic emission theory as shown in eqn. 1 [3].

$$J = A^*T^2 e^{-qV_{b,eff}/kT}(e^{qV/n_{eff}kT} - 1) \tag{1a}$$

$$V_{b,eff} = (kT/q)\ln(A^*T^2/J_s) \tag{1b}$$

$$n_{eff} = \frac{q}{kT}\left(\frac{\partial \ln J}{\partial V}\right)^{-1} \tag{1c}$$

where A^*, the effective Richardson constant for InP, is $9{\cdot}4\,A\,cm^{-2}K^{-2}$ [6]. $V_{b,eff}$ is the I–V effective Schottky barrier height at zero bias. J_s is the extrapolated saturation current density, and n_{eff} is the effective ideality factor obtained from the I–V curves. The forward current characteristics of different diodes are shown in Fig. 2*a*. In the log (I)–V curve of the diode with a higher effective barrier height, the small inflection at 0·05 V may be due to the Schottky–Read–Hall recombination current in the surface depletion region [10].

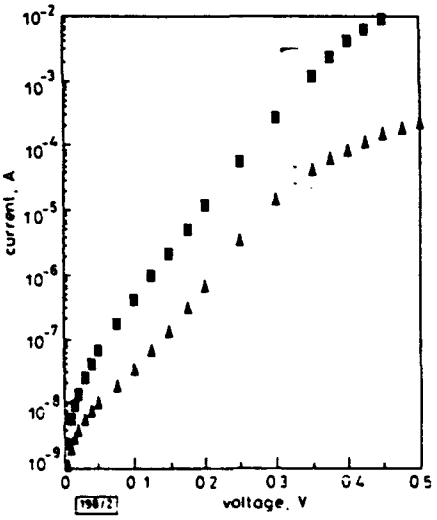

Fig. 2 *Forward I–V characteristics of Au–InP Schottky diodes with different effective Schottky barrier heights*

■ V_b = 0·656 eV, n = 1·192
◆ V_b = 0·732 eV, n = 1·197

The relationships between the effective barrier height and the doping level as well as the thickness of the surface layer are shown in Table 1. It is clear that the effective barrier height increases either with the doping concentration or with the thickness as expected. A barrier height as large as 0·73 eV can be obtained, much higher than the original value of 0·42 eV. We performed a theoretical I–V barrier-height calculation, following previous workers [7–9]. Under the electrostatic condition, the electron energy band diagram was obtained by solving the Poisson equation with Boltzmann statistics. The effective barrier height was defined from the Fermi level in the bulk region to the conduction bandedge in the surface doped layer, as shown in Fig. 1*b*. It is also possible

Table 1 EXPERIMENTAL AND THEORETICAL VALUES OF ENHANCED THERMIONIC EFFECTIVE BARRIER HEIGHT AND EFFECTIVE IDEALITY FACTOR OF *n*-TYPE Au-InP SCHOTTKY DIODES

Sample	No. 344, $t_p = 125$ Å, $p = 2.5 \times 10^{18}$ cm^{-3}	No. 343, $t_p = 150$ Å, $p = 2.5 \times 10^{18}$ cm^{-3}	No. 346, $t_p = 90$ Å, $p = 1 \times 10^{19}$ cm^{-3}
$V_{b,eff}$ (experiment)	0.66 eV	0.73 eV	0.66 eV
$V_{b,eff}$ (theory)	0.66 eV	0.77 eV	0.68 eV
n_{eff}	1.19	1.20	1.12

to obtain the effective ideality factor and surface depletion region width from these calculations.

Owing to the space-charge region associated with the counterdoped surface layer, the band maximum in the surface layer is actually a function of the applied bias and the doping level. In eqn. 1*a*, the thermionic barrier height is obtained from the extrapolated zero-bias value. The effective ideality factor will then become a function of applied bias and doping level. The experimental values of the effective ideality factor were obtained from the current to voltage gradient in a specified range, and these values are generally larger than the original n_0, which is supposedly near unity. This relation was confirmed by the experimental data. The exact depletion region width can be readily obtained from the depletion capacitance value of the Schottky diode. This was measured by a HP4284A LCR meter at 1 MHz. When we assumed the surface layer would be completely depleted, the calculated zero-bias depletion region width, for sample no. 346, is 3150 Å, and the measured value is 3315 Å. Comparing these two values, we believe our assumption of complete depletion to be correct.

It should also be pointed that due to the surface space charge region, the C–V barrier height (the intersection of $1/C^2$ against voltage axis) is expected to be larger than the I–V barrier height because the C–V barrier height is obtained by extrapolating toward the metal–semiconductor interface, from the energy band bending in the *n*-type substrate region [7]. The corresponding C–V barrier height of sample no. 346 was 0.69 eV, as shown in Fig. 3, which was higher than the value 0.66 eV from the I–V measurement analysis. Therefore, it is more proper to measure the effective Schottky barrier height by the I–V method for this structure. However, it is still valid to use $\partial(1/C^2)/\partial V$ to obtain the free carrier concentration in the bulk region because the depletion region already extends into the substrate and the capacitance value is measured by depleting the free carriers in the nearly uniformly doped substrate region.

The forward and reverse current characteristics of the diode with a barrier height of 0.66 eV are shown in Fig. 4. At reverse bias of 6.0 V, the reverse leakage current density is about 3.05×10^{-3} A/cm^{-2}. The breakdown voltage of the diode was larger than 9 V, which is particularly important for high-power devices. Furthermore, for a $1 \times 100\,\mu m^2$ diode (a typical gate area for FET) the corresponding leakage current would be smaller than 35 nA. This is acceptable for device application, and it is much lower than the leakage current of 800 μA as mentioned previously [11].

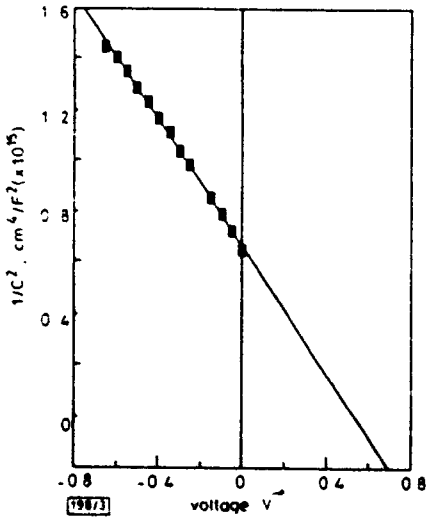

Fig. 3 *$1/C^2$ against voltage of Au–InP Schottky diode with effective barrier height 0.66 eV*

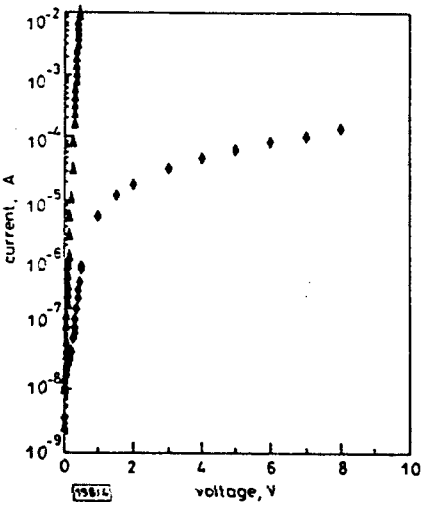

Fig. 4 *Forward and reverse I–V characteristics of Au–InP Schottky diode with effective barrier height 0.66 eV*

▲ forward current
◆ reverse current

Conclusion: InP Schottky diodes with high effective I–V barrier heights, obtained from a thin, heavily doped *p*-type surface layer on *n*-type InP substrate, were fabricated and tested. The results agree well with theoretical calculations. Moreover, it is possible to modulate the barrier height by changing the doping level or thickness of the surface layer. The moderate reverse leakage current density and the high breakdown voltage make this technique promising for device application.

Acknowledgment: We wish to express our appreciation to S. S. Lau, J. T. Chow and P. M. Asbeck for making their C–V and I–V measurement facilities available to us. We also would like to acknowledge the Office of Naval Research for financial support.

1st November 1991

M. C. Ho, Y. He, T. P. Chin, B. W. Liang and C. W. Tu (*Department of Electrical and Computer Engineering, University of California, San Diego, La Jolla, CA 92093-0407, USA*)

References

1 AHAMAR, A., FELER, M. D., KOREN, U., and MILLER, B. I.: 'DC and microwave characteristic of modulation doped $Ga_{0.47}In_{0.53}As$ InP HFET', *Electron. Lett.*, 1988, 24, pp. 702–703

2 HOSSEINI THERANI, A., DECOSTER, D., VILCOT, J. P., and RAZEGHI, M.: 'Monolithic integrated photoreceiver for 1.3–1.55 μm wavelength: association of a Schottky photodiode and a field effect transistor on GaInP–GaInAs heteroepitaxy', *J. Appl. Phys.*, 1988, 64, pp. 2215–2248

3 RHODERICK, E. H., and WILLIAMS, R. H.: 'Metal–semiconductor contacts' (Oxford Science Publications, London, 1987), p. 74
4 LEE, P. Z., FAN, C., MEINERS, L. G., and WIEDER, H. H.: 'Interfacial properties of InAlAs/InGaAs HIGFETs and MIS capacitors', *Semicond. Sci. Technol.*, 1990, **5**, pp. 716–720
5 LOUALICHE, S., GINUDI, A., LE CORRE, A., LECROSNIER, D., VAURDY, C., HENRY, L., and GUILLEMOT, C.: 'Low-temperature DC characteristics of pseudomorphic $Ga_{0.18}In_{0.82}P/InP/Ga_{0.47}In_{0.53}As$ HEMT', *IEEE Electron Device Lett.*, 1990, **11**, pp. 153–156
6 HATTORI, K., and TORRI, Y.: 'A new method to fabricate Au/n-type InP Schottky contacts with an interfacial layer', *Solid-State Electron.*, 1991, **34**, pp. 527–531
7 SHANNON, J. M.: 'Control of Schottky barrier height using highly doped surface layer', *Solid State Electron.*, 1976, **19**, pp. 537–543
8 WU, C. Y.: 'Barrier height enhancement of the Schottky barrier diode using a thin uniformly-doped surface layer', *Solid State Electron.*, 1981, **9**, pp. 857–862
9 EGALSH, S. J., NEWMEN, N., PAN, S., MO, D., SHENAI, K., SPICER, W. E., PONCE, F. A., and COLLINS, D. M.: 'Engineered Schottky barrier diodes for the modification and control of Schottky barrier heights', *J. Appl. Phys.*, 1987, **61**, pp. 5159–5169
10 PEARTON, S. J., REN, F., ABERNATHY, C. R., HOBSON, W. S., CHU, S. N. G., and KOVALCHICK, J.: 'Carbon and zinc delta doping for Schottky barrier enhancement on n-type GaAs', *Appl. Phys. Lett.*, 1989, **55**, pp. 1342–4344
11 ABID, Z., GOPINATH, A., WILLIAMSON, F., and NATHAN, M. I.: 'Direct Schottky contact InP MESFET', *IEEE Electron Device Lett.*, 1991, **12**, pp. 279–280

PARALLEL ACQUISITION OF MR IMAGES USING TIME MULTIPLEXED COILS

S. W. Wright and J. R. Porter

Indexing terms: Image processing, Signal processing, Data acquisition, Biomedical electronics, Magnetic resonance

A new technique for parallel acquisition of magnetic resonance images is described. Two RF coils are time multiplexed into a single receiver channel, halving the effective image acquisition time with no degradation in signal-to-noise ratio. Noise filtering is performed with RF bandpass filters. In principle, the method can be extended to additional coils.

Introduction: Parallel image acquisition using independent radio-frequency (RF) coils and receiver channels has been suggested as a method of increasing throughput in MR imaging by acquiring multiple images simultaneously [1]. This technique has been proposed for imaging large fields of view without sacrificing image quality [2], and reducing imaging time for a specified field of view by reducing the number of phase encoding steps needed to obtain a certain resolution [3]. Unfortunately, there is a high cost for the additional receiver channels.

This Letter presents an alternative technique for simultaneous data acquisition from multiple coils. The proposed method eliminates the need for additional receiver channels by multiplexing the signals from each coil to a single channel. This technique requires minimal additional hardware and simple reconstruction software while still allowing multiple images to be obtained from different coils simultaneously.

Methods: A Siemens 1·0T Magnetom was modified for multiplexed imaging from two receiver coils. A block diagram of the modified receiver system is shown in Fig. 1. Each coil requires at least one preamplifier and one bandpass filter. A *pin* diode switch (SCM-12D-250, Merrimac Devices, West Caldwell, NJ) was used to multiplex the filtered signals from each coil into the original receiver channel. A separate preamplifier was added after each bandpass filter to compensate for a 29 dB insertion loss in the filters. Although a single preamplifier with higher gain could have been used, this allowed the existing surface coil preamplifiers to be used for the input stage in both single channel and multiplexed imaging for pur-

Two minor modifications to the receiver channel were required. First, a TTL level end-of-conversion signal available on the analogue-to-digital convertor (ADC) board was brought out through an optoisolator to control the RF switch. A digital phase shifter was constructed to allow adjustment of the timing of this signal. Secondly, the audio-frequency lowpass (LP) filters normally used after demodulation were bypassed, as filtering was performed at RF. On the Magnetom GBS I system, this is carried out by a simple front panel connection. On some systems, a wide LP filter may be needed to eliminate noise from the imager electronics.

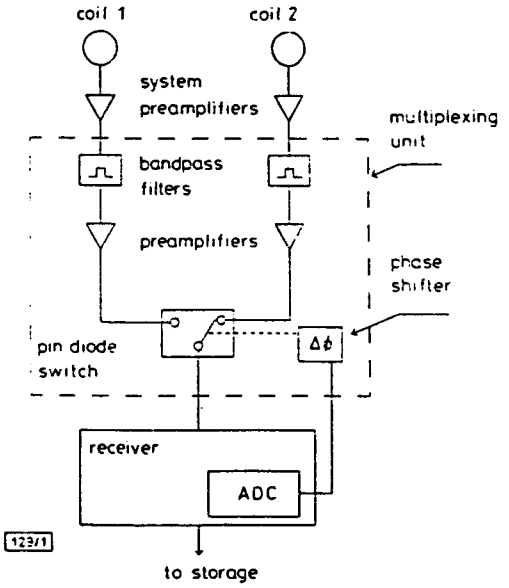

Fig. 1 *Block diagram of modified MR receiver system*
Hardware added for multiplexing is outlined

To obtain the desired resolution from each coil, the sampling rate is increased by a factor of two as compared to a single coil image with the same image parameters, and a standard oversampled data set is acquired. In this manner, no modifications are made to the data acquisition system. The resulting data set is transferred to a standalone processor where it is parsed into separate raw data files which are reconstructed into two independent images. Each resulting image has the same SNR as obtained from separately obtained single channel images, resulting in a halving of effective imaging time. In principle, this method can be extended to additional coils. Practical limitations include the maximum sampling rate of the data acquisition system and the bandwidth of the receiver system.

Although this method requires only minor modifications to the existing MR system, the RF filters require extremely narrow bandwidths. Each coil is filtered by an RF bandpass filter whose bandwidth is determined by the sampling rate for a single coil image with the same resolution. Crystal filters were designed and constructed to obtain a sufficiently narrow bandwidth. While these filters are somewhat restrictive due to their fixed bandwidth, problems occur when the multiplexed signals are passed through the conventional LP filters. Cross-talk between images, which occurs due to the averaging effects of the filter, can be removed by inserting a second switch after the demodulator to separate each signal to its own set of LP filters. However, this method results in a decrease in SNR. Owing to the switching after the receiver, the signal samples are averaged with the interleaved signal voids in the AF filter, resulting in a net decrease of the time average signal power by a factor of 2. The noise, due to its random nature, only suffers a $\sqrt{(2)}$ loss, resulting in a total $\sqrt{(2)}$ loss in SNR.

Results: To test the system, two small phantoms were placed on two 6·5 cm round surface coils spaced 21 cm apart, centre to centre. Spacing of the coils was sufficient to achieve an $S_{12} < -20$ dB, effectively decoupling the two coils. Images were obtained in single channel and in multiplexed modes.

To be published in MRS
Symp. Proc. 1991.

LOW-TEMPERATURE GROWTH AND CHARACTERIZATION OF InP GROWN BY GAS-SOURCE MOLECULAR-BEAM EPITAXY

B. W. Liang, Y. He and C. W. Tu
Department of Electrical and Computer Engineering, University of California, San Diego, La Jolla, CA 92093-0407.

ABSTRACT

Low-temperature (LT) growth of InP by gas-source molecular-beam epitaxy has been studied. Contrary to GaAs, InP grown at low temperature (from 200 °C to 410 °C) shows n-type, low-resistivity properties. The electron concentration changes dramatically with growth temperature. A model of P antisite defects formed during LT growth was used to explain this experimental result. Ex-situ annealing can increase the resistivity, but only by a factor of about 6. Heavily Be-doped LT InP also shows n-type property. We believe this is the first report of an extremely high concentration of donors formed in LT InP and n-type doping by Be in III-V compounds.

INTRODUCTION

Annealed GaAs layers grown at low temperature exhibit extremely high resistivity [1-3] and short carrier lifetime [4, 5], but unexpectedly high mobility [4]. High resistivity is desirable for both field-effect transistors and optoelectronic devices. Short carrier lifetime combined with high mobility, is advantageous for ultra-fast switches. Low-temperature growth of various arsenides has become one of the most interesting topics today. Different models have been proposed to explain the properties of LT GaAs [6, 7].

As another important member of the III-V family, InP grown at low temperature and its properties have not been investigated. In this paper, we have systematically studied the growth of InP by gas-source molecular-beam epitaxy (GSMBE) at low temperature (from 200°C to 410°C), and the properties of both as-grown and annealed LT InP thin films by reflection high-energy electron diffraction (RHEED), Hall-effect measurement, I-V characteristics, and photoluminecence. Extremly high concentration of donors and anomalous doping behavior of Be in LT InP grown by GSMBE has been observed for the first time.

EXPERIMENTAL PROCEDURE

The samples were grown in an Intervac (Varian) Gen-II MBE machine modified to handle arsine and phosphine. An Intervac gas cracker for cracking group-V hydrides and EPI effusion cells for In, Ga, Be and Al were used. The growth rate of InP was fixed at 1 monolayer per second. The growth temperature was calibrated by a pyrometer and the melting point of InSb. The cracker temperature was 1000°C. The LT InP layers were grown in the growth temperature range of 200°C to 410°C, and with a phosphine flow rate range of 0.8 sccm to 2.4 sccm. Ex-situ annealing was performed in forming gas (15% H_2 and 85% N_2). During proximity annealing, the sample surface was protected by another piece of InP substrate. RHEED pattern was used to monitor the growth front. Hall-effect measurements and I-V curves were used to characterize electrical properties of LT InP grown on (001) semi-insulating and n^+-InP substrates, respectively. Photoluminecence was used to characterize optical properties of LT InP .

RESULTS AND DISCCUSION

Among growth parameters, the growth temperature is the most important. Figure 1 shows the electron concentration of undoped InP as a function of growth temperature at a phosphine flow rate of 1.5 sccm. Below 500°C, the electron concentration of undoped InP, similar to InAs [8], increases with decreasing growth temperature. At 340°C, the electron concentration is as high as 4.5×10^{18} cm^{-3}. When the growth temperature decreases further, the electron concentration begins to decrease. We believe that native defects dominate electricalproperties of LT InP. At a fixed phosphine flow rate, the lower the growth temperature is, the higher the phosphorus incorporation into the layer. The species of native defects in InP are P_i (phosphorus self-interstitial), P_{In} (phosphorus antisite defect), In_i (In self-interstitial), In_P (In antisite defect) and V_P (phosphorus vacancy) for In-rich InP; or combination of theses defects. Of

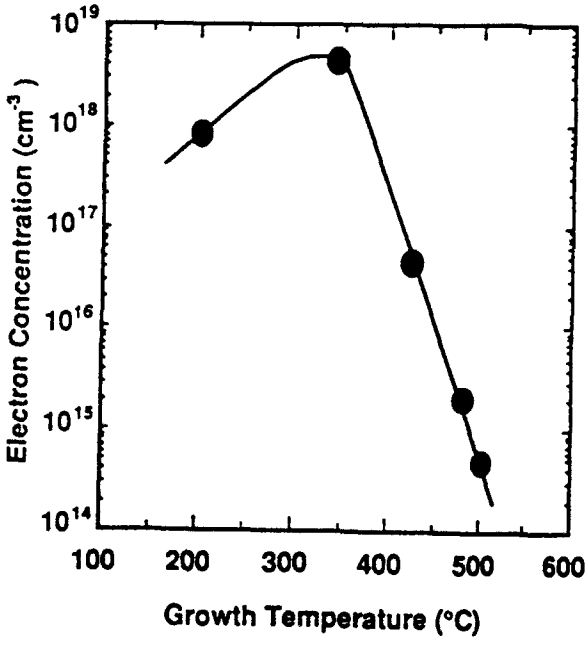

Fig.1 The electron concentration of GSMBE InP vs. growth temperature at 1.5 sccm of phosphine flow rate and 1.0 monolayer per second of growth rate.

these, P_{In}, In_i and V_P are donors, and the others are acceptors. Because phosphorus atoms are much smaller than In atoms, it is expected that more P atoms will occupy the In sites, instead of interstitial sites. This can then explain that undoped LT InP is n-type. However, when the growth temperature decreases further, more P_i may be present because many extra phosphorus atoms become incorporated into the deposited layer. Therefore, the electron concentration decreases. Photoluminecence measurements at 40 K show that the full width at half maximum (FWHM) is 2 meV for a sample grown at 500 °C, 11 meV for a sample grown at 410 °C, and no luminecence for samples grown at temperatures below 400 °C.

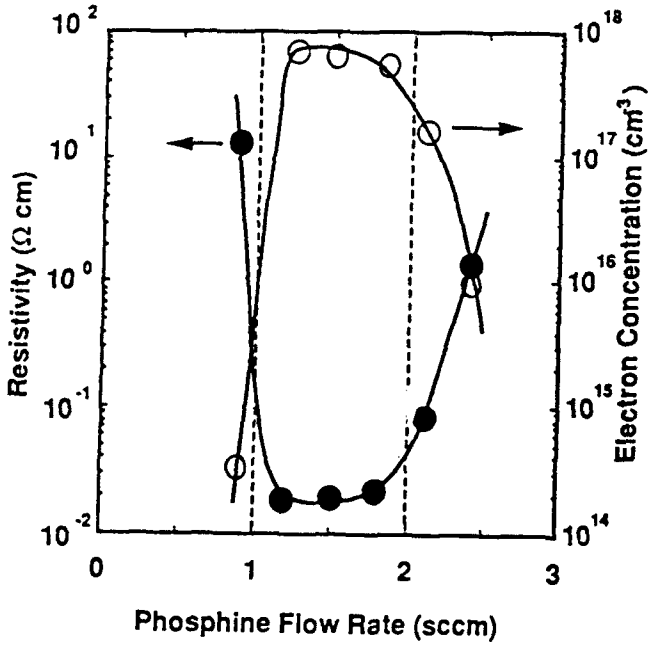

Fig.2 The resistivity (solid circles) and electron concentration (open circles) of LT InP (200°C) vs phosphine flow rate. Growth temperature was 200°C and growth rate was 1.0 monolayer per second. The depodit layers were polycrystalline-like InP if phosphine flow rate below 1.0 sccm or above 2.0 sccm.

Figure 2 shows the resistivity and carrier concentration of undoped LT InP as a function of phosphine flow rate at a growth temperature of 200°C. Between 1.0 sccm and 2.0 sccm of the phosphine flow rate, the electron concentration of undoped LT InP is about $7x10^{17}$ cm^{-3} with a resistivity about 0.02 Ω-cm. Mirror-like surface morphology of these samples were obtained. On the other hand, if the phosphine flow rate is below 1.0 sccm or above 2.0 sccm, LT InP grown at 200°C is polycrystalline according to the RHEED pattern, and its resistivity (carrier concentration) increases (decreases) with increasing nonstoichiometry. The surface morphology of these samples becomes either white (In rich) or black (P rich). At a fixed growth temperature and In-beam flux, the crystallinity and surface morphology of LT InP layers deteriorate with increasing PH_3 flow rate above 1.0 sccm. For the LT InP layer grown on an n^+-InP substrate, Au dots are evaporated on the surface. I-V curves show very good ohmic contact characteristics between Au and LT InP without any alloying.

Be is a popular p-type dopant for InP grown by molecular-beam epitaxy (MBE) [9]. One can obtain an acceptor concentration as high as $3x10^{19}$ cm^{-3}. However, as shown in Figure 3, we can not obtain p-type InP by Be-doping in LT InP, even the Be doping level is as high as $1x10^{19}$ cm^{-3} of acceptor concentration for normally grown InP in our system. With increasing

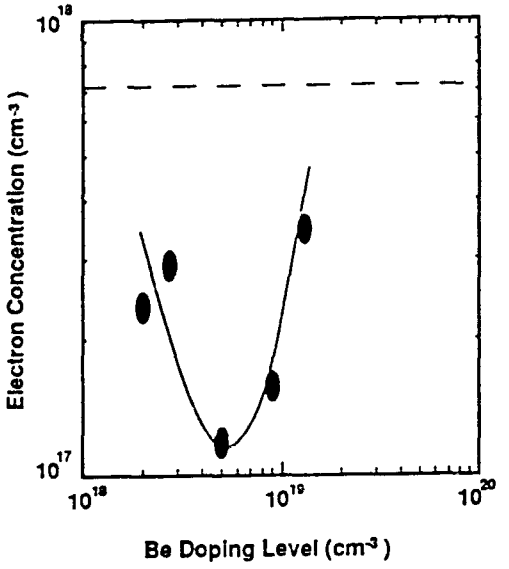

Fig.3 The electron concentration of Be-doped LT InP vs Be doping level. The dashed line shows the electron concentration of undoped LT InP. Growth temperature was 200°C. Phosphine flow rate was 1.5 sccm.

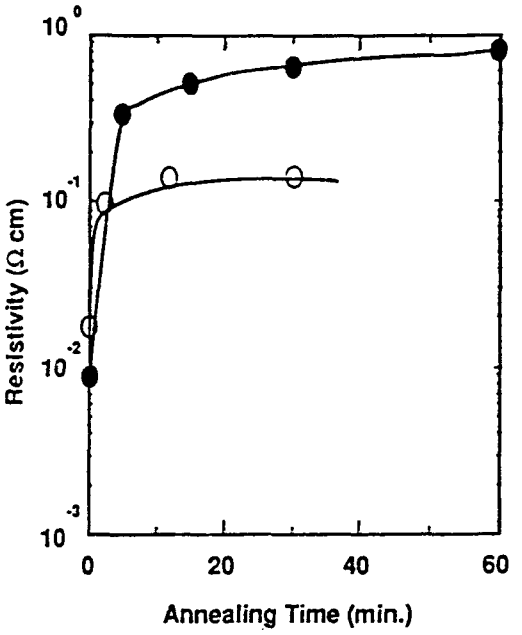

Fig.4 The resistivity of undoped (open circles) and Be-doped (solid circles, Be-[illegible]0°C) LT InP vs ex-situ annealing time (in forming gas). Anneal temperature was 500°C.

Be doping level the electron concentration in LT InP decreases first and then increases. We believe that there must be some interaction between native defects and Be atoms. Because Be is a group-II element, the only possibility for Be being a donor in InP is that it is self-interstitial. Therefore, in LT InP, if the Be doping level is not too high ($< 5x10^{18}$ cm^{-3}), a fraction of the Be atoms still occupy In sites as acceptors. When the Be doping level is high ($> 5x10^{18}$ cm^{-3}), more Be atoms may prefer to occupy interstitial sites and form (Be_{In}-Be_i) complex, which has been taken as a deep donor [10]. *Ex-situ* annealing at 500°C for 30 minutes in forming gas can increase the resistivity of undoped and Be-doped LT InP by factors of 6 and 60, respectively, as shown in Figure 4. Part of the initial increase in resistivity upon annealing may be due to reactivation of impurities and defects that have been passivated by hydrogen which comes from cracked phosphine.

The presence of hydrogen during growth is an important difference between GSMBE and MBE. Hydrogenation of defects and impurities in III-V compounds has been studied by several groups [11-15]. In GSMBE, at a relatively high, normal growth temperature, hydrogen species from cracked group-V hydrides are not incorporated in the deposited layer. However, hydrogen passivation of defects and dopants may occur during LT growth. At low growth temperature, hydrogen is able to be incorporated into the deposit layer and may passivate some defects and dopants. To investigate this possibility, we grew Si-doped and Be-doped InP layers on (001) semi-insulating InP substrates at a normal growth temperature of 500°C. Then, the sample

temperature was decreased to about 200°C while the layer was exposed to the cracked-phosphine beam for 30 minuets. The cracker temperature was kept at 1000°C. For Be-doped InP, the carrier concentration decreased from $3.5x10^{17}$ cm^{-3} to $2.3x10^{17}$ cm^{-3}, but for Si-doped InP, the carrier concentration remained the same. A similar behavior has been reported in ref. [15] with p^{+}-InP:Zn using hydrogen plasma. Compared to the result in ref. [15], hydrogenation of Be is not as effective as that of Zn. The difference may result from different elements or different hydrogen source. Therefore, the hydrogen presence during GSMBE can affect the properties of deposited layers, especially for LT grown materials. Even though we could not distinguish how much of the resistivity change come from dehydrogenation of native defects and/or impurities in Figure 4 at this time, hydrogenation of defects and impurities during LT GSMBE, we believe, is one of the most important factors that dominate the property of LT grown materials. Further studies on the effect of hydrogen on the deposited layer properties is being performed in this group.

CONCLUSION

The properties of LT InP have been studied systematically. Contrary to GaAs, LT InP shows n-type, low resistivity. Be in LT InP exhibits abnormal doping behavior. P-type LT InP:Be can not obtained. *Be interstitial has been assumed to explain this anomalous* experimental result.

ACKNOWLEDGEMENT

This work is partially supported by the Office of Naval Research. We wish to thank Messrs. T. P. Chin and M. C. Ho for assistance in photoluminecence measurements and the GSMBE system.

REFERENCES

[1] F. W. Smith, A. R. Calawa and C. Chen, IEEE Electron Device Letters EDL-9, 77 (1988).

[2] R. A. Puechner, D. A. Johnson, K. T. Shiralagi, D. S. Gerber, R. Droopad and G. N. Maracas, J. Crystal Growth 111, 43 (1991).

[3] M. R. Melloch, K. Mahalingam, N. Otsuka, J. M. Woodall and A. C. Warren, J. Crystal Growth 111, 39 (1991).

[4] A. C. Warren, N. Katzenellenbogen, D. Grischkowsky, J. M. Woodall, M. R. Melloch and N. Otsuka, Appl. Phys. Lettters 58, 1512 (1991).

[5] F. W. Smith, H. W. Le, V. Diadiuk, M. A. Hollis, A. R. Calawa, S. Gupta, M. Frankel, D. R. Dykaar, G. A. Mourou and T. Y. Hsiang, Appl. Phys. Letters 54, 890 (1989).

[6] M. Kaminska and E. R. Weber, Proc. 20th Inter. Conf. on the Physics of Semiconductors (ICPS) 1990.

[7] M. R. Melloch, N. Otsuka, J. M. Woodall, A. C. Warren and T. L Freeout, Appl. Phys. Lett. 57, 1531 (1990).

[8] B. W. Liang, K. Ha, J. Zhang, T. P. Chin and C. W. Tu, SPIE Proc. 1285, 116 (1990).

[9] M. B. Panish, R. A. Hamm, D. Ritter, H. S. Luftman and C. M. Cotell, J. Crystal Growth 112, 343 (1991).

[10] E. V. K. Rao, F. Alaoui, Y. Gao, J. L. Benchimol and H. Thibierge, Semiconductor Sci. & Tech. 6, 125 (1991).

[11] A. R. Calawa, Appl. Phys. Lett. 15, 1020 (1978).

[12] S. J. Pearton, W. C. Dautremont-Smoth, J. Chevallier, C. W. Tu, and K. D. Cummings, J. Appl. Phys. 59, 2821 (1986).

[13] N. Pan, S. S. Bose, M. H. Kim, G. E. Stillmen, F. Chambers, G. Devane, C. R. Ito, and M. Feng, Appl. Phys. Lett. 51, 596 (1987).

[14] H. Hirayama and T. Tatsumi, Appl. Phys. Lett. 54, 1561 (1989).

[15] W. C. Dautremont-Smith, J. Lopata, S. J. Pearton, L. A. Koszi, M. Stavola, and V. Swaminathan, J. Appl. Phys. 66, 1993 (1989).

Highly carbon-doped p-type $Ga_{0.5}In_{0.5}As$ and $Ga_{0.5}In_{0.5}P$ by carbon tetrachloride in gas-source molecular beam epitaxy

T. P. Chin,[a] P. D. Kirchner, and J. M. Woodall
IBM Research Division, T. J. Watson Research Center, Yorktown Heights, New York 10598

C. W. Tu
Department of Electrical and Computer Engineering, 0407 University of California, San Diego, La Jolla, California 92093-0407

(Received 26 August 1991; accepted for publication 25 September 1991)

Highly carbon-doped, highly p-type $Ga_{0.5}In_{0.5}As$ and $Ga_{0.5}In_{0.5}P$ epilayers were grown by gas-source molecular beam epitaxy (GSMBE) using carbon tetrachloride (CCl_4). Growth temperatures slightly below conventional values were used to increase the carbon incorporation, and a short-duration post-growth anneal near the growth temperature was necessary in order to obtain the highest hole concentrations, which were $p = 3\times10^{19}$ cm^{-3} for $Ga_{0.5}In_{0.5}As$ and $p = 5\times10^{18}$ cm^{-3} for $Ga_{0.5}In_{0.5}P$. This is the first report of significant p-type carbon doping for $Ga_{0.5}In_{0.5}P$ and the highest concentration from carbon doping yet reported for both ternary compounds. Reversible acceptor passivation from hydrogen species in the growth environment is a plausible explanation for the annealing behavior.

Carbon, a p-type dopant in the GaAs/AlGaAs material system, has been of great interest and widely investigated.[1–4] GaAs film of carrier concentration 1×10^{20} cm^{-3} and 1×10^{21} cm^{-3} have been demonstrated by organometallic vapor phase epitaxy (OMVPE)[5] and metal-organic molecular beam epitaxy (MOMBE)[2] or chemical beam epitaxy (CBE), respectively. The main advantage of carbon in these materials is the low diffusivity[6,7] that accompanies the high dopant activity, permitting thin, highly conducting layers to be used in devices such as the heterojunction bipolar transistor.[8]

However, obtaining a high p-type doping level from carbon in indium-containing materials such as $Ga_{0.5}In_{0.5}As$ (on InP) and $Ga_{0.5}In_{0.5}P$ (on GaAs) has not been as successful. Kamp *et al.*[9] demonstrated that $Ga_{0.5}In_{0.5}As$ layers grown with methyl or ethyl precursors and arsine were n type. Secondary ion mass spectroscopy (SIMS) showed carbon to be incorporated in the $Ga_{0.5}In_{0.5}As$ layer, but Hall mobility measurements showed high compensation attributed to amphotericity. Similar doping behavior was observed for implanted carbon. However, Abernathy *et al.*[10] achieved $p = 1\times10^{19}$ cm^{-3} by MOMBE using trimethylgallium (TMG) in a helium carrier gas, elemental indium, and solid arsenic. They found that this was far below the hole concentration of approximately 10^{21} cm^{-3} in GaAs grown with comparable TMG flow rate and solid arsenic. Thus the means by which carbon was introduced and incorporated into the crystal appears to determine its activity, and the presence of indium has a pronounced effect.

It is even more difficult to incorporate and activate carbon in $Ga_{0.5}In_{0.5}P$ films. de Lyon *et al.*[11] showed that $Ga_{0.5}In_{0.5}P$ grown with triethylgallium (TEG), elemental indium and phosphine at 560 °C is n type, and the carbon concentration was below the SIMS detection limit. Decreasing the growth temperature to 500 °C increased the carbon incorporation (carbon = 5×10^{18} cm^{-3} by SIMS) but the carrier density was still at the n-type background level. de Lyon *et al.*[12] also showed that CCl_4-doped films grown at 515 °C from elemental group-III sources and cracked phosphine were weakly p-type with 5×10^{16} cm^{-3} holes despite a carbon level of 5×10^{19} cm^{-3}. In this letter we demonstrate that carbon-doped p-type $Ga_{0.5}In_{0.5}As$ and $Ga_{0.5}In_{0.5}P$ can be grown by gas-source MBE using CCl_4 as the doping source. After a post-growth anneal, $p = 3\times10^{19}$ cm^{-3} and $p=5\times10^{18}$ cm^{-3} for $Ga_{0.5}In_{0.5}As$ and $Ga_{0.5}In_{0.5}P$, respectively, were achieved.

The growth was performed in a Varian Gen-II MOMBE system. Thermally cracked hydrides and elemental group-III effusion cells were used as sources. High-purity (but not redistilled) CCl_4 was supplied through a standard "alkyl" delivery system using hydrogen carrier gas, a CCl_4 bubbler, and an injector operated at 50 °C. The growth temperature was monitored by a thermocouple which had been calibrated by an optical pyrometer. All layers were grown on (100) semi-insulating substrates without buffer layers in order to avoid the effects of parallel conduction in electrical characterization. A CCl_4-doped GaAs layer was grown as a reference, and the Hall-effect hole concentration was measured to be 6×10^{19} cm^{-3}. The CCl_4 flux was then set at the same value for all subsequent growth runs. The composition was examined by x-ray rocking curves. Van der Pauw samples were fabricated on 5 mm squares by alloying pressed indium-zinc alloy contacts for 5 min at specified temperatures. Hall measurements were performed to determine the carrier concentrations.

First, we discuss two $Ga_{0.5}In_{0.5}As$ samples grown on InP(100) at 420 and 460 °C, respectively, with In, Ga, and arsine. These two temperatures were chosen so (2×1) or (2×4) reflection high-energy electron diffraction (RHEED) patterns were observed on the substrate[13] under the same phosphine flow rate (5 sccm) before growth. However, no difference between these two samples was

[a]Permanent address: Department of Electrical and Computer Engineering, University of California, San Diego, La Jolla, CA 92093-0407.

 0003-6951/91/472865-03$02.00

TABLE I. Comparison of carbon-doped $Ga_{0.5}In_{0.5}As$ in Refs. 9, 10, 16, and this work.

Source (carrier gas)				Growth temp. (°C)	Carrier concentration (cm^{-3}) as grown	Carrier concentration (cm^{-3}) *ex situ* 420 °C anneal	
TMG	TMI	Arsine		477	$n = 5\times10^{17}$		Ref. 9
TMG	TEI	Arsine		477	$n = 3\times10^{17}$		
TEG	TMI	Arsine		477	$n = 7\times10^{16}$		
TEG	TEI	Arsine		477	$n = 2\times10^{15}$		
TMG(He)	TMI(H_2)	As_4		500	$n = 7\times10^{16}$		Ref. 10
TMG(He)	TMI(H_2)	Arsine	(low V/III)	500	$n = 3\times10^{16}$		
TMG(He)	TMI(H_2)	Arsine	(high V/III)	500	$n = 1\times10^{17}$		
TMG(He)	In	As_4		500	$p = 1\times10^{19}$		
TMG(He)	In	As_4		450	$p = 1.2\times10^{18}$		Ref. 16
TEG(H_2)	In	Arsine	$CCl_4(H_2)$[a]	420	$p = 4\times10^{18}$	$p = 5\times10^{19}$	This work
TEG(H_2)	In	Arsine	$CCl_4(H_2)$	420	$p = 4\times10^{18}$	$p = 3\times10^{19}$	
Ga	In	Arsine	$CCl_4(H_2)$	460	$p = 3\times10^{18}$	$p = 3\times10^{19}$	
Ga	In	Arsine	$CCl_4(H_2)$	420	$p = 3\times10^{18}$	$p = 3\times10^{19}$	
Ga	In	Arsine	$CCl_4(H_2)$[b]	420	$p = 3\times10^{19}$		

[a]Consists of an $(InAs)_2/(GaAs)_2$ short period superlattice.
[b]Annealed *in situ* after growth at 420 °C.

observed by Hall measurement. In/Zn contacts were alloyed at 320 °C. A hole concentration of $\simeq 3\times10^{18}$ cm^{-3} was measured after the formation of ohmic contact. Subsequent anneals of these samples were then performed under forming gas or nitrogen at different temperatures. The hole concentration increased to 3×10^{19} cm^{-3} after a 420 °C anneal without surface degradation. Hole mobility of these samples were approximately 50 cm^2/V s.

A third sample was grown at 420 °C, remained in the chamber for 5 min at the same temperature without arsine overpressure after growth. After taking out the sample, we measured $p = 3\times10^{19}$ cm^{-3} by forming In/Zn contacts with a 320 °C anneal. This result shows that the post-grown anneal is necessary to obtain high hole concentration for CCl_4 doped $Ga_{0.5}In_{0.5}As$ in gas-source MBE and reveals that hydrogen may play an important role in the activation mechanism. More discussion will be made in later sections.

Yet higher hole concentration was achieved in one of two other samples grown with In, TEG, and arsine. One sample was a random alloy $Ga_{0.5}In_{0.5}As$, and the other sample was composed of a 2-monolayer InAs/2-monolayer CCl_4-doped GaAs short-period superlattice. CCl_4 flow rate was doubled in this superlattice sample in order to achieve the same average carbon dose as the other samples. As grown samples show $p = 4\times10^{18}$ cm^{-3}, but hole concentration of $p = 3$ and 5×10^{19} cm^{-3} was achieved after a 420 °C, 5 min anneal. Although the short-period superlattice approach results in higher doping level, the growth process was complex, and its was difficult to maintain a two-dimensional growth mode. Table I compares our results with previous reported data. Ito *et al.* observed that the conversion of conducting type in carbon-doped $Ga_{1-x}In_xAs$ was a function of x and sensitive to growth condition,[14] which may explain that no n-type $Ga_{0.5}In_{0.5}As$ was observed in our experiments.

The $Ga_{0.5}In_{0.5}P$ sample was grown on GaAs(100) substrate at 530 °C using In, Ga, and phoshine. CCl_4 was delivered at the same rate as for the $Ga_{0.5}In_{0.5}As$ samples and the GaAs standard. As observed by de Lyon *et al.*,[12] and in contrast to previous attempts to obtain p-type doping with carbon from metal alkyl sources,[11] Hall samples were weakly p type when ohmic contacts were first formed upon anneal at 350 °C and $p = 2\times10^{17}$ cm^{-3} was observed. A higher-temperature anneal was necessary to maximize the hole concentration: after a 550 °C anneal $p = 5\times10^{18}$ cm^{-3} was achieved. The known differences between this sample and the earlier work[12] are a reduced phosphine flux from 10 to 6 sccm and the use of a post-growth anneal at 550 °C for 5 min versus an approximately 300 °C contact anneal for 30 s.

Our results are the first unequivocal observation of p-type doping activity of carbon in $Ga_{0.5}In_{0.5}P$ and show the highest hole concentrations to date obtained with carbon in $Ga_{0.5}In_{0.5}As$ and $Ga_{0.5}In_{0.5}P$ grown by MBE-related techniques. At low substrate temperatures carbon from CCl_4 incorporates efficiently into these alloys. The net acceptor concentration relative to GaAs under the growth conditions specified above was found to be about 50% for $Ga_{0.5}In_{0.5}As$ and about 10% for $Ga_{0.5}In_{0.5}P$. It is possible that higher hole concentrations could result from higher CCl_4 delivery rates or the use of higher efficiency halocarbons such as CBr_4.[15] No reduction in growth rate or deviation from intended composition was observed. Therefore, using a separate source for carbon other than the sources for Ga, In, As, or P allows the alloy composition and its lattice constant to be decoupled from doping. Moreover, the hole concentration obtained from a given flux of CCl_4 proves to be far less sensitive to the alloy composition than found in previous reports. Thus while CCl_4 gives about a factor of two less doping in $Ga_{0.5}In_{0.5}As$ than in GaAs, TMG with arsenic in MOMBE gives a factor of about 100 less doping in $Ga_{0.5}In_{0.5}As$[10] than in GaAs.[2] Furthermore, while CCl_4 gives about a factor of ten less

doping in $Ga_{0.5}In_{0.5}P$ than in GaAs, alkyls that are efficient carbon-acceptor sources for GaAs and GaP have essentially no net acceptor activity in $Ga_{0.5}In_{0.5}P$.[11]

The previous observation by de Lyon *et al.* of CCl_4 doping in $Ga_{0.5}In_{0.5}P$ yielding 5×10^{19} cm^{-3} carbon and netting 5×10^{16} cm^{-3} holes was not a definitive evidence of net acceptor activity due to carbon. Because carbon is incorporated from CCl_4 at about 1% efficiency,[11,12] an efficient dopant contaminant at a concentration of 10 parts per million of the CCl_4 could produce the observed hole concentration. However, our *p*-$Ga_{0.5}In_{0.5}P$ results represent a hundredfold increase in net acceptor activation efficiency and reduce the possible influence of a noncarbon or non-CCl_4 contaminant.

While amphotericity may play a role at higher temperatures,[9] the high acceptor activation resulting from our short, 420 °C anneals suggests that the two alloys share another carbon compensation mechanism. The results of $Ga_{0.5}In_{0.5}As$ annealed *in situ* or *ex situ* suggest that hydrogen may affect the activation of carbon in these layers. This assumption is also supported by the work of Abernathy *et al.*[10] and Shirakashi *et al.*[16] who obtained *p*-type carbon-doped $Ga_{0.47}In_{0.53}As$ only under hydrogen-free environment and Woodhouse *et al.*[17] who observed H—C bond in carbon-doped GaAs. Hydrogen incorporation in semiconductors, mainly GaAs and Si, has been extensively studied and summarized.[18] Cole *et al.* and Antell *et al.* demonstrated that Zn or Cd in InP grown by MOVPE was passivated by hydrogen.[19,20] The hydrogenated Zn was reactivated after a 400 °C, 245 s anneal, but Zn became passivated again after an anneal under hydrogen (from arsine) at 450 °C.[20] Theys *et al.*[21] demonstrated the hydrogen neutralization of Zn in Zn-doped $Ga_{0.47}In_{0.53}As$, and hydrogen passivation and reactivation were observed at 250 and 375 °C, respectively. Our data suggest that carbon in $Ga_{0.5}In_{0.5}As$ and $Ga_{0.5}In_{0.5}P$ may also be passivated by hydrogen. In these layers, hydrogen would be incorporated from the hydrogen carrier gas (for the CCl_4) and/or cracked arsine. The higher annealing temperature used in our experiments can be qualitatively explained by the H—C bond strength of 80.9 kcal/mol as compared to 20.5 kcal/mol for H—Zn bond.[22] Pearton *et al.*[23] demonstrated that the activation energy for recovery of electrical activity in *n*-type GaAs is proportional to the hyrogen-dopant bond strength. Measurements of the bonding between carbon and hydrogen in $Ga_{0.5}In_{0.5}As$ and $Ga_{0.5}In_{0.5}P$ before and after anneal are in preparation.

In conclusion, we have demonstrated that highly *p*-type carbon-doped $Ga_{0.5}In_{0.5}As$ and $Ga_{0.5}In_{0.5}P$ can be grown in gas-source MBE using CCl_4 as the doping source. Record net carbon acceptor densities $p=3\times10^{19}$ cm^{-3} and $p=5\times10^{18}$ cm^{-3} were achieved for $Ga_{0.5}In_{0.5}As$ and $Ga_{0.5}In_{0.5}P$, respectively. These are relative to $p=6\times10^{19}$ cm^{-3} for GaAs and probably do not define the upper doping limit of halocarbons for $Ga_{0.5}In_{0.5}As$ and $Ga_{0.5}In_{0.5}P$ grown by gas-source MBE. We find that the growth rate and composition are essentially decoupled from the doping level, and the doping levels are orders of magnitude less sensitive to alloy composition than reported for TMG as a carbon doping source. Post-growth anneal at a temperature close to the growth temperature was required to obtain such high hole concentrations. Activation from these relatively low-temperature, short-duration anneals suggest that hydrogen passivation of carbon is present and reversible in these alloys. An InP/$Ga_{0.5}In_{0.5}As$ HBT with CCl_4-doped base has already been fabricated and will be reported elsewhere.

The authors would like to thank M. S. Goorsky and J. C. P. Chang for x-ray measurements and T. J de Lyon, H. Ito, B. W. Liang, and P. M. Asbeck for valuable discussions. C. W. Tu is supported by the Office of Naval Research.

[1] N. Putz, E. Veuhoff, H. Heinecke, M. Heyen, H. Luth, and P. Balk, J. Vac. Sci. Technol. B 3, 671 (1985).
[2] M. Konagai, T. Yamada, T. Akatsuka, K. Saito, E. Tokumitsu, and K. Takahashi, J. Cryst. Growth 98, 167 (1989).
[3] C. R. Abernathy, S. J. Pearton, R. Caruso, J. Ren, and J. Kovalchik, Appl. Phys. Lett. 55, 1750 (1987).
[4] T. J. de Lyon, J. M. Woodall, M. S. Goorsky, and P. D. Kirchner, Appl. Phys. Lett. 56, 1040 (1990).
[5] P. M. Enquist, Appl. Phys. Lett. 57, 2348 (1990).
[6] T. J. Kuech, M. A. Tischler, P. J. Wang, G. Scilla, R. Potemski, and F. Cardone, Appl. Phys. Lett. 53, 1377 (1988).
[7] B. T. Cunningham, L. J. Guido, J. E. Baker, J. S. Major, Jr., N. Holonyak, Jr., and G. E. Stillman, Appl. Phys. Lett. 55, 687 (1989).
[8] D. B. Slater, P. M. Enquist, F. E. Najjar, M. Y. Chen, and J. A. Hutchby, IEEE Electron. Device Lett. 11, 146 (1989).
[9] M. Kamp, R. Contini, K. Werner, H. Heinecke, M. Weyers, H. Luth, and P. Balk, J. Cryst. Growth 95, 154 (1989).
[10] C. R. Abernathy, S. J. Pearton, F. Ren, W. S. Hobson, T. R. Fullowan, A. Katz, A. S. Jordan, and J. Kovalchick, J. Cryst. Growth 105, 375 (1990).
[11] T. J. de Lyon, J. M. Woodall, P. D. Kirchner, D. T. McInturff, G. J. Scilla, and F. Cardone, J. Vac. Sci. Tech. B 9, 136 (1991).
[12] T. J. de Lyon, N. I. Buchan, P. D. Kirchner, J. M. Woodall, D. T. McInturff, G. J. Scilla, and F. Cardone, J. Cryst. Growth 111, 564 (1991).
[13] T. P. Chin, B. W. Liang, H. Q. Hou, M. C. Ho, C. E. Chang, and C. W. Tu, Mater. Res. Soc. Symp. Proc. 216, 517 (1991).
[14] H. Ito and T. Ishibashi, Jpn. J. Appl. Phys. 30, L944 (1991).
[15] T. J. de Lyon, N. I. Buchan, P. D. Kirchner, J. M. Woodall, G. J. Scilla, and F. Cardon, Appl. Phys. Lett. 58, 517 (1991).
[16] S. Nozaki, R. Miyake, J. Shirabashi, M. Qi, T. Yamada, E. Tobumitsu, M. Konagai, K. Takahashi, and K. Matsumoto, Extended Abstract of the 1991 International Conference on Solid State Devices and Materials, Yokohama, 1991, p. 356.
[17] K. Woodhouse, R. C. Newman, T. J. de Lyon, and J. M. Woodall, Semicond. Sci. Technol. 6, 330 (1991).
[18] J. I. Pankove and N. M. Johnson, Eds., *Hydrogen in Semiconductors*, Vol. 34 of *Semiconductors and Semimetals* (Academic, New York, 1991), Vol. 34.
[19] S. Cole, J. S. Evans, M. J. Harlow, A. W. Nelson, and S. Wong, Electron. Lett. 24, 929 (1988).
[20] G. R. Antell, A. T. R. Briggs, B. R. Butler, S. A. Kitching, J. P. Stagg, A. Chew, and D. E. Sykes, Appl. Phys. Lett. 53, 758 (1988).
[21] B. Theys, A. Jalil, J. Chevallier, A. M. Huber, C. Grattepain, P. Hirtz, and B. Pajot, Physica B 170, 421 (1991).
[22] R. C. Weast, Ed., *CRC Handbook of Chemistry and Physics*, 70th ed. (CRC, Boca Raton, FL, 1990), p. F-198, F-199.
[23] S. J. Pearton, W. C. Dautremont-Smith, J. Lopata, C. W. Tu, and C. R. Abernathy, Phys. Rev. B 36, 4260 (1987).